

Feasibility study for usage of optical partial discharge detection in HV Cable termination

by

Sweta Kumari

to obtain the degree of Master of Science, in Electrical Engineering,
Department of Electrical Sustainable Energy
at the Delft University of Technology,
to be defended publicly on Friday July 27, 2018 at 14:30.

Student number:	4598202	
Supervisors:	Dr. ir. Armando Rodrigo Mor	
	Dr. ir. Alex Tsekmes	
	Ing. Remko Koornneef	
Thesis committee:	Prof. dr. ir. Rob Ross,	TU Delft
	Dr. ir. Armando Rodrigo Mor,	TU Delft, supervisor
	Dr. ir. Milos Cvetkovic,	TU Delft

This thesis is under embargo

An electronic version of this thesis is available at <http://repository.tudelft.nl/>.

Acknowledgements

This thesis would not have been possible without the kind support and help of many individuals. First and foremost, I would like to thank my supervisors, Dr. Armando Rogrigo Mor and Dr. Alex Tsekmes for introducing me to this research topic and giving me the opportunity to do my master thesis in collaboration with Prysman Group. Their constant encouragement and valuable comments during weekly meetings throughout the thesis inspired me and guided me towards the right direction.

This thesis was experiment based and therefore I am thankful to my lab supervisor, Ing. Remko Koornneef for his guidance, support, patience and advice right from the start of my thesis, especially on the optical sensor. He helped me made a lot of critical decisions throughout my thesis and would constantly encourage me to think creatively and scientifically. Without his guidance, this thesis would not have been possible. I am also grateful to Ir. Radek Heller, Mr. Wim Termorshuizen and Ing. Paul Van Nes for always be willing to help me in my thesis. These people really helped me gained insights of High Voltage Laboratory.

I would like to extend my gratitude to Prof. Peter Vaessen and my thesis committee chair Prof. Rob Ross for providing significant comments and expert advice on the regular basis and also for reviewing my tasks and thesis report. I would also like to thank Dr. Milos Cvetkovic for taking time for being part of my thesis committee. I am thankful to all the colleagues I met at Prysman, Delft for their kind support and cooperation throughout my thesis. It was a privilege to work for a prestigious company and with friendly people.

I would like to thank all my friends in Delft especially Ayesha and Sagar and my friends back in India for their kind love and persistent belief. Finally, I must express my very profound gratitude to my parents and family for providing me with unfailing support and continuous encouragements throughout my years of study. I thank my parents and my brother for encouraging me for higher studies here at TU Delft. This accomplishment would not have been possible without them.

*Sweta Kumari
Delft, July 2017*

Abstract

Cable terminations are essential for connecting a cable to a piece of equipment such as a circuit breaker, transformer, motor, etc. Proper terminations are of great importance in order to provide faultless cable systems. Improper terminations could result in overheating, partial discharges, eventual breakdown, flashover and breakdown in the system. There are several defects that can take place in terminations because of environmental, ageing and imperfections caused during manufacturing and installation. A potential defect is the contamination of oil with water due to sealing failures.

Water contamination can lead to partial discharges that, when produced over the insulation result in accelerated ageing. Typically, online electrical measurements of partial discharges can be used for termination monitoring. However, online monitoring suffers from noise and interferences, and localisation of partial discharges can be a problem. To overcome the challenges of electrical measurements, optical means of detecting partial discharge is researched in this thesis. The main goal of the thesis is to study the feasibility of using the optical PD detection method in oil-filled cable termination. The aim was to detect surface discharges at the rubber-oil interface through an optical sensor.

The identification of parameters for selection and final choice of optical sensor for PD detection application were done. Various setups to produce the surface discharge at the rubber-oil interface were investigated and one of the method was finalized. The simultaneous measurements of PD with electrical and optical sensors were conducted in dry oil and oil with different moisture content. The analysis of data obtained from optical sensor in comparison with electrical sensor based on sensitivity, PD pulse, PRPD pattern and correlation factor are discussed. It is noted that most of the characteristics of optical measurements is comparable to the electrical measurements. Thus, it can be said that this thesis contributes towards initial step of using the optical PD detection for online monitoring of HV components.

Contents

List of Figures	ix
List of Tables	xiii
1 Introduction	1
1.1 Oil-filled termination in power system	1
1.1.1 Degradation of oil-filled termination due to water ingress	1
1.2 Previous research work	2
1.3 Motivation	4
1.4 Goals and research objectives.	5
1.4.1 Goal	5
1.4.2 Research objectives/questions	5
1.5 Thesis research methodology	6
1.6 Thesis outline	7
2 Literature study	9
2.1 Partial discharge detection	9
2.1.1 Basics of partial discharge	9
2.1.2 Types of partial discharge detection	11
2.1.3 Electrical partial discharge detection	12
2.1.4 Acoustic partial discharge detection	14
2.1.5 Chemical partial discharge detection	14
2.1.6 Optical partial discharge detection.	15
2.2 Research in optical partial discharge detection till date.	15
2.2.1 Optical interferometric detection	16
2.2.2 Fabry-Perot interferometer sensor.	17
2.2.3 Combination of lens, fibre cable and optical sensor	18
2.2.4 Combination of fluorescent fibre cable and optical sensor	18
2.2.5 Direct measurement through optical sensor.	20
2.3 On-line optical PD detection	20
3 Measurement System and test circuit description	23
3.1 Selection of optical sensor	23
3.1.1 Measurement of transmittance index of the oil	25
3.1.2 Choice of optical sensor for PD detection application	27
3.2 Setup for APD optical sensor	30
3.2.1 Specifications and characteristics of APD130A2	30
3.2.2 Layout of optical test setup.	32
3.3 Equipments for electrical PD detection	35
3.3.1 Sensors for electrical detection	35
3.3.2 Measurement instrument and analysis software	35
3.4 Finalized circuit for electrical and optical detection	39
4 Test setup design and oil sample preparation	41
4.1 Test setup design to produce surface discharge	41
4.1.1 Different orientation of electrodes and samples.	42
4.1.2 Design of electrodes	45
4.1.3 Introduction of foreign particles on the surface of rubber sample	48
4.2 Finalized setup/Conclusion	51
4.3 Oil sample preparation	52
4.3.1 Measurement of water content in the prepared oil sample	53

5	Measurement and results from electrical and optical PD detection	55
5.1	Preliminary testing with optical sensor	55
5.1.1	Corona Source	55
5.1.2	Surface discharge on rubber sample in air	58
5.2	Surface discharges on rubber sample in dry oil.	61
5.3	Surface discharges on rubber sample in oil with added moisture content	63
5.3.1	Sample 1: Saturated oil with water activity of 0.82	64
5.3.2	Sample 2: Water activity of 0.69.	66
5.3.3	Sample 3: Water activity of 0.58.	67
5.4	Measurements of treeing phenomena.	69
6	Analysis of results from electrical and optical PD detection	73
6.1	Basic Performance of optical based PD detection	73
6.1.1	Typical output PD pulse	73
6.1.2	Electromagnetic immunity	75
6.2	Sensitivity analysis	76
6.2.1	Partial discharge inception voltage	76
6.2.2	Lower limit of detection.	77
6.3	Pulse resolution time :Weibull plots	79
6.4	Phase resolved partial discharge pattern	81
6.5	Correlation between electrical and optical output.	82
6.5.1	Corona PD	83
6.5.2	Surface discharge in air	84
6.5.3	Surface discharge in oil	85
7	Conclusion and recommendation	89
7.1	Conclusion	89
7.2	Future scope and recommendations	91
8	Bibliography	93
	APPENDIX	94
A	Appendix: Chapter 3	95
B	Appendix: Chapter 4	97
C	Appendix: Chapter 5	101
D	Appendix: Chapter 6	103
E	Appendix: Chapter 7	107

List of Figures

1.1 HV cable termination [4]	2
1.2 Defects/Failure due to water ingress ion [2]	3
1.3 Failures rate in cable and cable accessories [7]	4
1.4 Work division	6
2.1 Various types of partial discharges (a) Corona discharge (b) Surface partial discharge (c) Surface partial discharge at interface (d) Internal discharge (e) treeing phenomena during internal discharge [11]	9
2.2 Equivalent circuit of (a) internal discharge (b) surface discharge (c) Corona discharge [12]	10
2.3 (a) Model representation of partial discharge (b) and (c) recurrent discharge phenomena [12]	11
2.4 Overview of PD Detection Methods	11
2.5 Standard PD circuit diagram [14]	13
2.6 Simple experimental setup of the optical interferometric detection of PD [18] . .	16
2.7 Illustration of principle behind Fabry-Perot Interferometric sensor[17]	17
2.8 Systematic representation of arrangement with lens, optic fibre and optical sensor [21]	18
2.9 Experimental setup for optical PD detection using combination of lens, fibre cable and optical sensor [22]	18
2.10 Systematic representation of arrangement with fluorescent fibre, optic fibre and optical sensor [21]	19
2.11 Experimental setup for optical PD detection using combination of fluorescent cable probe, fibre cable and optical sensor [23]	19
2.12 Experimental setup showing use of optical sensor directly [10] [24]	20
2.13 Example of online detection in transformer [21]	21
2.14 Example of online detection in termination [25]	21
3.1 Example of signal to noise ratio [26]	24
3.2 Crosstalk and afterpulse phenomena [26]	25
3.3 Spectrophotometer used for measurement of transmittance of A12 oil	26
3.4 Measured transmittance of A12 oil	27
3.5 (a) Basic structure of PMT sensors [26] (b) Basic structure of SiPM sensors [27]	27
3.6 APD working principle [28]	29
3.7 Finalized APD sensor used in this thesis	31
3.8 Layout of the sensor for measurement purposes	32
3.9 Calculation of distances from lens	34
3.10 Finalized assembled optical measurement setup	34
3.11 (a) Quadripole front pannel (b) HFCT sensor	35
3.12 Measurement using DDX 9101 PD detector	36
3.13 Measurement using Techimp PDBaseII [31]	37
3.14 Measurement using Tektronix DPO7354C Oscilloscope	37
3.15 (a) Internal circuitry of the synchronization box (b) Synchronization connection box (c) Synchronization signal to acquire phase of PD pulse [32]	38
3.16 (a) PRPD pattern from DDX9101 PD Detector (b) PRPD pattern from Techimp PD Detector (c) PRPD pattern from PDflex from signal captured using DPO7354C oscilloscope	38
3.17 Finalized Circuit diagram for PD detection	39

4.1	Experiments done with cylindrical electrodes at different positions	42
4.2	Breakdown in the oil	43
4.3	Experiments with different needle electrodes configurations	43
4.4	PRPD pattern observed at 25 kV from 1 st needle configuration (shown in Figure 4.3a)	43
4.5	PRPD pattern observed at 15 kV from 2 nd needle configuration (shown in Figure 4.3b)	44
4.6	PRPD pattern observed at 42 kV from 3 rd needle configuration (shown in Figure 4.3c)	44
4.7	(a) Breakdown at 42 kV (b) Treeing observed on rubber sample during inspection	45
4.8	(a) Model prepared in AUTOCAD (b) Test setup for experiments	45
4.9	PD pattern at 35 kV	46
4.10	(a) Breakdown at 35 kV (b) Breakdown path viewed after the inspection	46
4.11	(a) Setup of design 2 (b) 2D COMSOL Simulation of the setup with potential and electric field plot	47
4.12	(a) PRPD pattern at 6 kV (b) PRPD pattern at 10 kV	47
4.13	Breakdown at 11 kV	47
4.14	Damage and electric treeing observed on the rubber sample	48
4.15	(a) Gold sputtering machine (b) Gold sputtering mechanism (c) Gold deposited sample	48
4.16	(a) Test setup with Gold deposit sample during experiment (b) PD pattern recorded at 35 kV	49
4.17	Process for creating salted rubber sample	49
4.18	(a) PRPD pattern recorded at 15 kV (b) PRPD pattern recorded at 25 kV	50
4.19	Experiment with conductive paint deposit on rubber sample	50
4.20	(a) PRPD pattern recorded at 15 kV (b) PRPD pattern recorded at 25 kV	50
4.21	Finalized sample used for final measurements in this project	51
4.22	Climate chamber used for oil sample preparation of different moisture level (water activity)	52
4.23	Vaisala MI70 indicator and MMP78 probe	53
4.24	(a) Sample collected for water activity measurement (b) Oil sample measurement using Vaisala	54
4.25	Vaisala measurements for sample 1	54
5.1	Corona source setup	55
5.2	(a) Current pulse observed by electrical detector at 6.8 kV (b) Voltage pulse observed by optical detector at 6.8 kV	56
5.3	Signal obtained using oscilloscope from corona source	57
5.4	(a) PRPD pattern obtained from electrical detector at 10 kV (b) PRPD pattern obtained from optical detector at 10 kV	58
5.5	Setup for creation of surface discharge in air	58
5.6	Setup for creation of surface discharge in air in particular area	59
5.7	Signal obtained using oscilloscope from surface discharge	60
5.8	Experiment setup used for testing in HV lab, TU Delft	61
5.9	Test object in dry oil	62
5.10	Signal obtained using oscilloscope from surface discharge in dry oil	62
5.11	Transmission index of saturated oil compared to dry oil.	64
5.12	Experimental setup with oil sample 1	64
5.13	Signals obtained at 20 kV in oil sample 1	65
5.14	Experimental setup of oil sample 2	66
5.15	Signals obtained at 20 kV in oil sample 2	66
5.16	Experimental setup of oil sample 3	67
5.17	Signals obtained at 20 kV in oil sample 3	68
5.18	Setup used for creating internal discharge	69
5.19	Sensors in position to capture the PD activity	70
5.20	Growth of tree during testing	71

6.1	(a) PD pulse captured by HFCT sensor for corona source at 10 kV (b) PD pulse captured for corona source by APD sensor at 10 kV	73
6.2	(a) PD pulse captured by HFCT sensor for surface discharge in air at 12 kV (b) PD pulse captured by APD sensor for surface discharge in air at 12 kV	74
6.3	Signals captured by HFCT and APD sensor during noise condition	75
6.4	Signals captured by HFCT and APD sensor during PD activity	76
6.5	PDIV values comparison for different PD models in the experimental setups used	76
6.6	Sensitivity plot based on PDIV in different oil samples	77
6.7	(a) Plot for minimum charge detected by both sensor (Positive Cycle) (b) Plot for minimum charge detected by both sensor (Negative Cycle)	79
6.8	Weibull distribution of the time intervals between successive PD events recorded by HFCT sensor (blue) and APD sensor (red)	80
6.9	Weibull distribution of the time intervals between successive PD events recorded by HFCT sensor (blue) and APD sensor (red)	80
6.10	(a) Positive cluster of PRPD pattern obtained from HFCT sensor (b) Positive cluster of PRPD pattern obtained from APD sensor to save data for positive cycle part analysis	82
6.11	Plot of voltage pulse detected by APD sensor Vs apparent charge PD magnitude by HFCT sensor for corona data	83
6.12	Plot of voltage pulse detected by APD sensor Vs peak current pulse (-ve) by HFCT sensor for corona data	83
6.13	Plot of voltage pulse detected by APD sensor Vs apparent charge by HFCT sensor for surface discharge in air (setup 1)	84
6.14	Plot of voltage pulse detected by APD sensor Vs apparent charge by HFCT sensor for surface discharge in air for positive cycle (finalized setup)	84
6.15	Plot of voltage pulse detected by APD sensor Vs apparent charge by HFCT sensor for surface discharge in dry oil for positive cycle	85
6.16	Plot of voltage pulse detected by APD sensor Vs apparent charge by HFCT sensor for surface discharge in oil sample 3 for positive cycle	85
A.1	Detector responsivity response of APD130A2	95
A.2	Output frequency response of APD130A2	96
A.3	Spectral noise response of APD130A2	96
B.1	COMSOL Simulation for cylindrical electrode (Setup 1)	97
B.2	COMSOL Simulation for cylindrical electrode (Setup 2)	97
B.3	COMSOL Simulation for cylindrical electrode (Setup 3)	98
B.4	Different needle electrode orientation	98
B.5	Plot of electric field without side ground electrode for 10 kV voltage applied . .	98
B.6	Plot of electric field with side ground electrode for 10 kV voltage applied	99
B.7	Vaisala measurements for sample 2	99
B.8	Vaisala measurements for sample 3	99
C.1	PRPD pattern of corona source 15 cm from ground at 10 kV (a) From electrical detector (b) From optical detector	101
C.2	PRPD pattern of corona source 18 cm from ground at 10 kV (a) From electrical detector (b) From optical detector	101
C.3	PRPD pattern collected with electrical signal triggered for surface discharge in dry oil at 22 kV (a) From electrical detector (b) From optical detector	102
C.4	PRPD pattern collected with optical signal triggered for surface discharge in dry oil at 22 kV (a) From electrical detector (b) From optical detector	102
D.1	(a) PD pulse captured by HFCT sensor for treeing phenomena at 25 kV (b) PD pulse captured by APD sensor for treeing phenomena at 25 kV	103
D.2	Plot of peak voltage pulse detected by APD sensor Vs peak current pulse by HFCT sensor for surface discharge in air for positive cycle	103

D.3	Plot of peak voltage pulse detected by APD sensor Vs apparent charge by HFCT sensor for surface discharge in air for negative cycle	104
D.4	Plot of energy of signal detected by APD sensor Vs energy of signal (-ve) by HFCT sensor for surface discharge in air for negative cycle	104
D.5	Plot of peak voltage pulse detected by APD sensor Vs apparent charge by HFCT sensor for surface discharge in dry oil for negative cycle	104
D.6	Plot of peak voltage pulse detected by APD sensor Vs peak current pulse (-ve) detected by HFCT sensor for surface discharge in oil sample 1 for negative cycle	105
D.7	Plot of peak voltage pulse detected by APD sensor Vs apparent charge by HFCT sensor for surface discharge in oil sample 2 for positive cycle	105
D.8	Plot of peak voltage pulse detected by APD sensor Vs peak current pulse detected by HFCT sensor during treeing phenomena for positive cycle	105
E.1	Idea presented in [25] for positioning the different kind of optical sensors inside termination	107
E.2	Idea for online PD monitoring using APD sensor	108

List of Tables

1.1 Advantages of optical over electrical detector	5
2.1 Comparison of all PD detection methods	16
3.1 Comparison of all the three optical sensors	30
3.2 Specification of APD130A2/M	31
4.1 Summary of methods examined to produce surface discharge setup	41
4.2 Settings used for preparation of different oil samples	52
4.3 Water activity measured for different oil samples	54
5.1 Comparison between electrical and optical measurements from corona source using Techimp device	56
5.2 Comparison between electrical and optical measurements at different distance of corona needle from ground	57
5.3 Comparison between electrical and optical measurements from surface discharge in air using Techimp device	59
5.4 Comparison between electrical and optical measurements obtained from oscilloscope from the setup shown in Figure 5.6	60
5.5 Comparison between electrical and optical measurements in the dry oil	63
5.6 Comparison between electrical and optical measurements in the oil sample 1	65
5.7 Comparison between electrical and optical measurements in the oil sample 2	67
5.8 Comparison between electrical and optical measurements in the oil sample 3	68
5.9 Comparison between electrical and optical measurements from treeing phenomena	70
6.1 PD pulse captured by both the sensor in different oil sample	74
6.2 Comparison of the charge detected by both the sensor (Positive Cycle)	78
6.3 Comparison of the charge detected by both the sensor (Negative Cycle)	78
6.4 Comparison of the PRPD pattern for different discharges captured	81
6.5 Correlation coefficient obtained from all the PD data.	86

Introduction

In this chapter, the overview of the research starting from the background is presented. An introduction to oil-filled terminations and the problems due to the introduction of water are discussed. A summary of previous research work done in the field is also presented in this chapter. Finally, the motivation, goals, research questions, thesis approach and outline of this thesis project are described.

1.1. Oil-filled termination in power system

The electric power system is the network comprising generation, distribution, transmission and utilization of electric power and electrical devices. The generation due to large power plants or renewable energy (such as onshore wind energy and large solar farm) require the transportation of electricity to consumers through long distance. This transportation is facilitated by a number of power components such as transformers, transmission lines, cable and cable accessories namely joints and termination.

A high voltage (HV) cable termination is one of the most important components in the electric power system. According to International Electrotechnical Vocabulary (IEV), the termination is defined as *“Devices fitted at the end of the cable to ensure electrical connection with the other parts of the system and to maintain the insulation up to the point of connection”* [1]. Therefore, terminations are necessary to connect the cable end to an overhead line, to switchgear or transformers. The main purpose of using the termination for this connection is to reduce the field enhancement when the connection to the conductor is made. This function is performed by a stress cone which is placed inside the termination body as seen in Figure 1.1. The stress cone smoothens and reduces the very high concentration of flux and therefore the high potential gradient between the shield termination and cable conductor is thus avoided by stress cone.

There are different types of cable terminations namely: oil-filled cable termination, dry-type cable termination, GIS (Gas Insulated Switchgear) cable termination, outdoor cable termination and indoor cable termination. The research in this thesis project is based on oil-filled terminations (wet type terminations) in which the insulating medium is Polyisobutylene(PIB), type A12 oil which is highly viscous in nature.

1.1.1. Degradation of oil-filled termination due to water ingress

Oil-filled cable termination has been used for decades in the power system networks. During many years of operations, there is a high probability of defects that may occur in the terminations due to several causes like environmental, mechanical, chemical and aging . Since the insulating medium is oil, there can be several possibilities of contamination of oil due to foreign contacts or particles. Oil filled termination may get exposed to moisture due to several reasons like sealing failure of the termination which may be caused due to poor tightening of top bolts [2] or can be caused due to indirect thermal cycling raised because of heating

from sun dragging water (rain) into installation via deteriorated old gaskets and o-rings [3]. Water may also get inside due to bad installation work or due to imperfections caused during manufacturing.

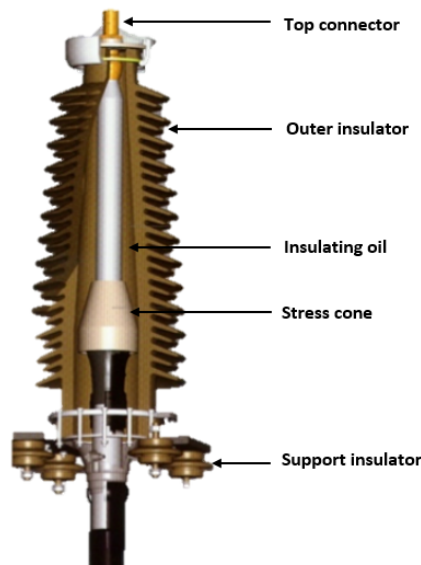


Figure 1.1: HV cable termination [4]

Therefore, water or moisture can be said to be one of the common contaminants of the insulating oil. It does not only degrade the quality of the oil inside the termination but also affects the interface between the rubber and oil during long run under certain conditions. The extremity of water incursion in oil filled termination can be illustrated by the picture shown in Figure 1.2. Due to foreign elements especially water which enters the termination due to above-mentioned reasons leads to surface treeing, localized discharges and eventually complete breakdown of the termination. Presence of moisture does not only lead to electrical failure but it also leads to chemical change in the insulating oil. Eventually, it causes regional overheating leading to accelerated aging of the material and faster malfunction of the termination with respect to its lifetime.

Hence, it is clear that moisture levels above a certain value increases the risk of unscheduled downtime and eventual termination failure. Moreover, the existence of moisture content is not felt immediately, but over times contributes significantly. Therefore, monitoring the oil and stress cone as a whole is a simple way of improving the reliability of the oil-filled termination.

1.2. Previous research work

The investigation of water effect in oil-filled cable termination started in 2016 at the Delft University of Technology in collaboration with Prysmian Group, Delft. Since then, two master thesis research focusing on this problem had been conducted.

The first research thesis named *“Condition assessment of water in high viscosity insulating cable termination oil”* focused mainly on studies based on phenomena surrounding water within the oil and the influence of water particles on the electrical performance of the oil [5]. 2D simulation of stress cone in COMSOL was done in order to know the highest electric field location with different position and size of the droplet in oil filled termination. The behavior of water droplets which can be in form of an emulsion or free water in oil was also studied with the effect of temperature and electric gradients (along with the movement of water in the oil). There were several tests conducted in order to know the influence of water in the

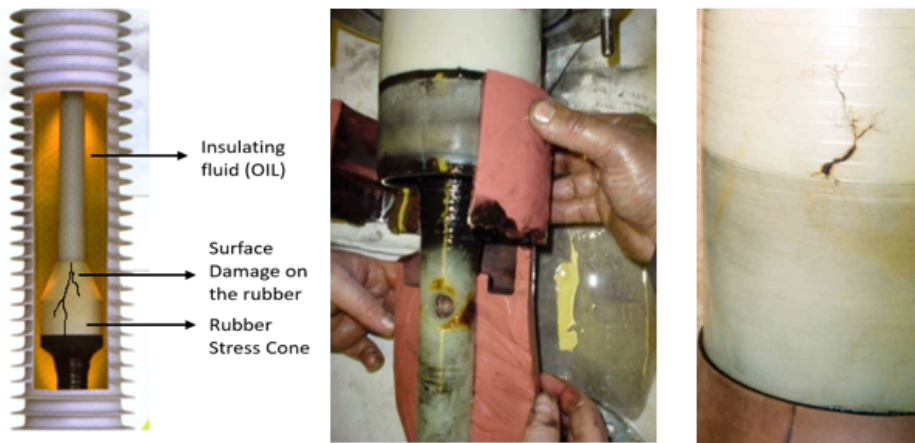


Figure 1.2: Defects/Failure due to water ingression [2]

oil like permittivity check, dielectric tan delta test, AC breakdown test and partial discharge test all with different content of water/moisture level in the oil. The following were the main conclusions from the first thesis research:

- The breakdown strength of the oil decreases exponentially with the introduction of moisture, with a critical point of approximately 80 ppm. The breakdown strength is also influenced by the size of water droplets.
- It was also concluded that there was no significant effect in the dielectric constant of the oil in the presence of moisture. However, some activities regarding dielectric constant and loss were observed at 40°C to 60°C.
- With the change in temperature, the viscosity of oil and conductivity of the liquids involved changes. The viscosity of oil reduces with increase in temperature whereas water conductivity increases with temperature rise.
- It was concluded after the analysis of all the tests performed that combination of heating (allow water to rise from the base of termination) and partial discharge detection can be used to know the influence of different amounts of water in the termination oil.

The second research thesis named *“Investigation on termination oil-rubber interface parallel to the electric field with water contamination”* focused on studying the influence of water on the surface of the stress cone [6]. It aimed at finding ways to detect the presence of water content in the termination oil using electrical methods. 2D and 3D models in COMSOL were developed to investigate the effect on the electric field with the change in size and number of the droplet on the oil-rubber interface. The main tests carried out were partial discharge tests and tan delta tests. Partial discharge experiments were conducted with different samples like water-oil emulsion samples with different ppm levels and also with different sizes and number of water droplets in oil. The following were main conclusions from the second thesis research:

- Water contaminations effect the electric field distribution based on positions of the water droplets, size of the droplets, the relative permittivity of water contamination and the number or coverage area of the water droplets.
- It was concluded in the thesis that PD activities due to water contamination on stress cone surface consist of both internal and surface discharges like pattern. It was mentioned that long-term measurement of 2 hours is required for extracting any information regarding the indication of water content in termination oil.
- No significant results were obtained from $\tan \delta$ measurements even with water-oil emulsion samples with rubber interface.

Apart from research done in above two thesis, there are several research done in the field of water contamination in oil-filled termination focusing on how water affects the electrical behavior of the termination as a whole. It is clear from research done before that PD measurement is one of the most sensitive and informative detection that can be conducted in order to get information regarding degradation caused by the water contamination in oil-filled termination.

1.3. Motivation

For the economic use of the operational high voltage components in the electric power systems, monitoring of these types of equipment is necessary and important. It has been observed that most failures occur in cable accessories, mostly terminations, rather than in cable. Below Figure 1.3 illustrates that in recent years most failures take place in terminations according to survey done by NEETRAC 2015 [7]. Oil filled terminations are expected to have a lifetime of about 40 years. In order to achieve this lifetime for oil-filled high voltage terminations, regular diagnostics and analysis of insulating parts and system have to be conducted. The potential problem of water presence in oil-filled termination has been discovered which has been researched a lot in the past. The final conclusion was to have partial discharge measurements and detection as most effective diagnostic technique. Partial discharge is one of the most sensitive, informative and non-destructive method for testing and monitoring the insulation condition in high voltage equipment. It acts as a preventive tool to safeguard the equipment from major failure and it is one of the most used testing methods for on-site high voltage components.

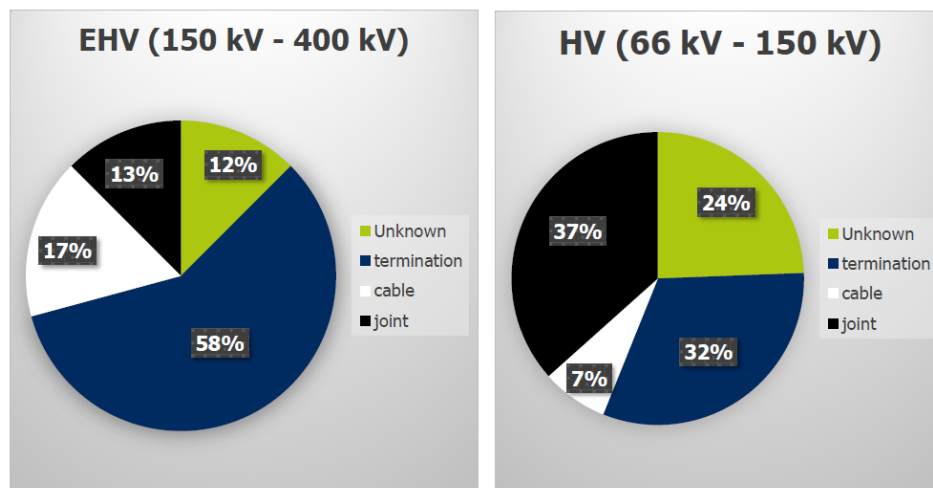


Figure 1.3: Failures rate in cable and cable accessories [7]

Electrical partial detection is the most commonly used diagnostic method till date based on IEC 60270. It is based on a simple circuit which can be attached parallel to test object in order to analyse the PD electrical signal. In fact, the same concept is applied to on-site detection of any high voltage equipment. Generally, high voltage laboratories are completely shielded to avoid any type of interference from noise and high-frequency sources from any surrounding elements. Hence, the PD level of less than 1 pC can also be detected with correct electrical oscilloscope and trigger level in the laboratory environment. However, during on-site testing such type of shielding and Faraday cage are missing. This leads to very high interference which sometimes goes up to noise levels greater than 100 pC [8].

Electromagnetic interference is one of the major drawbacks of electrical PD detection especially during on-site or on-line monitoring of high voltage equipment. The interpretation of the results can be considerably hindered and sometimes even impossible due to the presence of external interference signals. Lots of measures have been taken in order circumvent

these problems during on-line measurements like the suppression of pulse and frequency interferer to distinguish external and device-internal PD sources or the use of the broadband spectrum of partial discharges in the VHF or UHF range [9]. But these methods are generally not suited for field use and have their own drawbacks.

This calls for an innovative and creative solution to these types of problem. As a result, this thesis focus on optical detection of PD. A lot of studies in the past have already shown that the optical sensor used for PD detection displays good immunity against the electromagnetic interference and noise [10]. In addition to that localization with optical PD detection will be much easier as compared to current conventional electrical PD detection. The following Table 1.1 will clearly state the advantage of using optical over the electrical detector.

Table 1.1: Advantages of optical over electrical detector

Conventional Electrical Detection	Non-Conventional Optical Detection
Easily influenced by electromagnetic interference	Immune to electromagnetic interference
Vulnerable to noise	Immune to surrounding noise
Localization of PD possible	Localization of PD possible
Large size comparatively	Small size, light weight
Additional elements required to receive ideal PD pulse	No additional elements required

The motivation for the present work is to contribute towards additional technique for condition assessment of oil-filled cable termination by means of optical investigations in the field of PD detection. It is believed that this research will not only help towards progress in the field of online use of optical PD detection in these types of terminations but also characterize and compare these types of sensor to conventional electrical PD detector. It will set a foundation and promote the more practical application of the optical PD detection approach in actual power equipment. Moreover, the optical sensor used in this research work has been introduced for the first time for these kinds of applications.

1.4. Goals and research objectives

This section of the chapter will state the overall goal of the research done in this thesis and also lay down important objectives or questions which need to be fulfilled or answered during the research.

1.4.1. Goal

The optical PD detection in oil-filled termination is quite a new topic which has not been significantly researched in the past. Therefore, the feasibility study on this technology will be the main focus.

The scope of this thesis is to study and propose feasibility of a partial discharge optical monitoring device that can be used to detect the discharges inside the HV cable terminations. The aim is to be able to detect surface discharges in the termination due to the presence of water in the oil by optical means.

1.4.2. Research objectives/questions

Following are the important topics which need to be researched on during this thesis:

1. Design for creating surface discharge

In order to replicate the real situation the design of a setup in order to produce surface discharge on stress cone material in oil insulation (oil-rubber interface) is required.

2. Parameters influencing the choice of optical sensor

The important factors/attributes based on which the optical sensor (for PD detection at

oil-rubber interface) should be selected need to be deduced.

3. Selection of optical sensor

There are different types of optical sensor available in the market. But according to above-mentioned factors and suitability, the optimal choice of the sensor should be done for this kind of application.

4. Testing of surface discharge in the oil by means of both electrical and optical sensor

The measurements of PD produced on the surface of rubber with different oil samples (dry oil and oil with the different amount of water content) should be conducted by both electrical and optical means. This will help to make the comparison of the results obtained from the selected optical sensor with that of the electrical sensor used.

5. Determination of optical sensor characteristics and possible relation with electrical detector

The results obtained during testing process need to be examined and compared in order to have in-depth knowledge about the characteristics of the optical sensor with respect to the electrical sensor.

6. Possibility of usage of the optical sensor in real on-field detection

If the feasibility study of the technology of optical sensor in the detection of surface PD in oil filled termination is achieved, the next step will be its implementation. Therefore, future recommendation and further steps should be formulated in order to achieve the ultimate goal of using the optical sensor for on-line detection of PD in oil filled termination.

1.5. Thesis research methodology

This section will give the overview of the approach that has been adopted in order to fulfil the above-mentioned goals and research objectives.

Below is the overall overview in the Figure 1.4 of the thesis methodology divided into steps and respective tasks which is explained below.

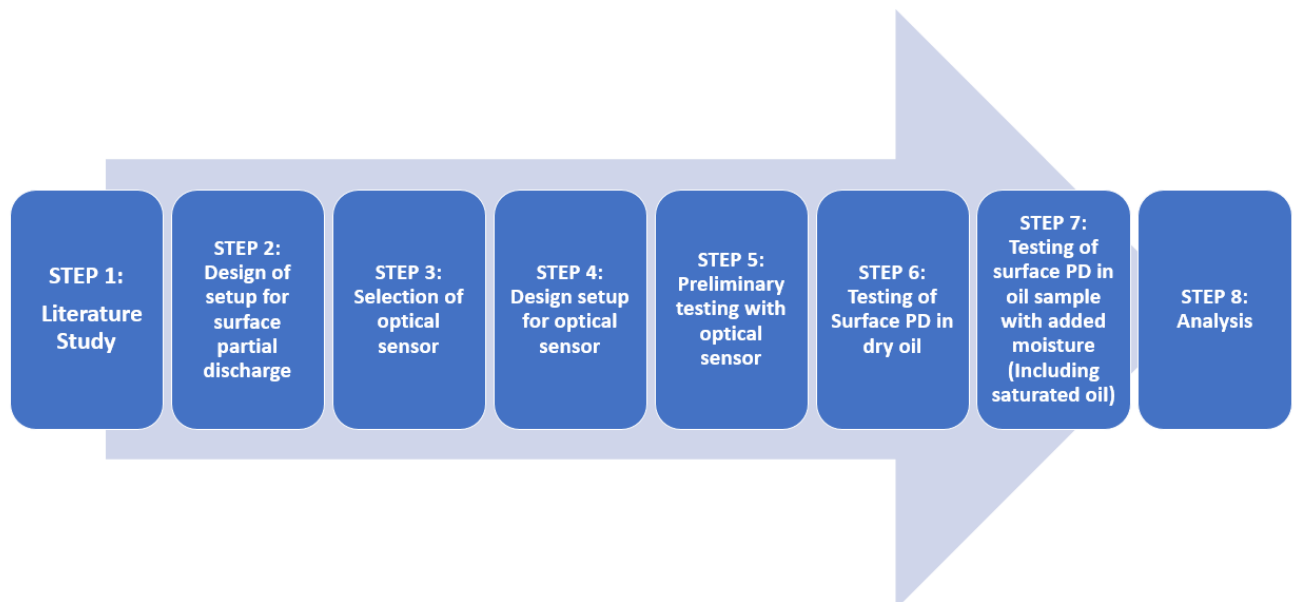


Figure 1.4: Work division

Step 1 starts with the literature study focusing on types of partial discharge and theory behind the optical partial discharge and research on the work done so far in this field of PD

detection. Next step starts with the testing of surface discharge on the stress cone material in oil insulation. Replicating the real scenario is very difficult but effort has been made to actually produce surface discharge with similar materials which are used in real terminations. It has to be made sure that the setup and sample preparation for surface discharge is reproducible since testing has to be conducted many times. In this step, the testing is conducted with the conventional electrical detector and HFCT sensor. Once the setup for surface discharge is finalized, selection of optical sensor based on spectrophotometer analysis and past research (on the sensor for PD detection application) is done.

After procurement of the selected optical sensor, the layout of the sensor is designed according to positionality and directionality calculation. The optical sensor selected is introduced for the first time in this thesis for this kind of application. Therefore, for knowing the behaviour of the sensor some initial testing with corona source and surface PD in the air is done and compared with the conventional electrical sensor. Step 6 will be simultaneous testing of the finalized setup obtained in step 2 by both optical and electrical detector. Once the testing with the dry sample with no water content is finished, different oil samples with water content are prepared and the same test setup as finalized in step 2 is used with different oil sample prepared (with water content) for both optical and electrical PD testing. The last step will be analyses of measurements collected in step 5,6 and 7 and these will, therefore, be used for characterizing the optical sensor used in this thesis. The last task should be having a line of thought towards the possibility of using this technology for on-line monitoring of termination.

1.6. Thesis outline

This section provides a brief introduction to the content of each chapter and guides the reader through the rest of this document.

Chapter 2 **Literature Study** highlights science behind the PD detection and different ways that is available till date. It discusses light detection of PD and also describes different ways of optical detection that has been done with air insulation, transformer oil insulation as well as with GIS. The last section also describes the possibility of on-line detection using the optical sensor and showcase some thought process behind it.

Chapter 3 **Experimental sensor description** starts with the introduction of instruments and sensor used for electrical detection while testing in this research. Then, it is followed by the selection of the optical sensor based on transmittance index measurement of termination oil and research on sensor suitable for the PD detection application. It explains the specifications and working principle of the selected APD (Avalanche Photo diode) optical sensor and how the layout is built based on positionality and directionality calculations. The finalized circuit with simultaneous optical and electrical detector is explained.

Chapter 4 **Design of test setup and sample preparation** explains the different approach used to produce surface discharges. The procedure to attainment of surface discharge is explained clearly in subsections namely: different orientation of electrodes and samples, design of electrodes and introduction of foreign particles on the surface of the rubber. It will conclude by summarizing the design which had positive outcome. The last section of this chapter is also dedicated to oil preparation with different water content and measuring the water activity (level of saturation) in the oil sample using Vaisala instrument.

Chapter 5 **Measurements and results from optical and electrical detection** presents findings and data of the simultaneous electrical and optical PD testing conducted in three parts namely: preliminary testing with optical sensor with corona source and surface discharge in air with rubber sample, surface discharge in dry oil and finally surface discharge with different moisture content in oil samples prepared as explained in previous chapter. The surface discharge in dry oil and partially saturated oil is done using finalized setup explained in chapter 4 and using the circuit diagram and instruments explained in chapter 3. At the

end, the treeing phenomena captured by the optical sensor is also discussed.

Chapter 6 **Analysis of the results** presents the comparison, interpretation and explanation of the findings obtained in chapter 5 on different parameters. The parameters to analyse electrical and optical detector are the PD pulse output, their sensitivity and stochastic pattern obtained through both electrical and optical detection. This chapter also discuss possible relation between output of optical and electrical sensor with different PD sources.

Chapter 7 **Conclusion and recommendation** highlights the outcome and conclusion drawn from the measurement and analysis of optical sensor with respect to the conventional electrical sensor. It also discusses the practical and effective use of the optical sensor in real on-line PD detection and how it can exploit the field of PD detection in transparent and translucent stress cone in the future. The chapter concludes by mentioning some recommendation for future work.

2

Literature study

This chapter takes a deep dive into the background theory behind the partial discharge and its detection. It evaluates the different methods available till date for PD detection focusing on state of art method developed for electrical PD detection and the theory behind method being assessed in this thesis which is based on light detection of partial discharge. The chapter is followed by the explanation of different procedure and arrangements that have been adopted in the past for the use of the optical sensor for PD detection. In the end, the possibility of using this technology in real time applications is discussed.

2.1. Partial discharge detection

2.1.1. Basics of partial discharge

Partial discharge is defined as “*localized discharge process (dielectric breakdown) where the distance between the two electrodes (high voltage and ground) is only partially bridged*” [11]. It implies that the insulation between the electrodes is partially punctured. The process can take place in gaseous, liquid and solid medium or insulation. There can be several reasons for the occurrence of partial discharge namely: void, contaminant, cracks, protrusions, electric treeing and many more. It can start with the very small hole and can build the bridge between high voltage and ground within time leading to complete failure of the equipment.

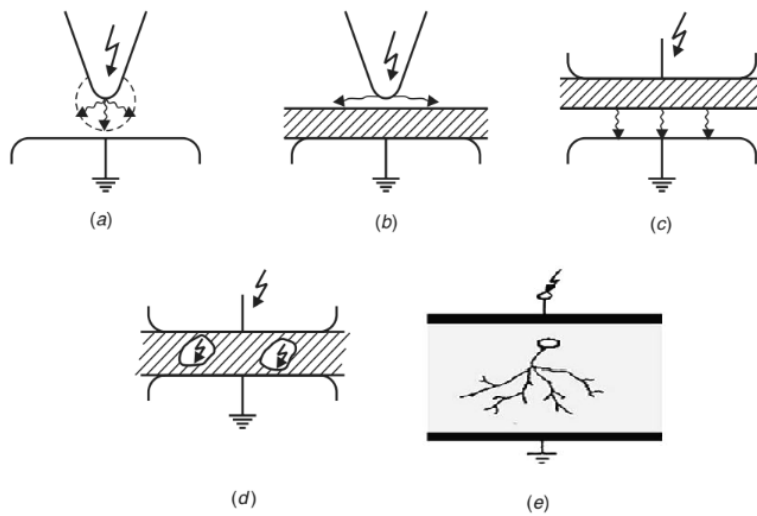


Figure 2.1: Various types of partial discharges (a) Corona discharge (b) Surface partial discharge (c) Surface partial discharge at interface (d) Internal discharge (e) treeing phenomena during internal discharge [11]

The partial discharge can be distinguished into three parts:

- **Corona or Gas Discharge:** These kinds of discharges occur due to the presence of sharp edges at the conductor which leads to the non-uniform electric field as seen in the Figure 2.1a. Generally, it occurs in gas however discharge due to the sharp point can also happen in the solid or liquid medium. When the sharp edge is present at the conductor which is connected to high voltage side, it is called as negative corona whereas sharp edge at the ground side of conductor results in the positive corona. It is not seen as great damage to the high voltage equipment but certainly can act as a source of interference when making PD measurements. Therefore, most of the high voltage equipment have rounded structure at the top or is even equipped with corona shield.
- **Surface Discharge:** As the name suggests, the discharge occurs at the surface of the insulation or at the interface of different dielectric materials like gas-solid, liquid-solid, solid-solid or gas-liquid when a substantial tangential field strength is present [12]. It can also takes place due to defects or protrusions at the surface of the insulation. The examples are illustrated in Figure 2.1b and c. Even though it is on the surface of the material, it becomes harmful if it happens inside the high voltage equipment. It will eventually degrade the material which can lead to ultimate failure. The testing conducted to record surface discharge in oil is presented in this thesis.
- **Internal or Cavities Discharges:** These are the types of discharges which occur inside the solid or liquid insulating medium due to the presence of cavities which are usually gas filled. The voids or cavities get overstressed and discharge as shown in Figure 2.1 d occur. This is followed by the high-intensity fields paving the path from small sharp edges of the voids thus deteriorating the whole insulating material. The continuous discharges so produced is called as treeing channels illustrated in Figure 2.1 e. This type of the discharges are the most dangerous one for insulation of high voltage equipment leading to damage and failure.

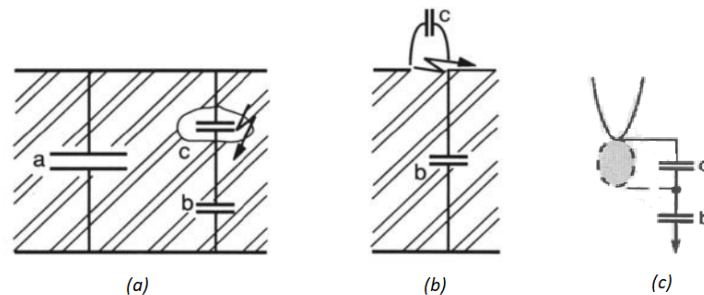


Figure 2.2: Equivalent circuit of (a) internal discharge (b) surface discharge (c) Corona discharge [12]

It is very important to understand the well known abc equivalent circuit (shown in Figure 2.2) before discussing about the different PD measurements technique. The voltage and current behaviour during internal, surface and corona discharge can be understood by the equivalent circuit represented in Figure 2.2 a, b and c respectively. The void or the defect in the insulation is represented by the capacitance c , the part of insulation in series with the void is represented by the capacitance b and a represents the void-free healthy part of the insulation parallel to the defect.

When the insulation has a void as shown above by capacitance c and if an A.C. voltage is applied to this insulations then a recurrent discharge phenomenon will occur as shown in Figure 2.3 b and c for internal or surface and corona respectively. If the A.C. voltage over the sample applied is greater than the breakdown voltage U_d , a discharge will occur. If the voltage rise is continuous and breakdown voltage is surpassed every time, discharge occurs again and therefore the recurring pattern occurs. For corona, as shown in Figure 2.3 c when

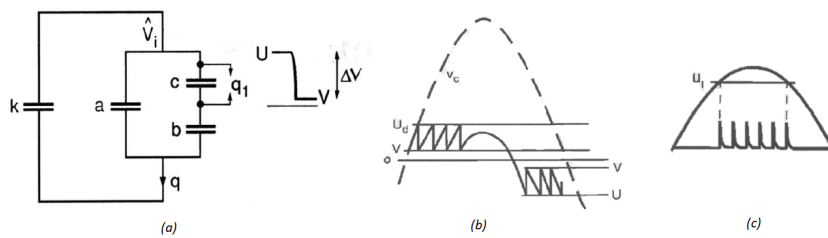


Figure 2.3: (a) Model representation of partial discharge (b) and (c) recurrent discharge phenomena [12]

the voltage is raised, the number of discharges increases rapidly but the magnitude remains about the same. As a result, corona pattern can be easily distinguished from other partial discharges. It should be kept in mind that actual cases are less stable than abc model. The value of U_d is not same for both positive and negative halves of the period and also there can be several discharge channels. Consequently, the discharges will also appear along the sine-wave with unequal size and behaviour.

The main parameter while measuring PD activities is the charge which defines the magnitude of the discharge also called as charge displacement q usually expressed in picocoulombs (pC). While measuring, the direct charge value from cavity, surface or corona discharge can not be calculated but the apparent charge deduced is a good representation of the intensity of the discharge which gives good knowledge of energy dissipation and the dimension of the discharge site.

2.1.2. Types of partial discharge detection

The PD activities as explained above can be detected in different ways. Partial discharges are regularly coupled not only by rapid current flow but also by electromagnetic (EM) radiations, mechanical vibrations, chemical change in the insulation material and light emission by the PD source. As a result, PD detection is not merely done by electrical signals but can be done using acoustic, chemical and optical signals. Below, Figure 2.4 gives an overview of the existing PD detection methods.

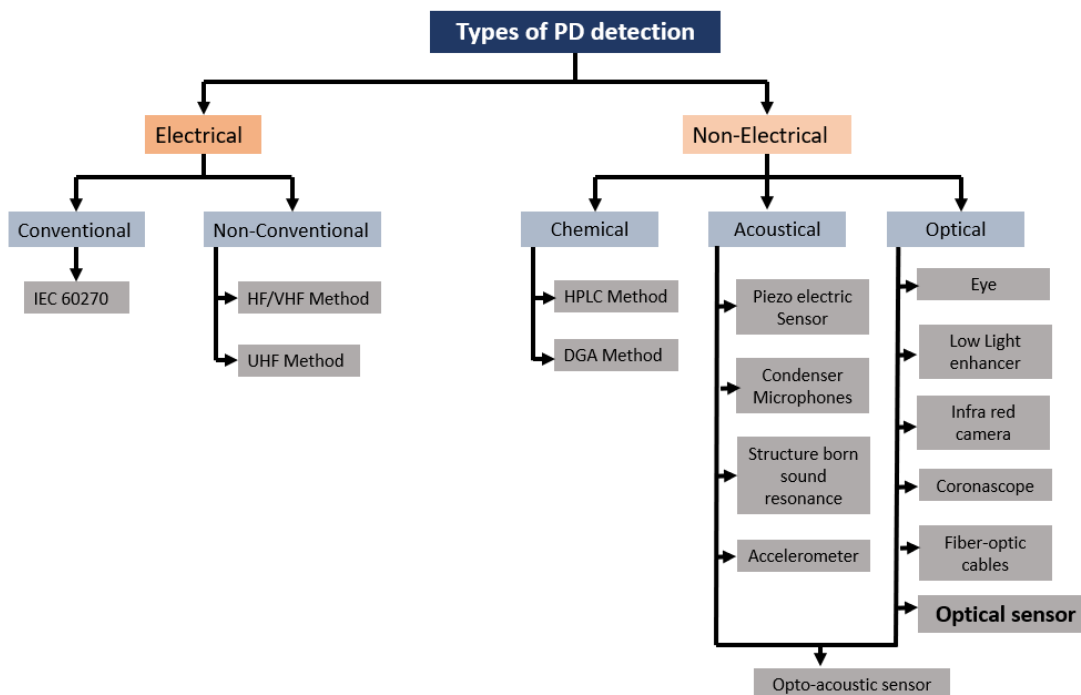


Figure 2.4: Overview of PD Detection Methods

Before reviewing several methods, there are some important standard parameters that should be kept in mind while conducting PD measurements as mentioned below [13]:

- Partial discharge pulse: The current or voltage pulse result from PD due to object under test. (Generally the test object produce current pulse, but according to IEC standards, the detector can give voltage or current output)
- Apparent charge: It is normally calculated as the area under the current pulse obtained during measurements. It is very good indication for categorization of PD source.
- Pulse repetition rate: It is defined as the ratio of the total number of PD pulses recorded in a selected time interval and the duration of this time interval.
- PRPD pattern: Phase resolved PD pattern is widely used to interpret the PD data. It display the number of pulse generated according to the phase of the sine wave. It is very useful for identifying the type of PD since each PD type has distant PRPD pattern.

2.1.3. Electrical partial discharge detection

Electrical PD measurement can be done in two methods: one method is state of art conventional method based on IEC 60270 and other one is non-conventional high frequency method. The detection based on IEC 60270 and some high-frequency equipment used for non-conventional electrical PD detection is explained in the following sections.

Conventional Electrical Detection

This section is based on the IEC 60270 standard of electrical PD detection. Figure 2.5 gives the respective circuit diagram. It consist of the test object C_a , coupling capacitor C_k , measuring system with input impedance Z_{mi} , coupling device (CD), connecting cable (CC), a high voltage supply and impedance Z in between supply and test object. The main criteria which should be fulfilled in-order to use this circuit are:

- The coupling capacitor should exhibit a sufficiently low level of partial discharges and should have capacitance greater or equal to the capacitance of test object in order to receive full signal of PD.
- The high voltage supply should be PD free.
- Impedance or filter should be present to reduce any type of noise or interference from supply side.
- The end of the cable should be properly terminated otherwise loss of signal can take place.
- The circuit should be calibrated before the measurement with step generator ΔV in series with small capacitor or calibrator. A discharge of known quantity is injected into the test object C_a and measured using the connected system in order to calibrate the measuring system. This step is very important to make sure the instrument is measuring the charge during experiment accurately.

The CD and CC represents coupling device, transmission system which can be connecting cable or optical link and measuring instrument (oscilloscope). CD is designed to optimize the sensitivity of the signal received from the PD source. It is generally a quadrupole which is active or passive four terminal network. Signals coming from this device are thus transferred by the connecting cable to the oscilloscope. CD also consist of either wide-band PD or narrow band measuring system having a fixed lower limit frequency, upper limit frequency and bandwidth. The wide band PD measurement system recommended values are $100kHz \leq \Delta \leq 400kHz$, whereas narrow band PD measurement has bandwidth of $9kHz \leq \Delta \leq 30kHz$. It is of very high importance that the PD signal is isolated from the 50Hz signal. The inductance in the Z_{mi} short circuit low frequency current that occur when 50 Hz voltage is applied whereas RC combination measure the high frequency component from PD

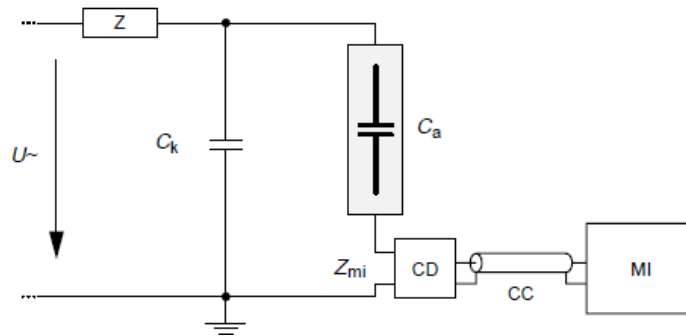


Figure 2.5: Standard PD circuit diagram [14]

pulses. After recording the accurate PD pulse using the correct instruments as mentioned above, its time for PD pattern recognition and analysis which can be done using time domain or frequency domain based methods [13].

Non-Conventional Electrical Detection

Non- conventional electrical PD detection generally can be categorized into three parts based on its working frequency range:

- HF (High Frequency) method – 3 MHz to 30 MHz
- VHF (Very High Frequency) method – 30 MHz to 300 MHz
- UHF (Ultra High Frequency) method – 300 MHz to 3 GHz

It is known fact that PD pulses consist of energy frequencies up to hundreds of MHz. Therefore, HF/VHF/UHF PD detection system is applied to detect partial discharges in a non-conventional electrical way. Classical detection loses some data and is difficult to minimize most noise related to the lower frequency band. With the increase in sampling rate and signal processing speed, PD detection with wider frequency band is needed. It provides result with suppressed noise or high signal-to-noise ratio. Thus, the use of these non-conventional techniques is growing fast especially for field measurements. There are lot of uses of UHF sensor in power cables and accessories, in GIS and in transformers.

The whole concept is based on the detection of the high-frequency signal generated from PD activities. The main instruments needed are PD sensors, triggering parts, spectrum analyzer and a computer equipped with PD software analysis. The circuit is similar to IEC 60270 method where the test object is in parallel to coupling capacitors. However, instead of quadrupole or CD, these high-frequency capacitive or inductive sensor are placed. These PD sensors work based on detection of high-frequency current pulses that occur during PD in the circuit. The PD pulses occur in very short time, the width and rise time of the pulses are in the nanoseconds region. As a result, generation of PD pulses with the energy in the range of frequency up to hundred MHz occur. The PD signal from the sensor then transferred through coaxial cable and amplifier to the spectrum analyzer. The computer with installed with PD software is connected to the spectrum analyzer and then the amplitude and number of PD pulses as a function of phase (phase-resolved pattern) can be performed and this pattern will be useful to recognize the type of defect in the test object.

In this thesis, electrical measurements have to be performed to compare it with the optical measurements. The conventional quadrupole instrument and non-conventional HFCT (High Frequency Current Transformer) is used for conducting the electrical measurements. At end, during simultaneously testing with optical sensor, HFCT is used.

2.1.4. Acoustic partial discharge detection

Acoustic partial discharge detection is one of the non-conventional and non-electrical techniques based on the fact that electrical discharges initiate wave pressures in the insulation [15]. The main fields of application are gas insulated switchgear and substations, transformers, cable accessories, current transformers, etc. It works generally in the frequency range of 10 Hz up to 500 kHz. It is based on the principle that sound propagates through a medium by means of wave motion, i.e., the propagation of a local disturbance through the medium takes place [16]. Therefore, due to PD activities when mechanical changes happen inside the insulation medium it leads to wave motion and the pressure wave is created, which can be detected by a suitable sensor, the output of which can be recorded and analyzed using conventional data acquisition system. As mentioned in Figure 2.4, there are several ways of doing acoustic PD measurements like using piezo electric sensor, condenser microphones, structure born resonance, accelerometer and opto-acoustic sensor.

The most commonly used acoustic sensor is piezoelectric transducers (PZT) [17]. It is used in GIS, transformers and HV cable. These sensors are for detection and monitoring of PD and are mounted outside of high-voltage equipment. Here, it uses electromagnetic interference for its measurements which requires the installation of PD coupler. The mechanical explosion which may happen due to PD activities inside equipment leads to the rise of an acoustic wave. Localization of PD is generally measured by estimating time of arrival of acoustic signal. The sensitivity of the acoustic methods does not vary with test object capacitance, so that acoustic PD detection is widely applied to large capacitors. This technique is most interesting one for on-site measurements as it has some inherent features and good immunity to noise and interference if conducted in the shielded system. But the main drawback is the complexity of pressure wave propagation in an insulating medium where the path and attenuation of signals are almost unpredictable.

2.1.5. Chemical partial discharge detection

The PD activities can also be detected chemically by observing the chemical changes in the composition of the insulating material. It is most commonly used in GIS and transformers. It is based on the principle that whenever PD activities occur, arc is formed leading to high temperature, at which the insulating medium like SF_6 or oil starts to decompose into various compounds which may be harmful to the equipment. There are two major ways to perform chemical PD analysis namely high performance liquid chromatography (HPLC) and dissolve gas analysis (DGA) depending on the type of medium. Sometime, fuel-cell type detector and hydrogen-oil detector is also used commercially.

During DGA test, sample from the equipment is collected like oil from transformers or insulating material from GIS. It is then sampled and analyzed in order to assess the level of gases such as methane, carbon dioxide, ethylene, hydrogen and acetylene [16]. These quantities of different gases measured should not exceed the levels specified for the condition when the oil insulation or insulation material breaks down. The downside of this method is that the level of dissolved gases and type of fault cannot be scientifically or experimentally correlated and calibrated.

The HPLC technique measures the by-product of the insulation breakdown of the transformer or GIS. Mostly the insulation breakdown of the transformer contains glucose [17]. Here also there is no known correlation between the amount of glucose discharged during the insulation breakdown to the type and the level of severity of the fault caused to the equipment under test. Besides, the collection of the adequate quantity of by-products of insulation breakdown and analysis takes too long for real-time monitoring.

One more technique commonly used in transformers is the hydrogen-oil detector [17]. This detector containing semi-permeable membrane is generally placed inside the oil filled transformer and then connected to portable gas chromatography. This will allow the measurement of the concentration of hydrogen gas at a regular interval of few hours.

It is true that chemical detection for oil filled type equipment is possible but the main disadvantage is it requires proper laboratory conditions to collect the sample and measure it accurately, hence not applicable for on-site detection. Also, as mentioned earlier no informa-

tion of type and severity of PD can be obtained by conducting chemical analysis. Moreover, these methods are also unable to locate the position of the PD signal source. Consequently, it cannot be used for online monitoring of high voltage equipment.

2.1.6. Optical partial discharge detection

Optical partial discharge detection is based on the potentiality of detecting light emission which is produced due to partial discharge activities. PD is always accompanied by light radiation during the entire process from primary ionization to its extinction. Therefore, the light been emitted during the entire process can be considered as the most intrinsic nature of the PD as a result of which optical detection can be considered most intuitive method to study basic properties of discharges namely discharge morphology, discharge energy, PD pulse and excitation spectra [10]. In connection with the electrical discharge, a radiation in the ultraviolet, visible and infrared area can be recognized [18]. The emission spectrum of the radiated light depends on the surrounding medium which can be air, SF_6 or oil and must be considered for the selection of optical detection system.

For a very long time, optical precise PD detections are only performed in laboratories based on setup and methods which will be discussed in next section of this chapter. However, due to big setup, great volume and high level of power supply requirements of the optical devices that can satisfy the requirements of photosensitivity, optical PD detection is limited to laboratories study. But nowadays with the improved manufacturing techniques used for producing optical sensors, there are sensors available with smaller size, higher sensitivity and greatly immune to electromagnetic and noise interference. However, a lot of research still needs to be performed based on the type of sensor which can be suitable for a particular type of high voltage equipment in order to have accurate optical PD detection.

There are different types of possibility for measuring light during PD activities as mentioned in Figure 2.4 such as eye, infrared camera, low light enhancer, coronascope, fibre optic cables, optic-acoustic method and most importantly using optical sensor. Coronascope is used mostly and can easily detect corona for outdoor insulation. Solar blind ultraviolet(UV) light measurements are already developed based on the physical fact that all solar UV is in the range of 240-280 nm. Sometimes in dark, an eye can easily detect some light at high voltage equipments. Infrared cameras are also installed in high voltage equipments to detect any activities related to PD. The optic-acoustic method is one of the oldest and mostly the first method combining both optics and acoustics physics to detect PD. Recently, most researches have been performed in the recent past using the low light detecting optical sensor like photomultiplier (PMT) and Silicone based photomultiplier (SiPM) with the different setup as explained in below section.

Table 2.1 exhibits a brief overview of all the PD detection methods discussed so far. There are several disadvantages of different PD detection methods based on electrical, acoustical signals and chemical changes as explained in the earlier section. However, considering the electromagnetic interference and noise immunity which is very important parameter when conducting online PD detection, optical detection method was chosen to be investigated as an option in this thesis, as it has the highest immunity compared to all other methods [10]. Therefore, this thesis is based on performing optical PD detection based on a relevant optical sensor in order to have proper feasibility study for its use in real time online detection of PD in oil-filled cable terminations. It is not claimed that optical PD detection will come out as the ultimate method of PD detection and so its advantages and limitation and scope for optimization will also be discussed in this thesis.

2.2. Research in optical partial discharge detection till date

This section is dedicated to past researches which have used optical PD detection techniques with different setup and medium or insulations. The study of each techniques aiming to be used at different high voltage equipments is also mentioned. This section is important in order to have an idea of what type and layout of the optical sensor should be chosen and designed for this thesis research.

Table 2.1: Comparison of all PD detection methods

Parameters	Electrical	Acoustical	Chemical	Optical
Advantages	<ul style="list-style-type: none"> Intensity, source, type, location of PD is assessable High precision measurements 	<ul style="list-style-type: none"> Localization of PD Immune to noise Relatively low cost 	<ul style="list-style-type: none"> High sensitivity and immune to noise Provide critical information and easy to measure in laboratory 	<ul style="list-style-type: none"> Highly immune against noise and electromagnetic interference Highly sensitive and localization of PD easily achievable
Disadvantages	<ul style="list-style-type: none"> High electromagnetic interference Relative expensive and sometimes difficult to apply on-site 	<ul style="list-style-type: none"> Low sensitivity Not good for continuous PD measurement 	<ul style="list-style-type: none"> No information about source, intensity and type of PD Not applicable for on-site detection of PD 	<ul style="list-style-type: none"> Night vision required for most of the optical sensor
Application	All HV equipment	<ul style="list-style-type: none"> Transformer GIS Cable accessories 	<ul style="list-style-type: none"> Transformer GIS Cable accessories 	<ul style="list-style-type: none"> Transformer GIS Cable accessories

2.2.1. Optical interferometric detection

This technique is based on the combination of both acoustic and optics and are also most commonly known as Mach-Zender interferometers. This is the most earlier methods of acoustic detection based on fibre optics essential interferometers such as fibre Michelson and Mach-Zender interferometers [16]. During the partial discharge in gas or oil, an acoustic wave in the sonic and ultrasonic range is produced. In the presence of optic fibre, this pressure wave will result in the deformation of this fibre cable. Consequently, the mechanical stress, stretch of the cable and the optical transmission characteristics of the fibre will get changed. [19]. Below Figure 2.6 display the experimental setup of the optical interferometric detection of PD.

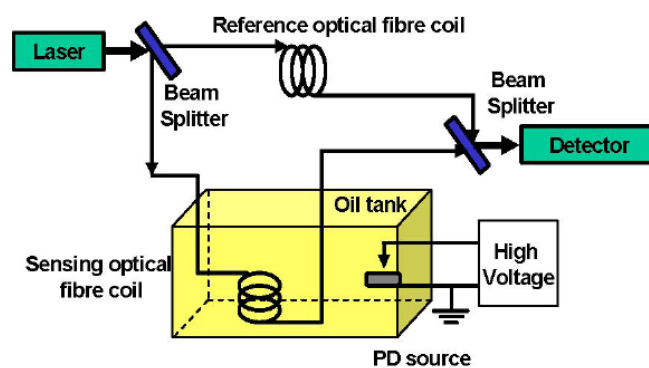


Figure 2.6: Simple experimental setup of the optical interferometric detection of PD [18]

The essential fibre uses a single fibre mode and laser. From a source, the light is been divided into two fibres with equal intensity of 3 dB via a beam splitter and fibre coupler. The first fibre is referred to as reference fibre and the second one as sensing optical fibre coil. In order to generate interference signals, the lights in the two coils are recombined at

the end by transmission using Mach-Zender interferometer or by reflection using Michelson interferometer [17]. The reference optical fibre coil has the original light source while the sensing optical fibre coil is kept in the vicinity of PD source and is allowed to be interfered by the acoustic wave induced by the PD. The essential fibre interferometer has high sensitivity when a long fibre is used during sensing. It can be observed that when acoustic wave infringes on the sensing fibre optic sensor coil, the phase of this optical signal changes compared to the reference sensor coil. The detector at the end will convert light source from the sensor coil to electrical signal (using optoelectronic transducer) and then can be amplified before being observed and analysed using the digital oscilloscope.

This method can be used for the transformer in the laboratory environment. Due to the complexity of the test setup and requirements of laser and proper acoustics source make it difficult for use in the real scenario.

2.2.2. Fabry-Perot interferometer sensor

This method is exactly based on the optical interferometric technique as discussed above. This is one of the oldest ways of detecting light using PD source using both optics and acoustics principle. The Fabry-Perot interferometric sensor has been used for many applications including detection of the wave being produced due to PD source. The sensing element used here is quite small in size known as Fabry-Perot cavity which is composed of two reflecting surfaces [17]. The basic principle behind the sensor is illustrated in the Figure 2.7 below.

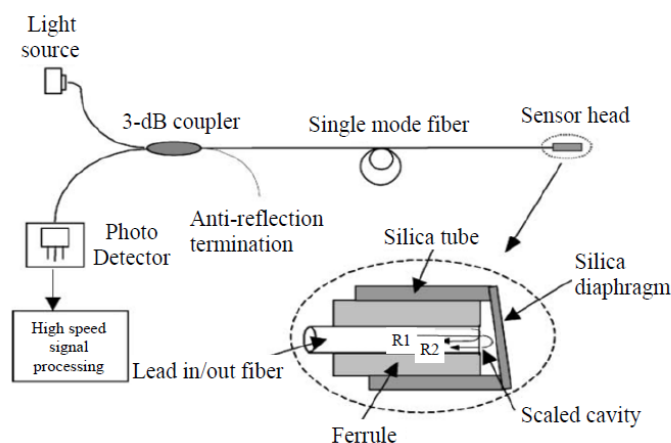


Figure 2.7: Illustration of principle behind Fabry-Perot Interferometric sensor[17]

The output of the LED light source is coupled into 2×2 coupler. The output of this coupler is feed into a single-mode fibre which is connected to sensor head whereas other arm leads to photo detector. As seen from Figure 2.7, the Fabry-Perot interferometer sensor is formed using a silica diaphragm and signal mode fibre at the sensor lead. The cleaved end of the fibre results in the first reflection and then the remaining light is transmitted from the end of the fibre and reflected off the silica disk as seen in the zoomed figure of the sensor in Figure 2.7. The ray that strikes at the centre of the diaphragm is coupled back into the fibre and interacts with the first reflection producing an interference pattern. This optical signal travels back down the fibre to a photo detector where the intensity is measured [20]. This optical signal travels to the photo detector where the optical signal is converted to the electrical signal. The electrical signal is thus sent to an amplifier and then to oscilloscope or a high-speed signal processor.

This sensor can be used for PD detection in the transformer as well as in GIS. From several tests in the past, it has been proven that this type of sensor is an excellent candidate to detect the acoustic signal induced by the PD in transformers or in GIS. However, use of many components apart from the sensor itself as explained above leads to complicated setup for use in the oil-filled termination.

2.2.3. Combination of lens, fibre cable and optical sensor

Another way of capturing the light which is been emitted due to PD source is by using the combination of lens, fibre optics cable and the optical sensor as is been researched in [21] and [22]. The whole system works on the principle as shown in Figure 2.8. This technique can be experimentally used as demonstrated in Figure 2.9.

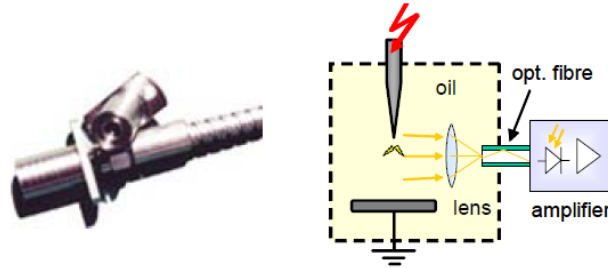


Figure 2.8: Systematic representation of arrangement with lens, optic fibre and optical sensor [21]

The normal optics lens of certain focal length is used for focusing on the PD source. The lens is coupled with fibre-optic cable which acts as a receiver unit which collects the emitted optical radiation of the partial discharge and then guides the signal to the optical sensor or receiver [21]. As observed in the experimental setup, direction and position of the optical sensor are very important as it should be focusing on the PD source in order to capture the light emitted by the PD activities. Therefore, the lens can be placed at different locations of the equipment and then the fibre optic cable from the different lens will be used to coupled to common a optical sensor placed at the end. This optical sensor will convert optical signal to electrical signal (current or voltage pulse depending on the configuration of the particular sensor used) and thus can be used to display on the oscilloscope or doing different analysis based on time or frequency domain in order to compare it with electrical measurements. The main parameters to consider while developing this type of step up are: focal length of the lens used, optical characteristics of the fibre cable and optical detector material (e.g: relative spectral sensitivity as a function of wavelength). This technique can be used in GIS as well as in transformers.

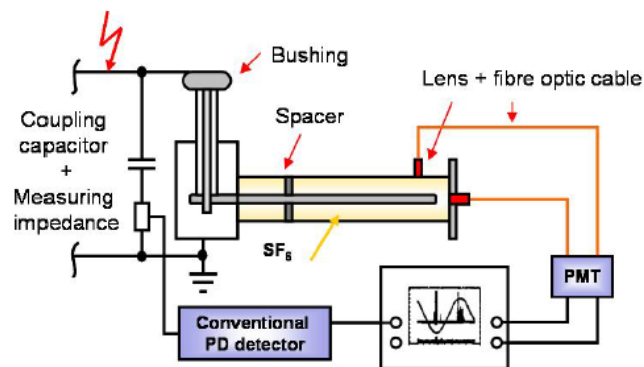


Figure 2.9: Experimental setup for optical PD detection using combination of lens, fibre cable and optical sensor [22]

2.2.4. Combination of fluorescent fibre cable and optical sensor

The use of the optical sensor in the combination with special fluorescent fibre and optical fibre cable is also researched in the past in [21],[22] and [23]. Figure 2.10 illustrates the systematic diagram of this type of approach. It works on exactly same principle as explained in the last section. The fluorescent fibre optic cable is placed just in the middle where the PD will occur

to collect the light emission. By this fibre, the light is linking over the surface of the fibre into the core. So the light is coupled into the cable and at the end, the optical signal line is transmitted to the optical sensor and further to the oscilloscope. By the use of a fluorescent fibre optic, a direction-independent light linking is possible.

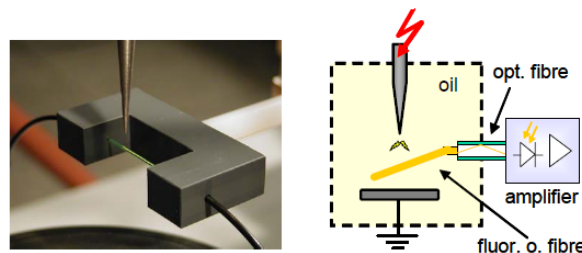


Figure 2.10: Systematic representation of arrangement with fluorescent fibre, optic fibre and optical sensor [21]

The experimental setup using this approach is illustrated in Figure 2.11. The discharge model uses the needle-plate gap to simulate PD signal generated by the typical out thrust insulation defect in the transformer [23]. The photomultiplier (PMT) is one type of optical sensor that is used in this experiment. The selection of fluorescent cable probe is very significant in this approach. The fluorescence fibre probe should have good insulation, corrosion resistivity and flexibility. The material of the fluorescent optical fibre probe substrate can be quartz fibre and plastic fibre. However, plastic is generally chosen because of its several advantages. The spectrum of the PD should lie within the excitation spectrum of the fluorescent substance used in the probe in order to ensure that most of the PD optical signal is received by the fluorescent optical fibre. Fluorescence emission spectra generally have the following characteristics [23]: firstly, the fluorescence emission spectra had nothing to do with the shape of the excitation wavelength and secondly, there is a relation of “mirror symmetry” between the fluorescent emission spectrum with its absorption spectrum. Due to the impact of Stokes Shift, the emission spectrum is always located on the long wavelength side of the excitation spectrum.

Another important parameter is the fluorescence quantum yield (Y_F) of the probe. Y_F is generally defined as the ratio between the number of fluorescence photons emitted and the number of the excitation photons absorbed after the fluorescent substance absorbs light [23]. Y_F is generally less than 1 and is determined by the chemical structure of the fluorescent substance. The value of Y_F closer to 1 display that the efficiency of the probe is higher. Therefore, the capacity of fluorescence fibre sensing optical signal can be improved by selecting appropriate fluorescent substance. The length of the probe also matters in this scenario and it should be proportional to the ability to receive optical signals. Research in the past has shown that length of the fluorescent fibre probe should not be greater than 2 meters in order to ensure the high transmission efficiency.

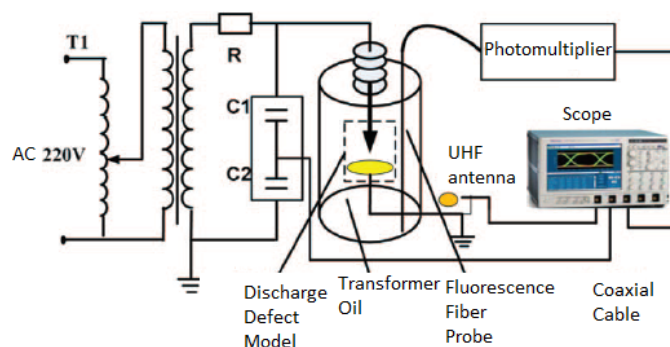


Figure 2.11: Experimental setup for optical PD detection using combination of fluorescent cable probe, fibre cable and optical sensor [23]

The advantage of these arrangements (using lens and fluorescent optics cable) is that the amplifier circuit is not arranged in the proximity of the high voltage set and therefore the electromagnetic influence can be minimized.

2.2.5. Direct measurement through optical sensor

The most simplified way of detecting the PD through optical means is direct measurements using the optical sensor. With a lot of development in the fields of sensor especially in the area of optics, there are several companies specializing in producing optical sensor. However, use of the optical sensor for PD detection application is not so common but some research has been done in the past and as a result, PMT (Photomultiplier) is the common sensor that has been used in most of the research done in this field. Last year, one of the sensors called SiPM (silicon Based Photomultiplier) is also researched for PD detection [10].

The Figure 2.12 shows two experimental setups where the optical sensor is directly focused on the PD source. The first setup is used under a closed and dark environment with two optical sensors namely PMT and SiPM. The second setup also uses PMT in direct view with the PD source. The output of the optical sensor is directly fed to the oscilloscope in order to analyse the data.

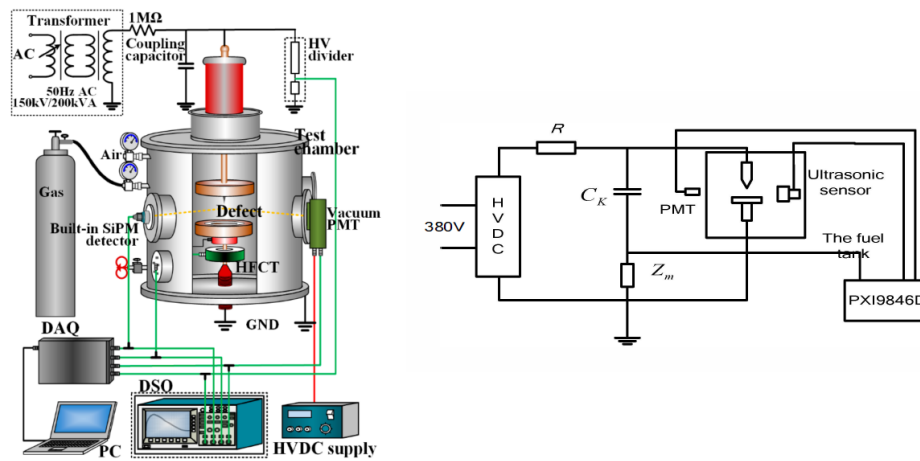


Figure 2.12: Experimental setup showing use of optical sensor directly [10] [24]

In all the methods explained above, the conventional electrical detector is also used simultaneously along with the optical detector. This is important in order to make comments about any correlation of measurements by an optical system with that of the results of the conventional measuring system. The research in past gives some ideas of how the layout and design for setup of the optical sensor should be. All the investigations in the past have been done in consideration of using the optical PD detection either in GIS or in the transformer. However, all the researches in the field of optical PD detection have laid a good foundation and give a solid concept for this thesis which is based on using the optical PD detection technique in the oil-filled termination.

2.3. On-line optical PD detection

On-line monitoring of PD can be big assets to the HV equipments present in the electrical power network. It will inform us the actual situation of the equipments without taking it off the grid. The possibility of the optical detection seems to be an appropriate method for the future for real-time applications with the advantage of discharge location and immunity to electromagnetic interference. This thesis will focus on the feasibility of optical PD detection in oil-filled termination. Furthermore, if the feasibility study is successful there will obviously be the rise of expectation to use this technology for the practical real situation i.e. online

monitoring of these termination using the approach researched in this thesis.

In the past, some research has been done in the field of online detection using the optical sensor. In the Figure 2.13, the use of optical sensors in the transformer has been projected. The lens can be located at different positions in the transformer where the possibility of PD occurrence is high. Then, using the fibre optic cable the signals from the various location can be coupled with the common optical sensor and can be analyzed using the computer at the far end.

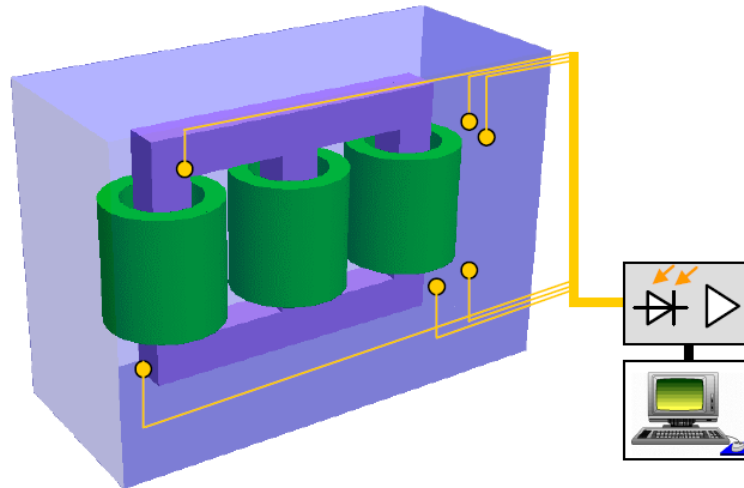


Figure 2.13: Example of online detection in transformer [21]

In [24], the idea of using optical sensor for PD monitoring in high voltage cable termination has been discussed. The idea can be illustrated using the Figure 2.14.

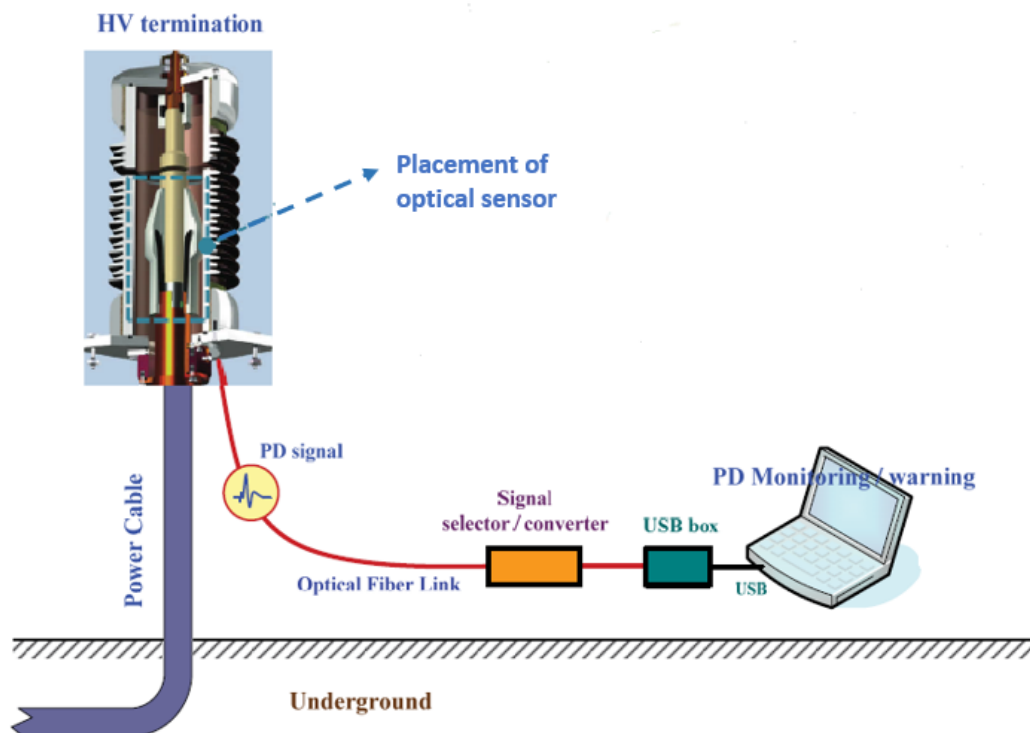


Figure 2.14: Example of online detection in termination [25]

The selected optical sensor or lens plus optical sensor can be placed in suitable position inside the termination near the start of the connection of cable-rubber stress cone. Then, the fibre optic cable can be fixed with proper converter and USB box which can be thus transferred maybe by radio (WiFi) channel to the respective cloud location and then can be analyzed on the computer. Thus, the real-time online measurement of the PD signal can directly be accessible for analysis. The inside into the housing of HV cable termination enables a night vision under low light conditions caused by partial discharges activity. The whole measurement system is galvanically isolated. There is no electromagnetic influence so that the optical PD detection is nearly immune against environmental noise signals. Therefore, it is possible to use the optical sensors for PD on-line monitoring in HV cable termination even if there will be high noise level and high electromagnetic interference in HV sub-stations.

Measurement System and test circuit description

This chapter explains the instruments and sensors used for the experimental measurements done in this research. The selection procedure and criteria adopted for optical sensor choice is discussed. Furthermore, the technique towards using the optical sensor along with its positioning is also explained. The different electrical detection instruments and measuring units adopted throughout the testing phase will be described. Lastly, the overall final circuit diagram used for simultaneous measurement of PD signal using optical and electrical system is presented.

3.1. Selection of optical sensor

The research in this thesis is about optical PD detection as a result selecting the appropriate optical sensor is highly necessary. The use of the optical sensor in the field of PD detection is quite new. Hence, there is no laid procedure or standards for choosing a right detector for optical diagnosis of the PD depending upon its type or medium. This section identifies some significant parameters which were considered as a base for the selection of the optical sensor for PD detection application in this thesis.

1. **Light power level:** This is the most fundamental criterion for selecting any detector related to light recognition. Here, since we are dealing with the light produced by the PD, we do not expect it to be high or even visible. Sometimes, the light produced by corona or PD in the air is visible in dark environment through naked eyes but in oil, detection of PD through light is tricky. Therefore, here the most prominent choice will be low light detection level even in the dark and closed environment.
2. **Light source spectral range:** The light source emits light radiation within a certain wavelength. This wavelength varies from medium to medium. Therefore, knowing the wavelength in which light is transmitted by the insulation medium where the PD activities take place is the first step towards short-listing the optical sensor. The next section 3.1.1 will explain the measurements and results obtained in order to find this wavelength for this research work.
3. **Quantum Efficiency (QE):** It is also termed as photon detection efficiency depending on the type of optical sensor used. A detector is not able to collect all the photons that have been emitted by the light source and convert them to electron-hole pairs. Therefore, quantum efficiency is defined as numbers of electrons produced per incident photon and is generally expressed as a percentage [26].

$$QE(\eta) = \frac{\text{Number of electrons produced}}{\text{Number of incident photons}} \times 100\% \quad (3.1)$$

4. **Gain:** This is also termed as current amplification. Most of the optical sensor gives the output in term of current. The light detected is of low level which needs to be amplified in order to reach the measurement system. It is calculated in different ways for different optical sensor. Mostly, it is described as a ratio of output current to the input current of the sensor. This also indicates the sensitivity of the sensor which is defined as the ratio between the output signal and measured property. High gain or sensitivity should be chosen in this scenario.
5. **Electrical bandwidth:** This refers to the bandwidth in which the measurements of the signal will be conducted by the optical sensor. It has been explained how the PD measurements take place at different frequency range depending upon the type of sensor used in the electrical detection which ranges from narrow to wide and then to ultra high-frequency range. Therefore, the bandwidth of the optical sensor should start from DC to MHz and can go higher according to the requirements.
6. **Signal to Noise Ratio (SNR):** The SNR ratio is the most significant parameter for an optical sensor if used for PD measurements application. Noise is a big disturbance in case of PD detection and thus is generally minimized or avoided. When observing the output waveform of an optical signal, there are two types of noise component that can be observed: one being present even without light input and the other is generated by the input of the signal light. Generally, these noise components are governed by the dark current generated by the photo-cathode thermionic emission and the shot noise resulting from the signal current. When the signal and noise waveforms as shown in Figure 3.1 is observed, it can be analyzed in following way [26]:

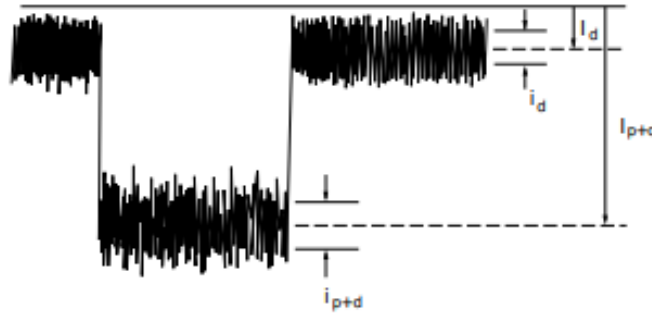


Figure 3.1: Example of signal to noise ratio [26]

Here, I_d = Mean value of noise component; i_d (r.m.s) = AC component of noise; I_{p+d} = Mean value of signal (noise component included); i_{p+d} = AC component of the signal (noise component included). Using these factors SNR is given by:

$$SNR = \frac{I_p}{i_{p+d}} \quad (3.2)$$

where I_p is the mean value of the signal component only, which is obtained by subtracting I_d from I_{p+d} . If the dark current I_d can be ignored ($I_p \gg I_d$), then SN ratio can be defined as:

$$SNR \approx \frac{I_p}{i_p} \quad (3.3)$$

where I_p is the mean value of the signal component and i_p is the A.C. component (r.m.s) of the signal. The optical sensor should be tested first for SNR before actual measurements in order to evaluate its performance.

7. **Other parameters:** There are several other small parameters of which the user should be aware when using the optical sensor. These are crosstalk, after pulse and jitter.

These features are mostly common in PMT sensors. Crosstalk is one type of optical noise. Most of the low light sensitive optical sensor undergo Geiger mode. During this Geiger discharge, hot plasma emits photons that are capable of producing electron-hole pairs. These electron-hole pairs and carriers injected in high field region create discharges in the neighbouring cell, thus creating another avalanche for emission of electron-hole pairs and therefore superimposing of the primary pulse at same time occur which give rise to phenomena called crosstalk. The Figure 3.2 illustrates a scenario of crosstalk observed in the oscilloscope.

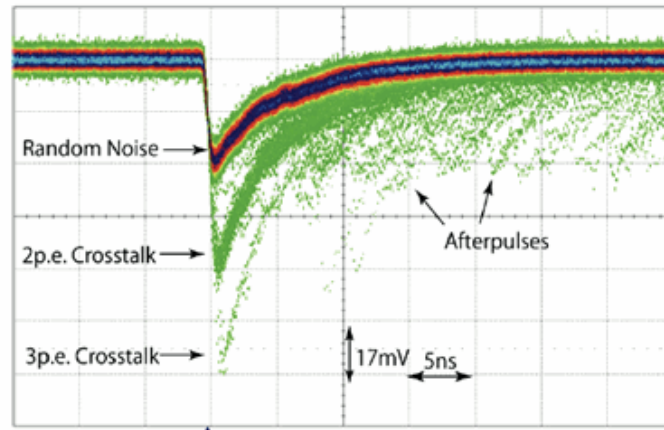


Figure 3.2: Crosstalk and afterpulse phenomena [26]

Another source of optical noise is afterpulse which is also called as delayed correlated noise. There are two sources for afterpulse: the delayed release of the trapped carrier and delayed optical cross-talk. Some carriers from the primary avalanche may get confined in a deep trapping level in the energy band. This lead to delayed release resulting in triggering of another avalanche leading to afterpulse signals. These noises can be avoided by improving the quality of wafer layer with an optimized gain of the optical sensor.

During measurement of optical signals, time resolution variation can be observed which is often termed as jitter. It is not a noise but can be seen as uncertainty during sensitive and low light measurements. Counting time is when the photon strikes the surface of the sensor to the time when output pulse reaches to the maximum. If every time the photon strike, the counting time is same, then the jitter will be zero. However, this is an ideal scenario and variation always occur in counting time which is called as jitter. This is very important if we are doing time-based measurements.

After reviewing all the parameters, the optical sensor with high sensitivity to low light should be selected with an appropriate spectral response which is discussed in the section below. The optical sensor should have good quantum efficiency in the range of spectral response with good gain. The electrical bandwidth chosen in this research should lie from DC to some MHz (similar to HFCT sensor used for electrical detection). The sensor should have good SNR value with no crosstalk, after pulse or jitter phenomena. Apart from that, basic requirements like the mechanical necessity of size, power consumption and operating temperature should also be considered. The final factor of the budget was also accounted for while selecting the sensor in this thesis.

3.1.1. Measurement of transmittance index of the oil

As mentioned in the last section, one of the important parameters while selecting optical sensor is its spectral response bandwidth. It defines the wavelength within which the optical

sensor is capable of working. In order to define this, we should know what will be the wavelength within which light is been transmitted in the medium under test. Here, the PD will occur on the surface of the rubber sample in the oil insulation. Therefore, the transmission characteristics of this insulating oil A12 (used in oil-filled termination) should be measured.

A Lambda 950 spectrophotometer instrument (owned by PVMD group, TU Delft) as shown in the Figure 3.3 was used for measurement of transmittance index of the oil in order to determine a suitable working range for the optical sensor.

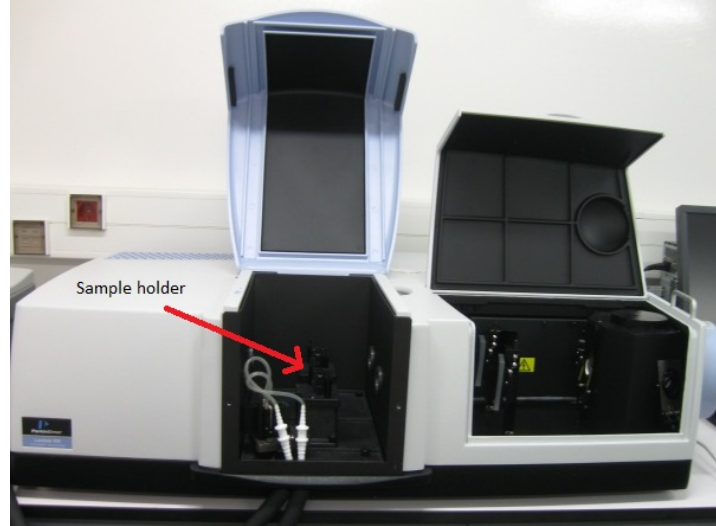


Figure 3.3: Spectrophotometer used for measurement of transmittance of A12 oil

The working principle is the combination of physics behind the double beam, double monochromator, ratio recording UV/Vis/NIR spectrophotometers based on different wavelength coupled with electronics and software controlled by a compatible personal computer. The system consists of D2 lamp (for UV range) and tungsten lamp (for visible range) as a source of light followed by lamp changer (lamp selector mirror) and the monochromator. The monochromator is used to restrict unwanted radiation and control spectral purity. It is then followed by CBM (Common Beam Mask), slit and CBD (Common Beam Depolarizer). CBM allows setting the height of the beam, therefore, adjusting the resolution whereas CBD is used to depolarize the radiation that comes from the monochromator. Slits allow to reduce the width of the beam and therefore reducing the energy passing through the sample, thus can be used to improve sample resolution. Then, comes the attenuators which reduce the signal noise. This is followed by the sample compartment where the oil filled in the suitable cuvette is kept. The next open compartment right of the sample holder compartment as seen in the Figure 3.3 consists of the detector (PMT and Pbs) and integrating sphere coated with a highly diffuse reflective material which reflects the light until it reaches the detector. PMT is used for UV and visible light detection whereas Pbs for near infrared detection. Therefore, the light produced through the source inside the spectrophotometer is passed through the oil contained in the cuvette which is then measured by detector present on the other side of the sample holder, thus recording the transmittance performance of the oil i.e. the ratio of light energy falling on a body to that transmitted through it.

Measurements & Results: The empty cuvette is placed first and then the transmittance in terms of percentage is obtained with respect to wavelength ranging from 200 nm to 2500 nm. The oil is then placed in the cuvette and rested for few hours in order to get rid of any air bubbles. The cuvette with oil is again placed in the sample compartment and measurement is thus carried out. Therefore, the transmittance index can be calculated as a ratio of transmittance measured with oil in the cuvette to transmittance measured with empty cuvette.

$$\text{Transmittance index} = \frac{\text{Transmittance measured of oil in cuvette}}{\text{Transmittance measured of empty cuvette}} \quad (3.4)$$

The results are thus displayed in Figure 3.4. The graph illustrates that the A12 oil can transmit the light in the wavelength ranging from 350 to 1100 nm approximately. Therefore, the optical sensor selected should have spectral response around this range. The graph shows values slightly higher than 1. This is due to using empty cuvette first and then filling it with oil, this could lead to different reflection at the surface of cuvette as at start there was only air in between and then it was filled with oil. Thus, reflection in air can be larger than oil. However, for our purpose this error can be neglected as it does not effect the wavelength range.

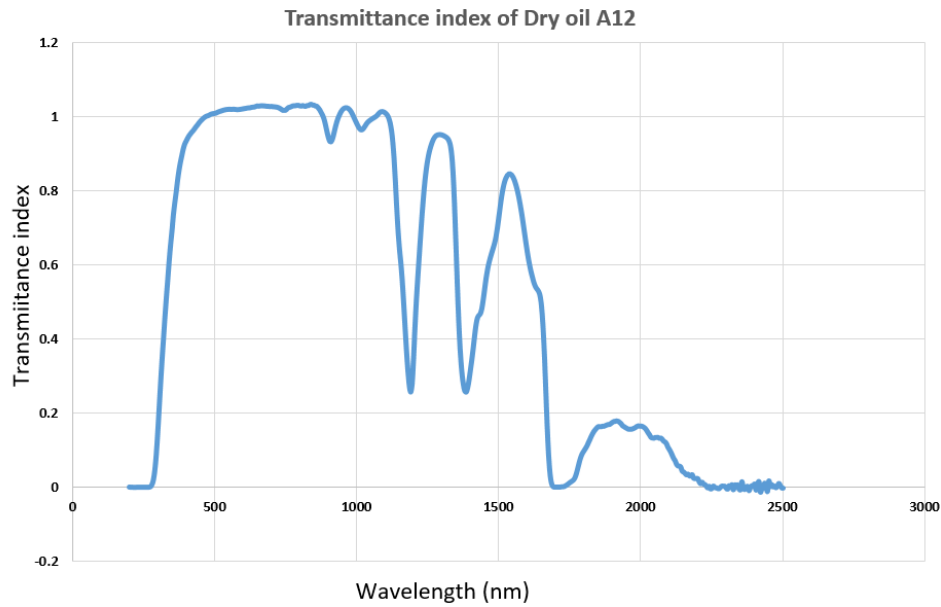


Figure 3.4: Measured transmittance of A12 oil

3.1.2. Choice of optical sensor for PD detection application

The above sections clarified the factors to be focused while selecting the optical sensor for PD detection application in this thesis. The requirements are low light detection, 350-1100 nm spectral range, DC to MHz electrical measurement bandwidth, high quantum efficiency, small and light weight with good SNR and no optical noise like crosstalk, after pulse and jitter. There many sensors in the market and the most suitable among them on basis of past and current researches are the three sensors discussed below.

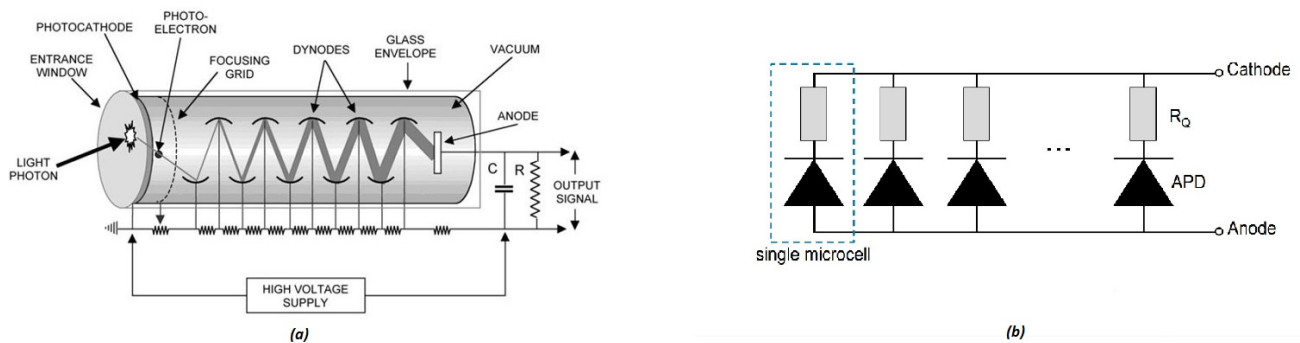


Figure 3.5: (a) Basic structure of PMT sensors [26] (b) Basic structure of SiPM sensors [27]

Photomultiplier tube sensor (PMT)

PMT is most commonly used sensors for low light detection. These sensors have been used in almost all the researches that have been done based on optical PD detection in the past.

Figure 3.5a demonstrates the basic structure and working of the PMT sensors. A photomultiplier tube sensor is a vacuum tube which consists of: an input/entrance window, a photocathode, focusing grid/electrode, dynodes and an anode which is usually sealed into evacuated glass tube [26]. The light which hit the effective area of the sensor passes through the input window. This light excites the electrons in the photocathode which emits the photoelectrons into the vacuum. These photoelectrons are then guided towards dynodes with the help of focusing electrodes where the multiplications of the electrons take place by the means of secondary electron emission. The secondary emission is repeated at each of the successive dynodes depending on the number of dynodes present in a particular PMT. The multiplied secondary electrons emitted from the last dynodes are finally collected by the anode. Thus, the output of the PMT will be in the form of current.

PMT sensors feature large gain, low noise and ultra fast response and they require high voltage to operate. They are available in different size from fingertip sized micro PMTs to the large 20-inch PMTs with a varying price. Generally, 115 - 1700 nm is the spectral range of the PMT but the variation can be done for individual PMT according to the material and construction of photocathode and window. It has highly sensitive light capturing mechanism but it is also mostly influenced by the external means. Since it is highly dependent on the emission caused by the dynodes, any disturbance to the path of these electrons can lead to erroneous results. This influence is more if the distance between the photocathode and first dynodes is large. Therefore, it is not immune to outside magnetic interference and needs housing protection. Anode dark current is also very often a problem since the main source here is thermionic emission so if the temperature rises, the dark current also increases. PMT also can be damaged by ambient light so the measurements should always be performed in the closed chamber and should be handled carefully.

Silicon photomultiplier (SiPM)

A silicon photomultiplier has recently been introduced in [10] for optical PD detection application. These are also called Multi-Pixel Photon Counter (MPPC). A silicon photomultiplier is a solid-state silicon based photodetector whose output is in form of a current pulse. Upon absorption of the single electron, it can give current pulse ten nanoseconds long with the gain of 10^5 to 10^6 electrons [27]. Figure 3.5b illustrates the most basic structure of the sensor. SiPM integrates a dense array of microcells in parallel to each other. These microcells consist of avalanche photodiode (APD) and quench resistor, each of which can independently work in a Geiger avalanche mode and fires in response to an absorbed photon. When the light fall on the active part of SiPM, the photoelectrons flow will be activated. This will result in charge carriers which will activate an avalanche in the gain region within the $p^+ - n^+$ structure. The avalanche produces multiple carriers which ultimately results in the gain. The role of quenching resistor is to restore the APD back to the Geiger mode. Whenever the Geiger avalanche takes place, it happens only in single microcell which is initiated in the avalanche process whereas other microcells during this period remain fully charged and ready to detect photons, therefore, ensuring a complete PD photon emission process.

Generally, the SiPM efficiency is known as photon detection efficiency (PDE). This PDE is the product of geometrical fill factor, quantum efficiency and a probability of Geiger discharge. Geometrical fill factor is the fraction of the active area sensitive to light. Quantum efficiency can be defined as probability that an incident photon generates a charge carrier which is capable of triggering Geiger discharge in the avalanche section of the depletion region. The gain of the SiPM is defined as the amount of charge created for each detected photon and is a function of the over-voltage and microcell size. It is a ratio of the product of a capacitance of the microcell and over-voltage to the electron charge.

A SiPM most resembles a PMT in operation and characteristics. They feature high gain comparable to PMT, excellent time resolution, high photon detection efficiency, low afterpulse and no jitter. Also, they are operated at low bias voltages compared to PMT. They can vary in size from a small 1×1 mm active area to larger arrays, and they are insensitive and immune to magnetic fields, unlike PMT. Generally, the spectral range is 320-900 nm. It is also more rugged compared to PMT, as a result, SiPM has begun to replace PMT in low-light applications such as positron emission tomography, light detection and ranging (LIDAR) or

radiation detection in high-energy physics. This type of sensor proves to be a good choice for our application in this thesis. However, the main concern remains the optical noise which is comparatively high in SiPM compared to PMT because of the neighbouring pixel which can cause more influence to optical crosstalk. Furthermore, the SiPMs available in the market are very specific and nothing we found were appropriate to us considering all the parameters and also the price.

Avalanche Photodetector (APD)

In addition to SiPM and PMT, Avalanche photodetector (APD) is one of the low light detecting sensor in the market. It is not generally used for optical PD detection application but has the capability of being used as it has similar features to that of SiPM and PMT. It is comparable to the normal photodiode and the schematic cross-section for a typical APD structure is illustrated in Figure 3.6. The structural design include absorption and multiplication region. The region across absorption area present electric field that serve to separate the photo-generated holes and electrons and sweep one carrier towards multiplication region. The multiplication region is designed to exhibit a high electric field so as to provide internal photo-current gain by impact ionization. When the light hit the active area of the APD sensor, the electron-holes pair is generated if the light energy is higher than the bandgap energy. Now when the electron-hole pairs are generated in the depletion layer of an APD due to reverse voltage applied to the PN junction, the electric field will cause the electrons to drift towards n^+ sides and hole towards p^+ side. With higher electric field, collision with crystal lattice will take place which will give rise to more electron-hole pairs, thus giving rise to ionization and this process repeats which leads to avalanche multiplication and finally deduced out as an output signal. APDs are similar to regular PIN diodes but operate with much higher reverse bias. The gain here is proportional to the applied reverse bias voltage. The amplification factor of APD is quite good of approximately 10^6 because of high reverse voltage.

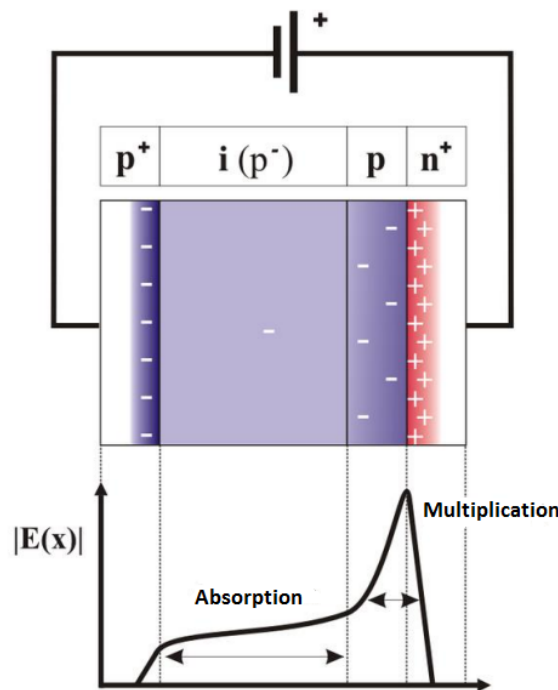


Figure 3.6: APD working principle [28]

APDs are available in different sizes with very compact structure and housing. They deliver a higher signal to noise ratio than normal photodiodes and have fast time response, low

dark current and high sensitivity. They are mechanically rugged, light weight and totally immune to damage due to ambient light exposure and magnetic interference and noise which is very critical during experiments.

There are a lot of varieties of sensors available in PMT, SiPM and APD type based on effective area, size, spectral response, electrical bandwidth and price. Table 3.1 gives a brief comparison on the basis of important parameters which was kept in mind while selecting sensor for this research. Finding the right sensor for this thesis took a lot of time and research. It should be kept in mind that there has to be a trade-off between some parameters but the basic factors influencing the performance of the sensor should always be considered. Finally after evaluating and researching on various aspects, **Avalanche Photodetector (APD) was chosen to be used in this thesis for optical PD detection** (mainly due to highlighted points in Table 3.1 under APD). The selected APD sensor specifications and structure of how it will be used is discussed in the following section.

Table 3.1: Comparison of all the three optical sensors

Photomultiplier Tube (PMT)	Silicon Photomultiplier (SiPM)	Avalanche Photodiode (APD)
<ul style="list-style-type: none"> • Expensive • Need Protection against magnetic interference (Not immune) • Can be damaged through ambient light exposure • Output Bandwidth: DC to 60 MHz • Larger size • Moderate spectrum range • Lower quantum efficiency • Highly sensitive 	<ul style="list-style-type: none"> • Low Cost • Immune against magnetic interference • No damage due to ambient light exposure • Output Bandwidth: DC to MHz • Smaller size • Moderate spectrum range • Moderate quantum efficiency • Low sensitivity than PMT 	<ul style="list-style-type: none"> • Moderate Cost • Highly Immune against magnetic interference • No damage due to ambient light • Output Bandwidth: DC to GHz • Smaller size • Large spectrum range • High quantum efficiency than PMT • Low Sensitivity than PMT.

3.2. Setup for APD optical sensor

Once the type of sensor was decided, i.e., APD sensor, the next step was what specific APD should be brought from the market. The APD sensor from the ThorLabs, **APD130A2/M Si Avalanche Photodetector** as seen in Figure 3.7 was selected for measurements in this thesis. The section below describes the characteristics, specification and layout adopted during the measurement.

3.2.1. Specifications and characteristics of APD130A2

The APD130A2/M sensor is temperature compensated avalanche photodetector which combines a high sensitivity Si avalanche photodiode with specially designed ultra-low noise amplifier for detection of optical signals from DC to 50 MHz [29]. The ultra low noise in this sensor is achieved using active low pass filter which efficiently suppresses out of band noise. APD130A2 have exceptionally low noise equivalent power which makes it ideal for fast low-level light detection applications such as spectroscopy, fluorescence measurements, laser radar and optical range finders. Due to its very high sensitivity, APD can easily replace PMT in many applications. APD cannot be damaged by any unwanted ambient light which is very critical for many PMT and SiPM sensors.



Figure 3.7: Finalized APD sensor used in this thesis

The working principle of APD130A2 is exactly same as explained in previous section. The amplification depends on the reverse bias voltage and is also termed as M (multiplication) factor. Due to internal process, M is temperature dependent. Therefore, at fixed bias voltage M will change with the temperature. M will decrease with higher temperature whereas M value will increase with lower temperature. However, this sensor is temperature compensated. It consists of thermistor inside the sensor's enclosure which senses the temperature and with the special electronic circuit controls the applied APD reverse voltage in accordance with the temperature change. As M factor depends on the applied reverse voltage, therefore the temperature dependency of the M factor can be reduced drastically with the help of thermistor.

The table 3.2 present all the technical specification of the APD130A2 sensor.

Table 3.2: Specification of APD 130A2/M

Parameters	Values
Detector Material type	UV-enhanced Silicon APD
wavelength range	200 to 1000 nm
Active area	1mm in diameter
Electrical bandwidth	DC to 50 MHz
Maximum APD responsivity	25 A/W @ 600 nm, M=50
Maximum conversion gain	2.5×10^6 V/W
Maximum output voltage	3.6 V (High Z load) 1.8 V (50 Ω)
Power Supply	± 12 V, 200mA
Weight	<0.1 kg

The input beam of light should be carefully aligned to the detector for efficient diagnosis. Therefore, an additional focusing lens or fibre adapters can be easily mounted on the optical input for optimal results. The fibre adapters can accommodate both multi-mode as well

as single-mode fibre. The output of the APD130A2 delivers an output voltage which is the function of incident light power (P_{opt}), detector's responsivity (R_M) at given wavelength and M (Multiplication/amplification) factor and transimpedance gain (G).

$$V_{out} = P_{opt} \times R_M(\lambda) \times G \quad (3.5)$$

The M factor is a factory set to 50 at 23° C ambient temperature for this sensor and cannot be altered. The amplifier transimpedance gain G is set to 100 kV/A. Responsivity generally is termed as an input-output gain of the detector system. The responsivity of this sensor at M=50 can be seen in appendix A Figure A.1 . The spectral noise spectrum shown in appendix A Figure Output frequency response of APD130A2 A.3 was measured using an electrical spectrum analyzer (resolution bandwidth 10 kHz). The optical input was blocked and the black curve was measured with the same setup when the detector was off in order to represent the measurements system's noise floor.

3.2.2. Layout of optical test setup

The sensor cannot be directly placed at the source of PD and require some mounting accessories. The sensor chosen has effective area diameter of 1 mm, as a result, the appropriate lens in front of the sensor was used in order to have enlarged area for capturing the light coming from PD activity. The use of the lens for more coverage area was chosen instead of fibre optic cable because coupling losses for the cable are more, leading to much more reduced output signal. Figure 3.8 illustrates the layout of the optical sensor in order to measure PD using the sensor APD130A2. The diagram presented is made using the *AUTOCAD Inventor 2017*.

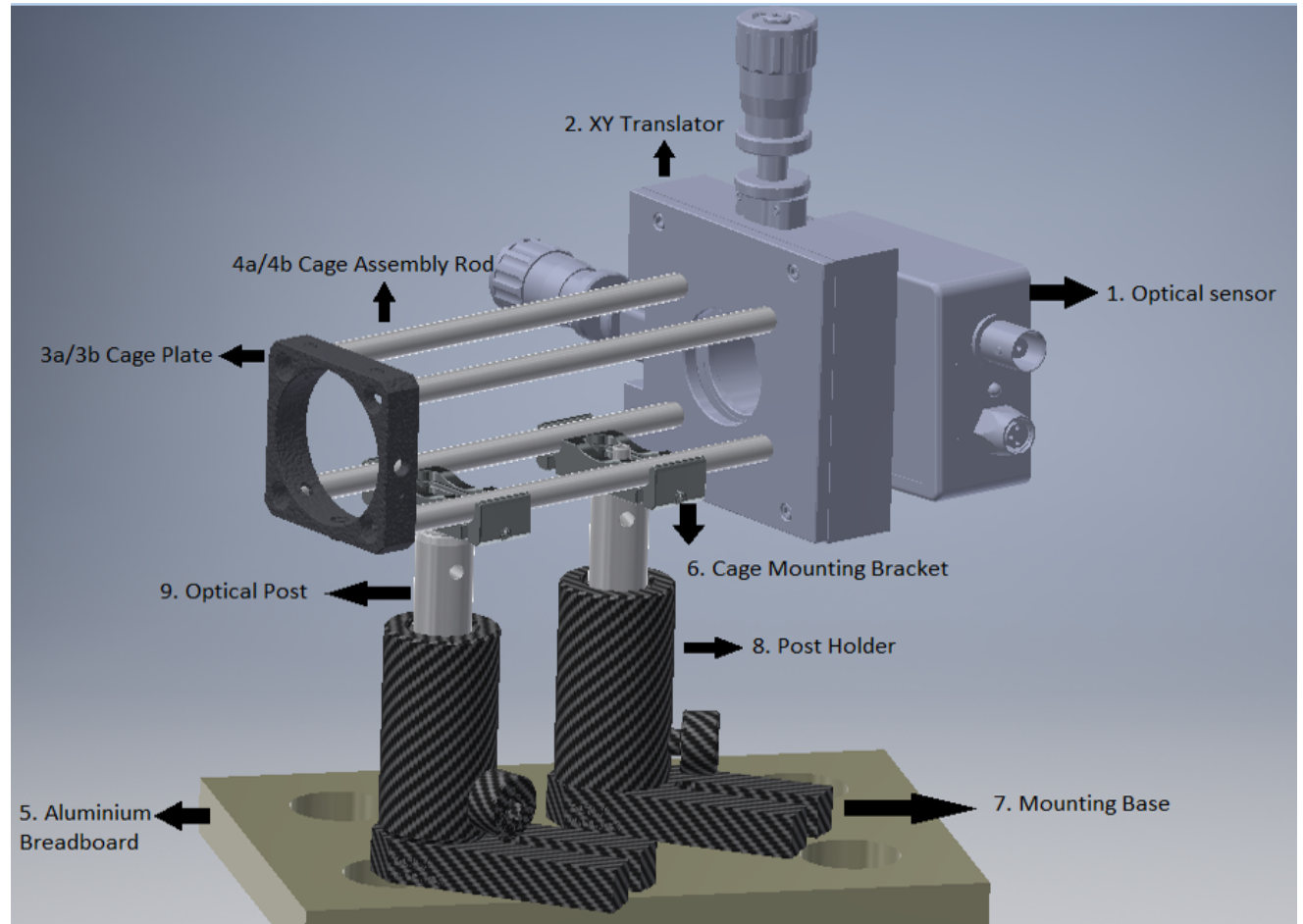


Figure 3.8: Layout of the sensor for measurement purposes

The following components from Thorlabs were used in order to build the structure for the optical sensor:

- **XY Translator** with differential drives, metric (ST1XY-D/M)
- **Cage plate**, 30 mm Cage plate with diameter of 1 inch Double Bore, M4 Tap (CP06/M)
- **Cage assemble rod**, 4 inches, diameter 6 mm (ER4-P4)
- **Aluminium Breadboard**, 100 mm × 150 mm × 12.7 mm, M6 Taps (MB1015/M)
- **Cage Mounting Bracket**, Snap-On 30 mm , M4 Tap (CPMA2/M)
- **Mounting Base**, 25 mm × 58 mm × 10 mm (BA1S/M-P5)
- **Post Holder**, 12.7 mm diameter, Spring-Loaded Hex-locking Thumbscrew of length 50 mm (PH50/M-P5)
- **Optical post**, 12.7 mm diameter, M4 Set screw with length 75 mm (TR75/M-P5)

As can be seen in Figure 3.8, the optical sensor will be mounted in the XY translator box in order to move it both in the horizontal and vertical direction according to the requirement during experiments. The cage plate will hold lens which will be fitted on the translator through the cage assembly rod (two type of cage plates and rods were ordered due to use of two different size of the lens in order to achieve maximum efficiency during the experiment). The components like mounting bracket, base, optical post, post holder and aluminium board are required to provide further support to the system in order to establish stable set up for optical sensor and lens.

Positionality and directionality calculation

The lens positioning has to be done accordingly so that maximum light that can fall on the sensor from the source which is area creating PD in this case. In order to align the lens at the right position from the sensor as well as from the PD source, requires some basics calculation and trail test. Therefore, lens formula and magnification formula as shown in below equations were used.

$$\frac{1}{S_1} + \frac{1}{S_2} = \frac{1}{f} \quad (3.6)$$

$$M = -\frac{S_2}{S_1} = \frac{f}{f - S_1} \quad (3.7)$$

$$M = \frac{h_o}{h_i} = \frac{f}{S_2 - f} \quad (3.8)$$

where, S_1 = Distance from PD source to lens

S_2 = Distance from sensor to lens

f = focal length of the lens used

h_i = height of the active area of optical sensor

h_o = height of the PD source area

M = Magnification factor

Now, the **biconvex lens** of focal length 25 mm was chosen after several trail and error tests. The PD source activities should lie within the cage plate shown in Figure 3.8 pointed by number 3a/3b as PD activities happening outside of this area will not be captured through the lens to the optical sensor. The cage plate actual size used for holding lens is circular in shape of around 25 mm in diameter. The image height is equivalent to the optical sensor effective area. Therefore, if the axis symmetry is considered, the height of the image/optical sensor is taken as 0.5 mm and height of PD source/object is taken 12.5 mm.

Figure 3.9 displays the idea behind the calculation of the sensor, lens and PD source positioning. Therefore, with the known quantities: focal length = 25 mm, h_i = 0.5 mm, h_o =

12.5 mm and with the equations 3.6, 3.7 and 3.8, the computation was made with following results:

- **Distance of the PD source to lens: $S_1 = 600$ mm**
- **Distance of the sensor to lens: $S_2 = 24$ mm**

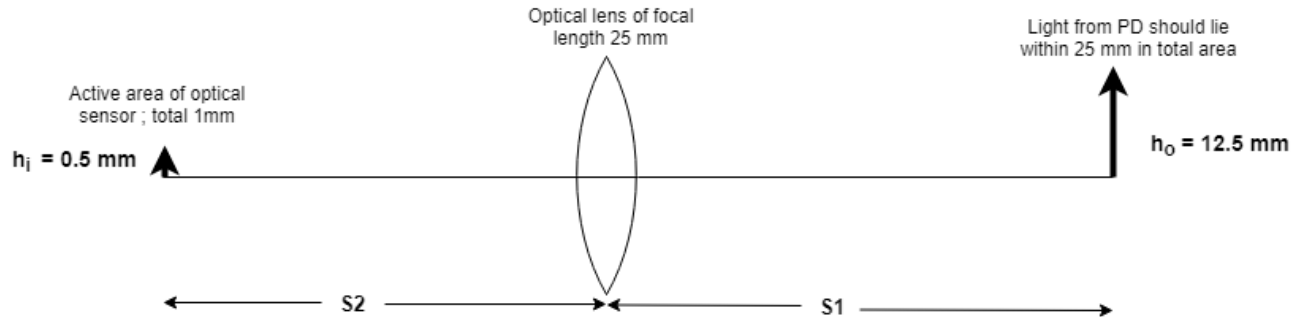


Figure 3.9: Calculation of distances from lens

The finalized assembled optical setup for PD detection is shown in Figure 3.10. The values calculated will give the exact optimum efficiency of the measurement using this optical sensor. However, the exact values cannot be taken while doing the testing but the calculated values should be kept in mind while adjusting the optical sensor in front of PD source in order to get proper output from optical detection. The basic test with a beam of light at a varying distance was also conducted in order to verify the optimum position and its measurement characteristics. Now, the optical sensor with the finalized layout is ready for the PD detection.

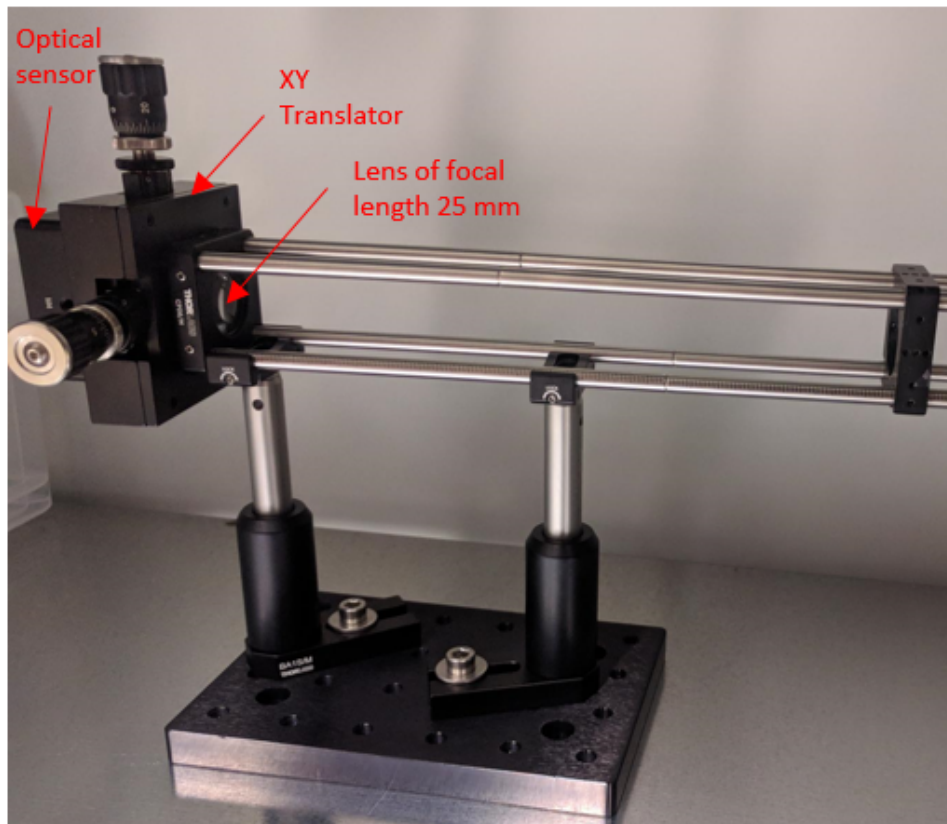


Figure 3.10: Finalized assembled optical measurement setup

3.3. Equipments for electrical PD detection

In order to verify our results of the optical sensor and know the proper intensity and magnitude of the partial discharge produced in our setup, use of proper electrical measurements is a pre-requisite. The basic electrical PD detection used in this thesis was according to IEC standards as explained in chapter 2 under electrical detection. However, unconventional electrical measurements of higher bandwidth are also used. This section will provide a detailed explanation of all the equipments used for PD measurements focusing on complete setup for electrical detection explaining the electrical sensor and all the instruments used for measurements and analysis of the PD output pulses.

3.3.1. Sensors for electrical detection

Below are the sensors that is used in this thesis for measurement of PD electrically.

1. **Quadripole:** AQS 9110a quadripole system with PD lower limit frequency of 50 kHz and PD upper limit frequency >5 MHz is used as shown in the Figure 3.11a. The input high connection should be connected to the low voltage end of the coupling capacitor. Generally, there should not be any other connection to this point on the capacitor. The input low connection should be grounded. The connection of the ground should be made using braid copper to give good low-inductance connection and should be small in order to minimize stray inductance. The PD output source should be connected using high quality 50 Ω BNC coaxial cables. The output of the quadripole should be fully isolated.



(a)



(b)

Figure 3.11: (a) Quadripole front pannel (b) HFCT sensor

2. **HFCT Sensor:** The HFCT sensor used in this thesis is the same one which is used in [30] as shown in Figure 3.11b. The high frequency current transformer is placed just below the coupling capacitor. This HFCT consists of five turns wound onto TDK N30 ferrite core and is terminated with 50 Ω BNC coaxial cable connected to an oscilloscope or the measuring instrument same as that of the quadripole output. Each turn is made of the flat strip 3 mm wide and each turn is evenly distributed along the core in order to reduce stray capacitance in the system. The bandwidth of this HFCT sensor is 34.4 kHz to 60 MHz.

3.3.2. Measurement instrument and analysis software

This project involves lot of experiments starting from finding the right setup for creation of surface discharge to the simultaneous measurements done using electrical and optical detection techniques. There were different measurement instruments used throughout the process. This change in measurement instruments also change the PD pattern, PD pulse

style, the recording method and the software used for analysing the PD. Therefore, this section will discuss all the measurement instruments used in this project along with the software used to analyse it later. Hence, this will clarify any different pattern observed in the rest of the chapters of this report.

1. **Haefely DDX 9101 PD detector with quadripole:** Haefely PD detector series named DDX 9101 is used in combination with quadripole AQS 9110a. The software called *Remote9101* is used along with the measurement device in order to record and analyse the data in NQP form. Figure 3.12 shows the exact setup used while doing the measurement using these instruments. The PD detector was used in scope mode where the PD scope with a phase based (sinusoidal) display of the discharge activity was shown. When connected with the software on the laptop, the full control of the detector can be done using the software. The change in amplifier gain, frequency bandwidth range and minimum charge trigger level can be adjusted depending on the magnitude and intensity of the PD pulses obtained while measurements. The detector is always advised to be calibrated before doing the actual measurements. After the pulse has been saved, the PD pattern can be accessed using NQP analysis module. It provides the plot of N-Q-P which stands for the frequency of occurrence against magnitude and phase which can be related to PRPD (Phase Resolved Partial discharge) pattern. The data can be shown on a 2D or 3D chart and the data is captured in blocks. It also provides an option of capturing the data in NQP form while performing the experiment and then a comparison can also be made between saved and current captured data.

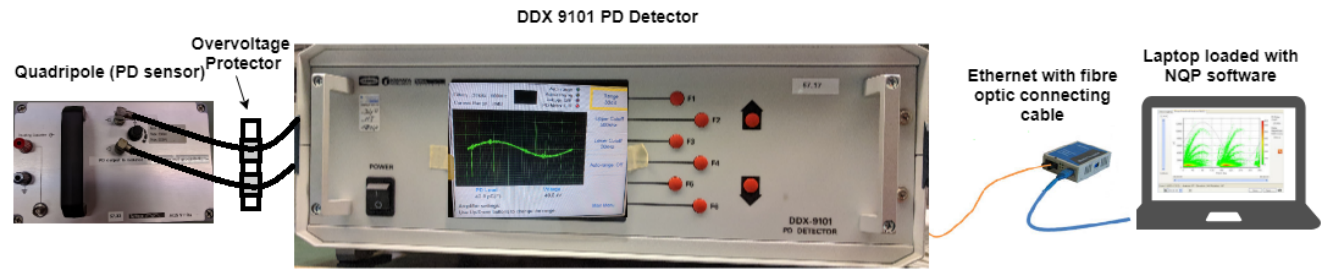


Figure 3.12: Measurement using DDX 9101 PD detector

2. **Techimp with HFCT sensor:** Techimp PDBaseII in combination with mostly HFCT sensor and optical APD sensor was also used. It is ultra wide band, 6 channel device, analogue to digital converters operating at 200 Ms/s with the bandwidth of 40 MHz. Figure 3.13 illustrates the connection made when used this device during the measurement of PD in the test setup. Generally, during the experiments two channels were used: one got the input from PD sensor and another from connection (synchronization) box shown in Figure 3.15b for voltage synchronization which will be explained later in this section. This connection obviously passes through over-voltage protection system. Techimp PDBaseII is provided with an Ethernet port which can be connected locally and remotely using TCP/IP communication protocol. Fibre optics cable and RJ-45 cable was used to connect PDBaseII detector to a computer containing dedicated software called PDBaseII control software. The PD data measured using this system not only capture PD pulse peak and phase but also capture each PD pulse waveform giving information about pulse shapes unlike the one used in case of Haefely detector. All the actions of the PD detector are controlled by the software right from first to last steps namely: calibration of the system, PD streaming, saving the data, acquisition of the data and pre-processing of the captured data. Different modes of bandwidth, pre-trigger level, maximum pulse number captured, dead time, time length, full scale, phase shift and scale limit can be altered according to the requirements during the measurement.

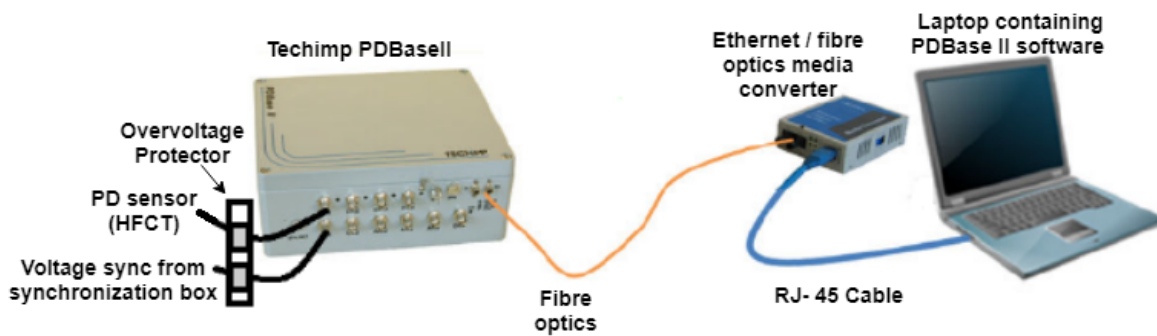


Figure 3.13: Measurement using Techimp PDBasell [31]

A software named *PDProcessing II* is also provided with the detector for further analysis of the data saved using PDBaseII control software. It provides the option of separating two types of PD if captured using same PRPD pattern, helps to separate noise from the actual PD pattern and also depicts different visualization of each PD pulse captured. It can display waveform graph (display individual pulse waveform in the time domain), spectrum graph (display pulse power spectrum in the frequency domain) and classification map (shows acquired pulses classified by equivalent time-length and frequency) of a PRPD pattern captured.

3. **High performance Tektronix DPO7354C oscilloscope with HFCT sensor:** A high performance Tektronix DPO7354C oscilloscope of 8 bits of vertical resolution was used with HFCT sensor and APD optical sensor in the configuration as shown in Figure 3.14. This oscilloscope simultaneously shows the optical as well as the electrical signal from the test setup at same time stamp. The signal shows each pulse and therefore in order to obtain the PRPD pattern or to perform further analysis of PD signals, each pulse is captured individually using “Fast Frame Acquisition” (in which the number of pulse to be captured is set according to the user requirements). The number of pulses, trigger value, time stamp and sampling frequency can be set before capturing the data. Once the data are captured, all the trigger events and channel signals are saved as the waveform in form of the “.wfm” and time stamp in “.txt” format all with a same file name. These waveforms are used by GUI based software tool called *PDflex*¹ developed at TU Delft itself [32] for further off-line analysis. No calibration of the test setup is required if the measurement and analysis is made using this combination.

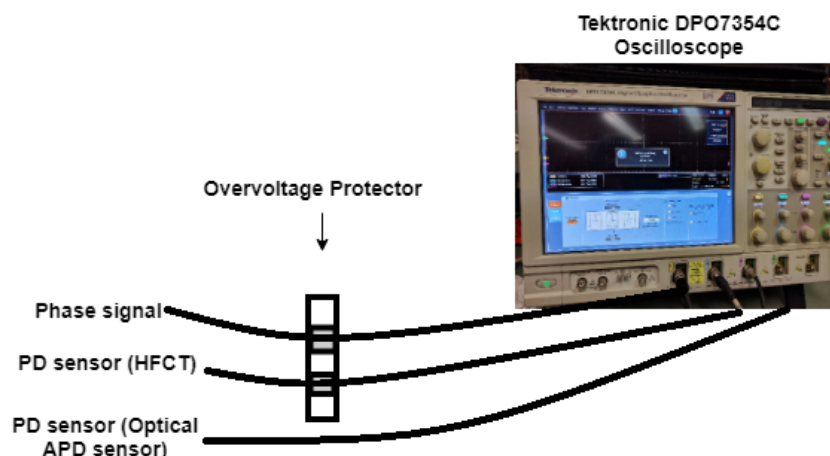


Figure 3.14: Measurement using Tektronix DPO7354C Oscilloscope

¹<http://pdflex.tudelft.nl/>

The software PDFlex requires synchronization signal in order to acquire PD pulse and to display it in form of PRPD pattern and other analysis plots. Therefore, the box was made as shown in the Figure 3.15b by Koornneef in HV lab, TU Delft. The internal circuit diagram of the box can be seen in Figure 3.15a. In order to create a phase resolved PD pattern, each PD pulse should be recorded along with the phase angle related to the test voltage at which it occurred. This phase angle is obtained using the sawtooth signal made by the box as seen in Figure 3.15c whose period is synchronized with the period of the test voltage. When a PD pulse amplitude is larger than the trigger, then the oscilloscope record both the signal from PD sensors and phase signal (sawtooth). The phase of the PD pulse is proportional to the ramp voltage magnitude at which the PD pulse occurred. The tests can also be conducted at different frequencies of the test voltage which is enabled by the trigger of the ramp at the zero crossing point of the applied voltage.

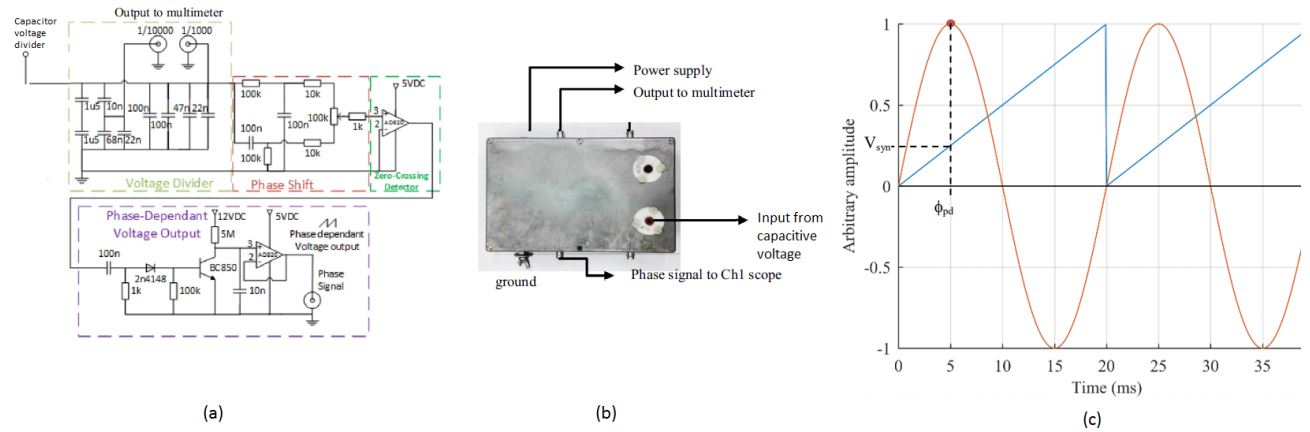


Figure 3.15: (a) Internal circuitry of the synchronization box (b) Synchronization connection box (c) Synchronization signal to acquire phase of PD pulse [32]

Once the waveforms from the oscilloscope are captured, they can be opened in PDFlex and can be analysed separately for optical and electrical signals. The PDFlex software gives us options for analysing AT plot (time evolution representation of the current pulse of each PD pulse), QT plot (time evolution representation of the charge of each PD pulse), $t_{rise} t_{fall}$ plot (cluster plot of the rise time and fall time of each PD pulse), IQE plot (cluster plot of the charge and the energy/charge ratio of each pulse) and FW plot (cluster plot of the frequency at which the peak of the Fourier spectrum occurs and the equivalent bandwidth). The further details of PDFlex software can be found in its manual [32].

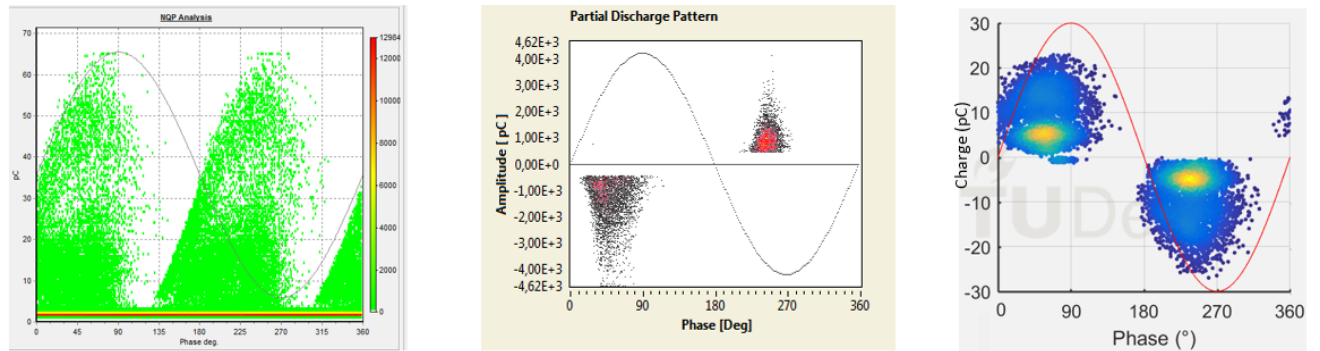


Figure 3.16: (a) PRPD pattern from DDX9101 PD Detector (b) PRPD pattern from Techimp PD Detector (c) PRPD pattern from PDFlex from signal captured using DPO7354C oscilloscope

The first measurement device of Haefely 9101 is only used for electrical PD detection while testing different setup for producing the surface discharge at oil-rubber interface. The rest two instrument: (two) Techimp and high end oscilloscope (separately) were used for simultaneous measurement of PD from both electrical and optical sensor. Hence, most of the testing and recording are done using these two measurements system. The analysis of the data obtained is mostly done using the PDFlex software. In order to give the reader clear picture of which signals or PD pattern is obtained from which measurement units, 3 PRPD pattern from each one (Haefely, Techimp and oscilloscope) are displayed in Figure 3.16. This will clarify and avoid the repeatability of mentioning which pattern is recorded from which measurement units throughout the report.

3.4. Finalized circuit for electrical and optical detection

After the selection of optical sensor and reviewing all the electrical sensors and measurements units that have been used throughout the testing phase, this section presents the finalized circuit diagram that is used in this thesis for simultaneous partial discharge measurements through electrical and optical means. Figure 3.17 display the circuit diagram of the finalized circuit.

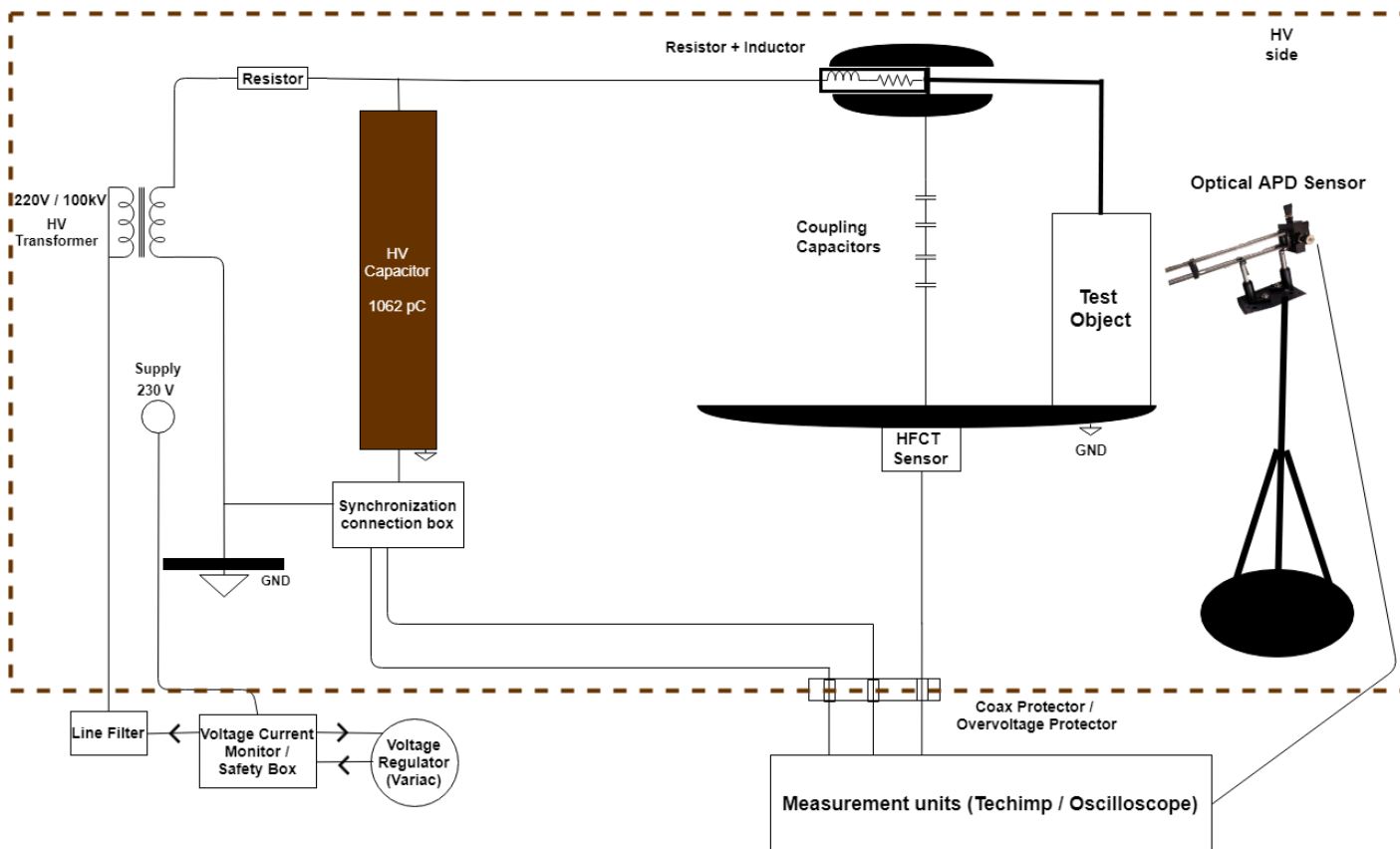


Figure 3.17: Finalized Circuit diagram for PD detection

The autotransformer or variac is used to change the voltage from 0 to 230 V according to the requirement. The safety box is connected to the variac in order to protect the system in case of any failure or overcurrent situation. The safety box switch off the voltage at overcurrent situation or due to fence opening during testing. This connection is then passed to HV transformer through a filter. The damping resistor is used to reduce the energy transferred to the test object in case of breakdown and also to suppress any unwanted disturbance from HV side. A HV capacitor is used in order to give input signal to the synchronization box whose function is already explained in previous section. The HV capacitor act as C1 and synchro-

nization box has C2 which is the capacitor at low voltage (both together act as voltage divider and thus the reading is taken from C2 i.e from lower voltage part). The output from the synchronization box are: phase signal (sawtooth) and the voltage to the multimeter monitoring the HV side according to the voltage applied by variac (LV side). The HV side is connected to the test object through inductor and resistor box along with the coupling capacitor in parallel. The blocking inductor is also placed along with resistor to block any unwanted disturbance from supply side. Four coupling capacitor each of 2 nF are used since upto 40 kV of voltage is achieved during testing process. The HFCT sensor for electrical detection is placed just below the ground plate with connection to the coupling capacitor. All the connection to the measurement unit are made by coaxial cable through coax protector/overvoltage protector (spark-gaps and TVS diode). The plates are round in profiles to avoid high electric field concentration and any sharp point or edges in vicinity of the test setup is avoided. The optical sensor is aligned in front of the PD source according to the length calculated previously. The output of the APD sensor is fed directly to the measurement system through coaxial cable. The measurement units shown in the circuit diagram can be any one of the instruments explained in the previous section. However, for simultaneous measurements mostly high performance Tektronix DPO7354C oscilloscope is used.

Test setup design and oil sample preparation

This chapter will give a detailed explanation of the different techniques adopted in order to create surface discharge at the rubber-oil interface. All methods and results tried in this research are presented. Only electrical detection methods were used in order to identify surface PD pattern as it is important to have a proper, reproducible setup to finally conduct experiments with optical sensors. At last, the oil sample preparation procedure with different level of moisture content is also described.

4.1. Test setup design to produce surface discharge

The oil-filled termination during the operation might face the problem of moisture ingress if it is not installed properly. During the inspection of such a case, it was revealed that the surface of the stress cone is highly damaged due to water contamination of oil. The damage of the stress cone surface can be replicated by conducting surface discharge experiments on the same material i.e rubber from the stress cone in the presence of the same insulation oil which is used in oil-filled cable terminations. The real size of the termination with stress cone and a large amount of oil setup for creating the surface PD was not feasible, and thus a small setup had to be designed in order to approximately represent what happens under real condition. The past thesis work and report [6] also describes some measures taken for creation of PD but creating surface PD with this thick viscous oil remained a challenge. With the research conducted in this thesis, finalized setup which is able to create surface discharge is short-listed after many tests conducted. There are different tests performed which are summarized in Table 4.1 and explained in the corresponding paragraphs.

Table 4.1: Summary of methods examined to produce surface discharge setup

4.1.1 Different orientation of electrodes and samples	<ol style="list-style-type: none"> 1. Cylindrical electrodes 2. Needle electrodes
4.1.2 Design of electrodes	<ol style="list-style-type: none"> 1. Design 1: Introduction of side electrodes 2. Design 2: Two electrodes on the top of the rubber sample
4.1.3 Introduction of foreign particles on the surface of the rubber sample	<ol style="list-style-type: none"> 1. Gold sputtering 2. Salted sample 3. Conductive paint

Before testing any setup, the oil with the sample in the bucket was placed in the vacuum chamber in order to get rid of any air bubbles. The electrodes were placed carefully at the start of each experiment so that fewer air bubbles were introduced. If more air bubbles are present due to insertion of electrodes, the setup was left for a day or two before starting an experiment, therefore making sure that no air bubbles are causing any PD activities in our setup.

4.1.1. Different orientation of electrodes and samples

The experiment to produce surface PD on the rubber sample in the oil insulation was started with electrodes which were already present in the HV laboratory at TU Delft. The rubber and oil sample were supplied by Prysmian Group. Different design of electrodes with different size and shapes of rubber sample were used as explained below.

1. **Cylindrical electrode:** A cylindrical electrode made of stainless steel of dimension 21 mm in height and 30 mm in width was used in the experiment. The corners of the electrode were properly smoothened to avoid any sharp turns or edges. The rubber sample was cut circular in shape with 50 mm of diameter and 17 mm of height. The high voltage was connected to the electrode and the bucket bottom part was grounded. Figure 4.1 shows different positions of the electrode tested with the rubber sample. The insights gained from this experiment with the mentioned configuration was that the surface discharge on the rubber is created if the tangential electric field along the surface of the rubber sample is high. The idea of trying varies position was to increase the stress level on the rubber interface. Figure 4.1b was tried in order to increase tension on the rubber sample (i.e the part indicated) which is in between HV and ground electrode. To provide a more sharp point for the rubber in between, the electrode was moved as shown in Figure 4.1c.

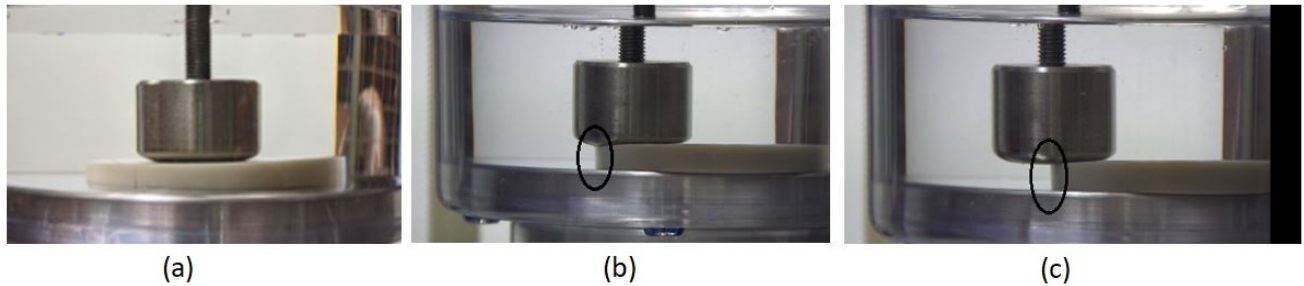


Figure 4.1: Experiments done with cylindrical electrodes at different positions

COMSOL 2D electrostatic simulation was also performed as shown in appendix B Figures B.1, B.2 and B.3 to get an idea of the electric field distribution of the different orientation that we tried experimentally. The permittivity of the rubber sample and oil was assumed as 3.1 and 2.1 respectively. The potential was applied to the electrode (10 kV in the simulation shown) and the bottom plate was grounded. The electric field at triple point (rubber, oil and HV electrode) has the highest field strength.

The voltage was applied at intervals from 0 to 40 kV with stepwise increase. No PD activities were detected with these orientations. However, the same setting in air resulted in high pC of surface discharge but due to the thick viscous oil, getting any PD activities with these orientations were very difficult. At last, after few minutes, the breakdown in oil was observed as seen in Figure 4.2 at 40 kV. However, through *COMSOL* simulation it was clear that electric field was almost uniform throughout the area starting from the stressed rubber interface at the edge of the electrode in the oil to the ground. Experimentally, the interface between the rubber-oil was stronger than the oil and thus the breakdown happened in the oil between the electrodes.

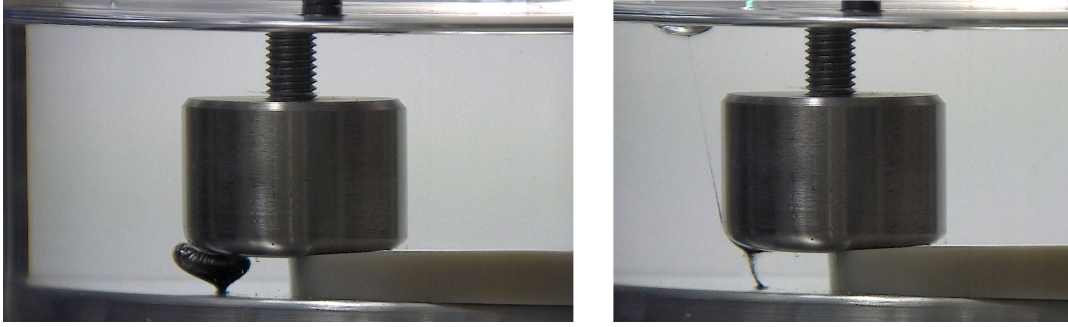


Figure 4.2: Breakdown in the oil

2. **Needle electrodes:** To increase the electric field on the surface of the rubber sample, much sharper electrodes were preferred as shown in Figure 4.3. The experiments were conducted with needle shaped electrodes (different thickness) along with different orientation, size and shape of rubber samples. The more detailed sketch of the setups with needle electrode configuration is presented in appendix B Figure B.4.

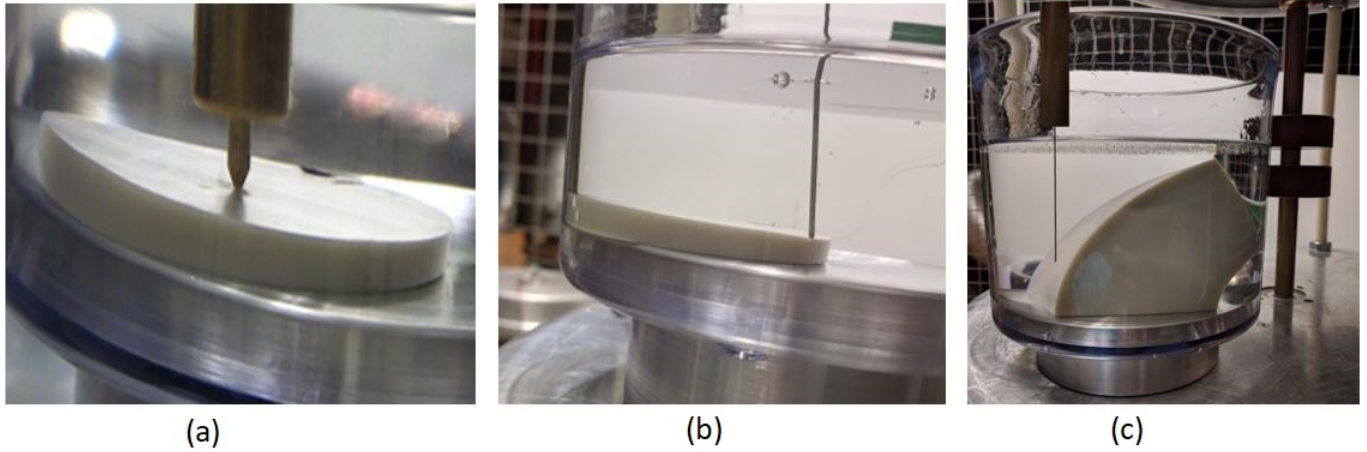
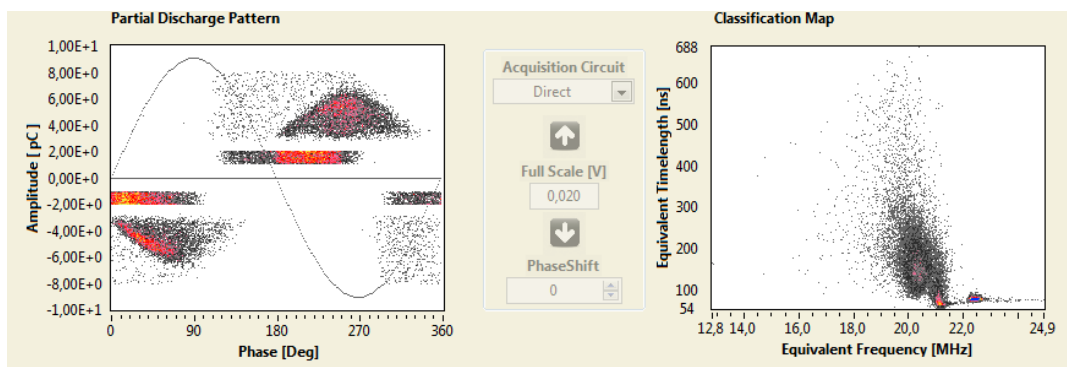


Figure 4.3: Experiments with different needle electrodes configurations

Considering the needle electrode shown in Figure 4.3a, the voltage was increased gradually from 0. At 25 kV as observed from the pattern presented in Figure 4.4, the PD activities were seen after the voltage was applied for 2 hours continuously.

Figure 4.4: PRPD pattern observed at 25 kV from 1st needle configuration (shown in Figure 4.3a)

It is clear from the pattern shown below that two types of discharges were taking place, one being internal and another on the surface of the rubber (can be floating too). The

internal discharge took place due to damage that the needle was causing to the rubber at high voltage. The possibility of having tree formation and a complete breakdown was high. Therefore, continuing with this electrode was not an option. Another configuration with the needle was tried as shown in Figure 4.3b in which the surface of the rubber between the HV needle and ground was aimed to be stressed. As observed from PRPD pattern presented in Figure 4.5, the surface discharge like pattern was definitely observed at 15kV when the voltage was applied for 15 minutes continuously. However, while testing it was observed that the PD activities were not so constant and the surface of the sample in contact with the needle was also deteriorating significantly.

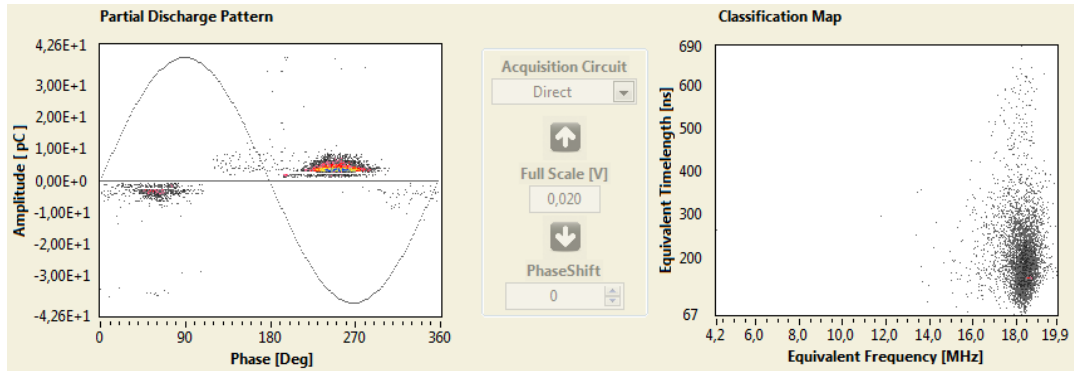


Figure 4.5: PRPD pattern observed at 15 kV from 2nd needle configuration (shown in Figure 4.3b)

Finally, the configuration displayed in the Figure 4.3c was tried. The different positioning of the rubber with much wider width was tested with the needle electrode. The idea behind this test setup was to get discharge across the sample. The needle was used in order to get high electric field due to a sharp point which would trigger the start of electrons along the surface of the rubber. The voltage was increased gradually till 42 kV and PD pattern as observed in Figure 4.6 was recorded.

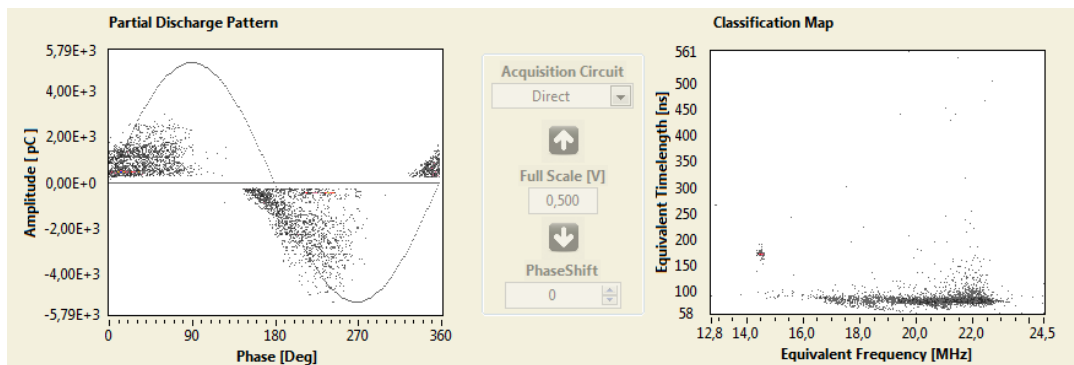


Figure 4.6: PRPD pattern observed at 42 kV from 3rd needle configuration (shown in Figure 4.3c)

Just after 2-3 minutes of the PD activities, a flashover from the needle to the ground as displayed in Figure 4.7a took place. After the inspection, it was confirmed that the pattern recorded was surface discharge as the treeing effect on the rubber surface was noticed as shown in Figure 4.7b. However, the needle electrodes along with these orientations, as shown above, showed the potential of producing surface discharge but it was not consistent and easily reproducible as oil needed to be changed each time the breakdown takes place. Furthermore, for the last setup, the time lag between the start of PD activities and the final breakdown was few minutes as a result capturing it with the optical sensor in order to obtain data for analysis in such short time would also be a challenge. Therefore, more options for test setup producing the surface discharge had

to be investigated.

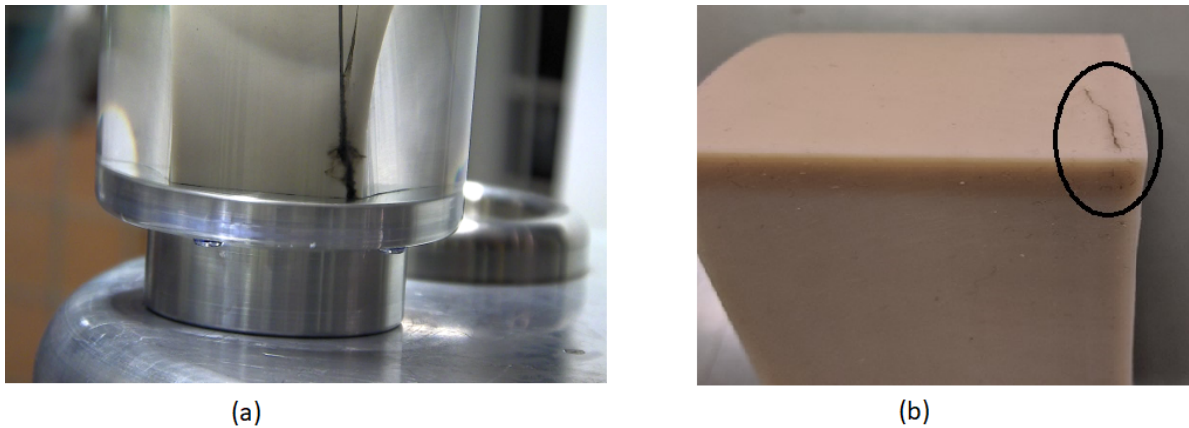


Figure 4.7: (a) Breakdown at 42 kV (b) Treeing observed on rubber sample during inspection

4.1.2. Design of electrodes

After trying all the existing electrodes, new test setup had to be designed to get a stable surface discharge. After design in *AUTOCAD* and simulation in *COMSOL*, there were two setups finalized designed by Termorshuizen as explained below.

1. **Design 1: Introduction of side electrodes:** The main aim of this setup was to stress the surface of rubber sample by introducing the side ground electrode. The testing with rubber sample as described in the previous section above lead to quick breakdown through the sample itself. Therefore, the main focus of the test object was to avoid flashover or breakdown through the sample as well as initiate surface discharge through sharp electrode towards the ground electrode which is placed at the side of the sample as shown in Figure 4.8 thereby also reducing the distance between HV electrode, sample and ground. The increase in tangential field at the oil-rubber interface due to introduction of side electrode can be observed through plot presented in appendix B Figure B.5 (without side ground electrode) and B.6 (with side ground electrode).

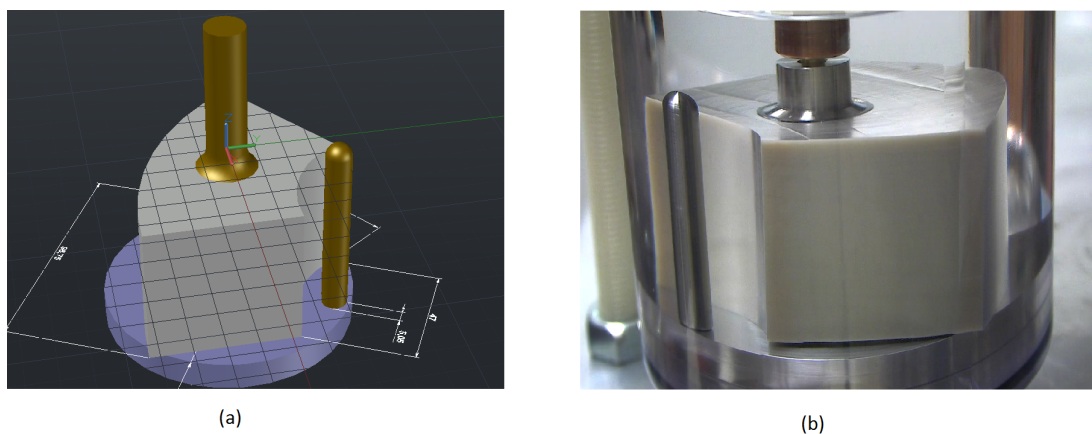


Figure 4.8: (a) Model prepared in AUTOCAD (b) Test setup for experiments

As can be observed from the Figure 4.8, the side electrode is grounded along with the bottom of the container. The height of the side ground electrode is kept little higher than the rubber sample and also the edge of the electrode is smoothened to avoid any field enhancements. Different design for the electrodes with varies angle of contact with sample was tried and simulated in order to get the best combination with the side

ground electrode. Finally, the new circular electrode was designed with stainless steel of diameter 25 mm with sharp edges to provide the high electric field with the side ground electrode. The electrode was designed circular in shape in order to reuse it from another side if the breakdown with side ground electrode caused damage to the edge of the circular electrode. The final setup (as seen from Figure 4.8b) was tested after keeping it in the vacuum chamber in order to avoid any air bubbles. The voltage was increased gradually and approximately at 35 kV, PD pattern displayed in Figure 4.9 was recorded.

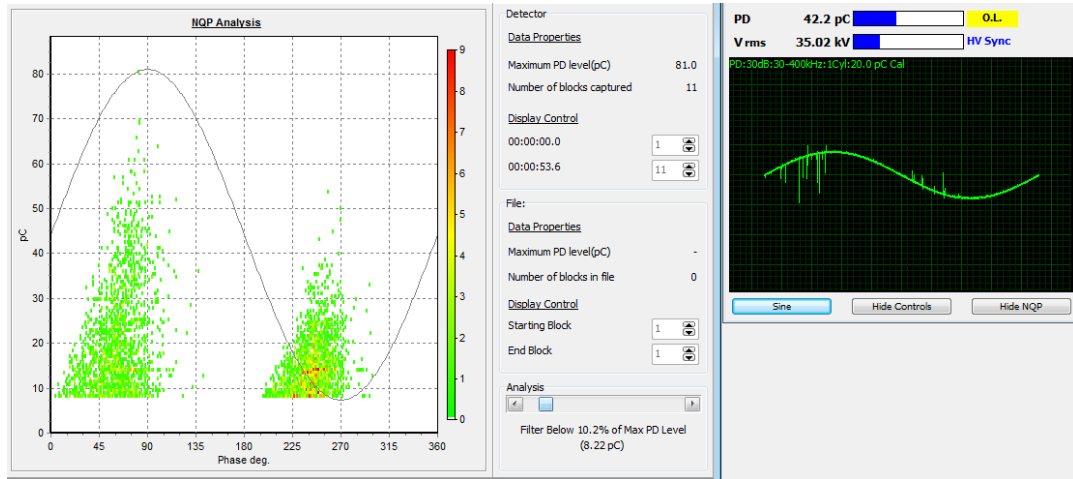


Figure 4.9: PD pattern at 35 kV

Observing the PRPD pattern, it can be either surface or internal discharge or can be a combination of both. The voltage of 35 kV was applied for 15-20 minutes and consequently, the breakdown in the setup was observed as shown in Figure 4.10a. This looked more like a surface discharge. However, during the investigation, it was found that the breakdown did not happen through the surface but happened inside the sample as can be observed in highlighted part in Figure 4.10b. The treeing activity started on the surface but the path was built through the sample.

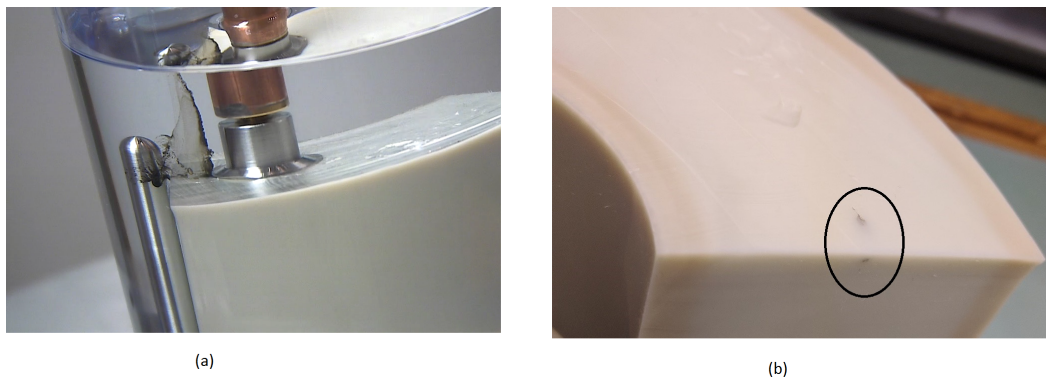


Figure 4.10: (a) Breakdown at 35 kV (b) Breakdown path viewed after the inspection

2. **Design 2: Two electrodes on the top of the rubber sample:** In the previous design of the setup, it was observed that the side electrode was exposed to whole rubber sample, as a result, the electrical stress was equal on both the surface of the sample and through the sample close to the surface. It was noticed that the breakdown took place from HV electrode to ground electrode through the sample close to the surface. Therefore, with modification it was tried to electrically stress only the surface of the sample rather than

the whole sample. Figure 4.11a shows the test setup prepared. Both the electrodes are identical: one is connected to HV side and other is grounded with the wire to the bottom of the container as shown. Figure 4.11b shows the COMSOL simulation showing the potential as well the electric field line plot for the same setup in 2D.

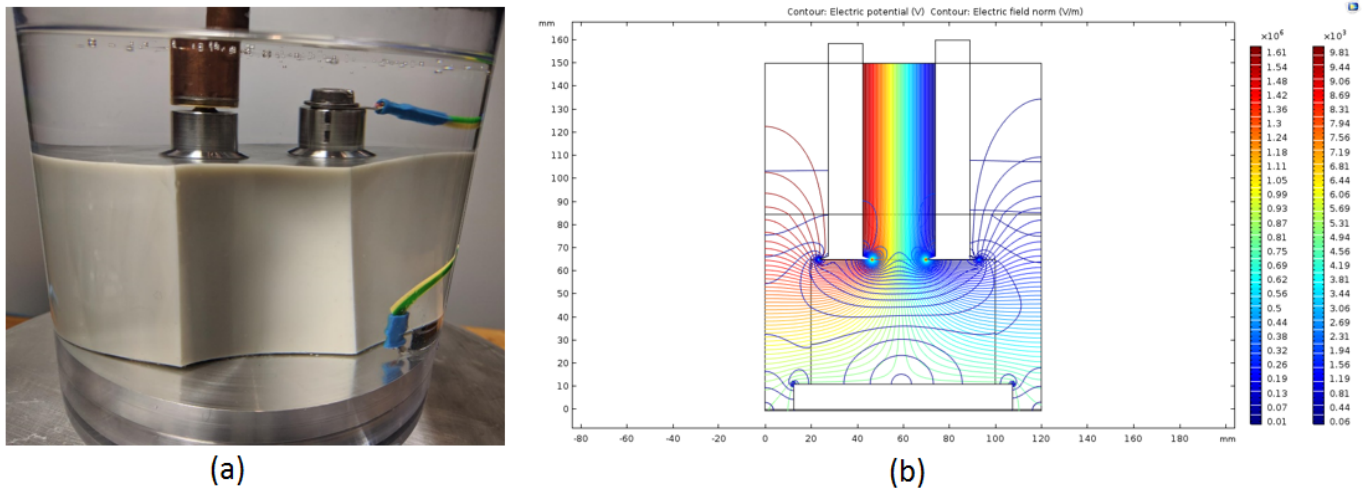


Figure 4.11: (a) Setup of design 2 (b) 2D COMSOL Simulation of the setup with potential and electric field plot

The voltage was increased gradually from 0 in steps of 5 kV at every 10 minutes. At 45 kV, there was a sudden breakdown without indication of the PD. Therefore, the experiment was repeated without any change and then the PD pattern at 6 kV was seen as displayed in Figure 4.12. The voltage was increased to 11 kV and within few minutes breakdown took place as observed in Figure 4.13.

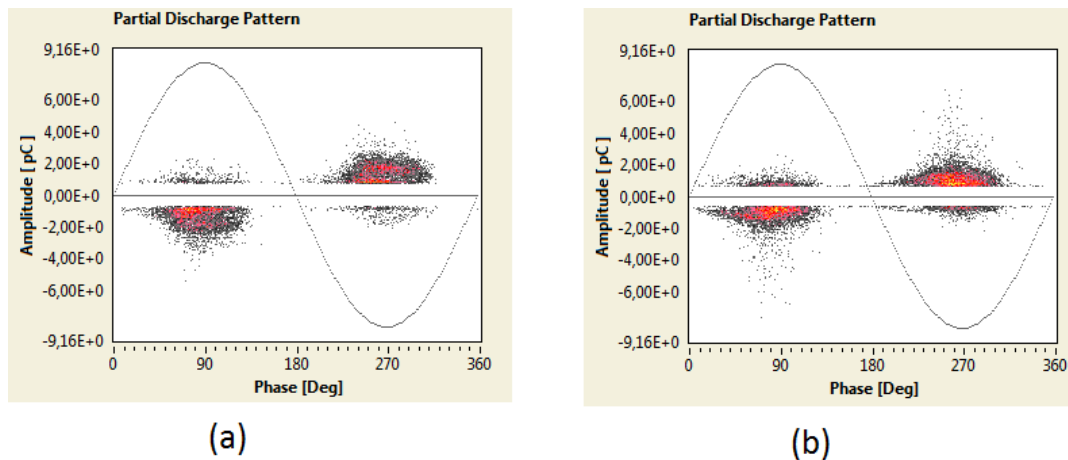


Figure 4.12: (a) PRPD pattern at 6 kV (b) PRPD pattern at 10 kV

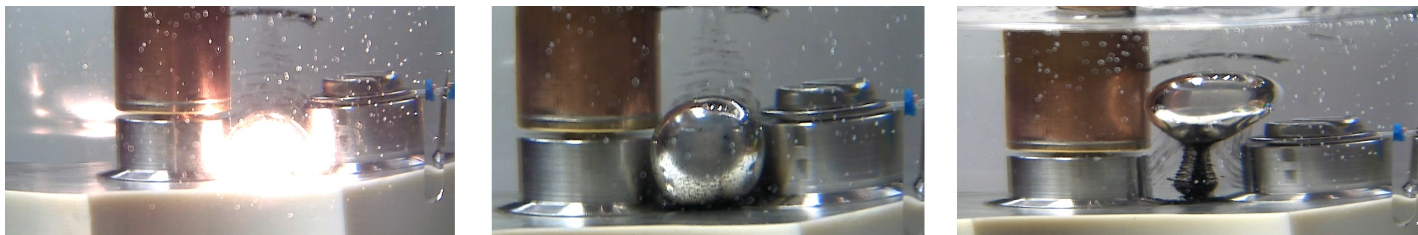


Figure 4.13: Breakdown at 11 kV

During the inspection, the damage on the rubber sample in the area between the electrodes was observed as shown in Figure 4.14. The small electric tree was also observed on the surface of the rubber. Therefore, it was concluded that the second design is able to give surface discharge on the rubber sample in the oil insulation. Also, it is evident with the PRPD pattern recorded as displayed in Figure 4.12.

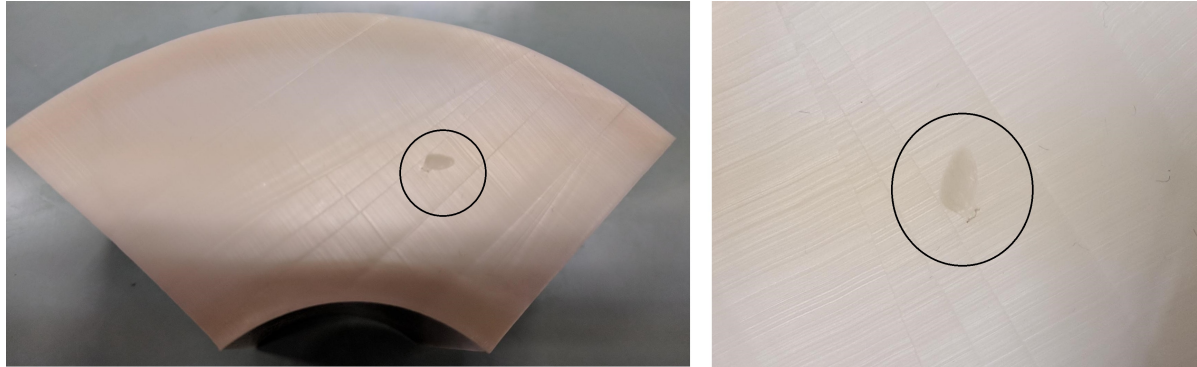


Figure 4.14: Damage and electric treeing observed on the rubber sample

4.1.3. Introduction of foreign particles on the surface of rubber sample

Different procedure were also explored in order to enhance the partial discharge process on the rubber sample in the oil medium. In order to do so, foreign particles in contact with the surface of the rubber sample were used. The idea was to use these foreign particles which will cling to the surface of the sample as a conductive floating particle which would enhance the PD activities. The plan to use this technique was not only to get PD activities for longer time but also to avoid the breakdown and change of sample every now and then. Different elements were used such as copper tape, gold deposit, salt and conductive paint which are explained hereafter.

1. **Gold sputtering:** The gold deposit was placed on the surface of the rubber sample using the gold sputtering machine as shown in the Figure 4.15a. Sputtering is the process by which the conductive particles are ejected from the target material to the sample on which we want the layer (mechanism illustrated in Figure 4.15b). In this experiment the sample was rubber from stress cone and the target was gold. The area where the layer of gold is required is exposed whereas rest of the area of the sample is covered by the mask. The end result from the machine is displayed in the Figure 4.15c.

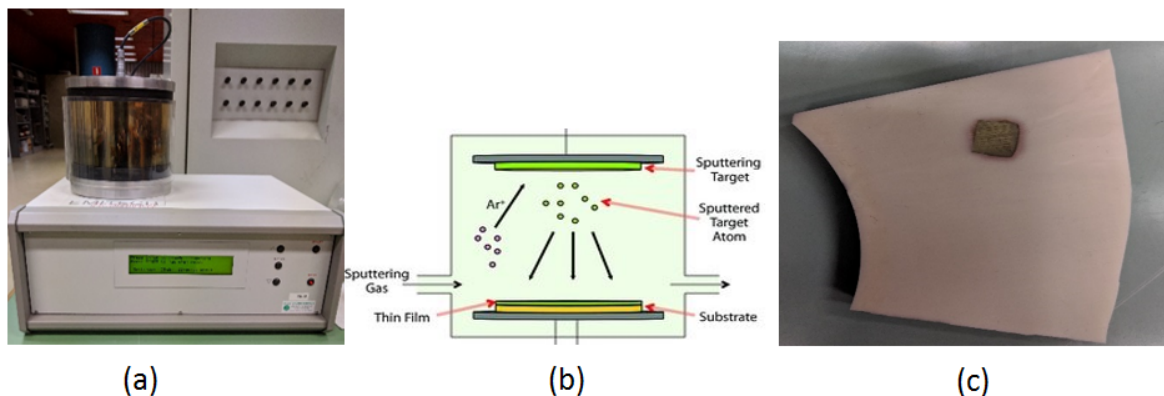


Figure 4.15: (a) Gold sputtering machine (b) Gold sputtering mechanism (c) Gold deposited sample

The sample was placed in the oil with the circular electrode kept near the gold deposit as shown in the Figure 4.16a. The high voltage was applied to the circular electrode.

The voltage was increased gradually in step of 5 kV with interval of 10 minutes. At 37 kV, PRPD pattern shown in Figure 4.16b was recorded. As can be observed, the PD magnitude is quite low and it also had very low repetition rate. The distance between the HV electrode and gold deposit was decreased and then a lot of PD activities was observed. However, the gold deposit was having some reaction with the electrodes placed very close, as a result, some bubbles formation also took place. This method was hence not considered further for the creation of surface discharge.

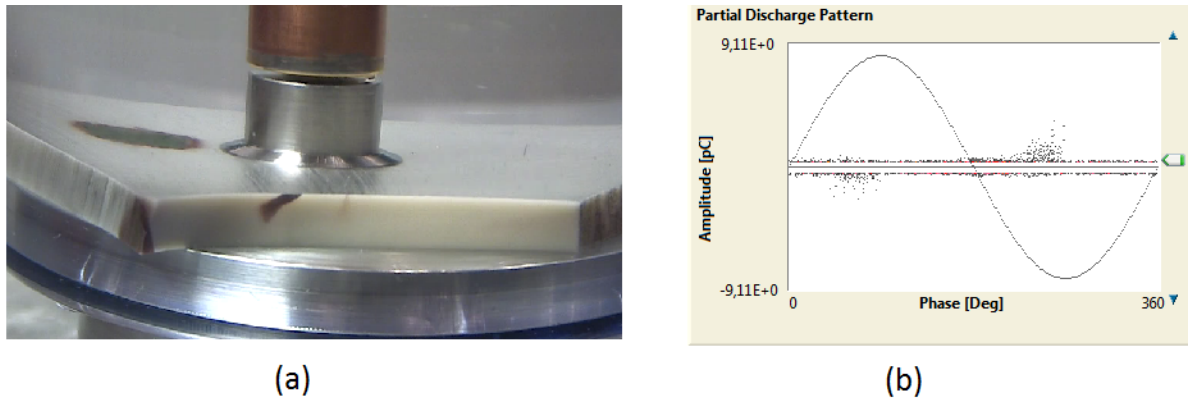


Figure 4.16: (a) Test setup with Gold deposit sample during experiment (b) PD pattern recorded at 35 kV

2. **Salted sample:** Another foreign particle used was salt as illustrated in Figure 4.17. The salt water was sprayed all over the sample and left for 4-5 days for the salt to dry on the surface of the rubber sample. Then, the sample was cleaned with dry tissues and placed inside the termination oil for testing. The idea of using salt water over the surface of the rubber is to degrade the sample so that surface PD can be obtained easily. However, the dried salt particles should be cleaned properly before placing it in the oil, as the salt particles can contaminate the oil and floating PD can also be observed. Therefore, it is important to make sure the sample is cleaned properly.

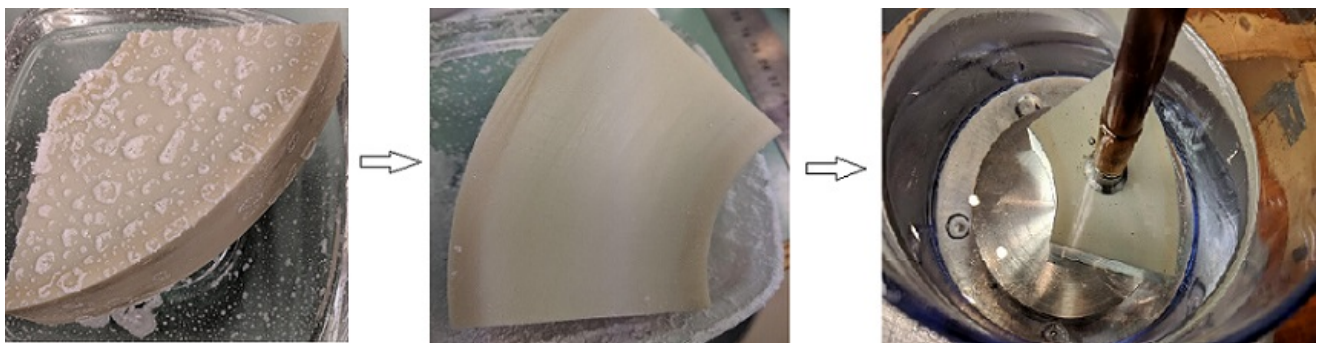


Figure 4.17: Process for creating salted rubber sample

The circular electrode was placed on the surface of the rubber sample and voltage was applied from 0. The inception voltage was 9.1 kV. The PD pattern obtained from the sample at 15 kV and 25 kV is shown in Figure 4.18. Using this technique, the surface discharge on the rubber in the presence of oil can be easily demonstrated. Although, preparation of these types of samples consumes time and proper precautions have to be taken to prevent contamination of the oil with salt particles.

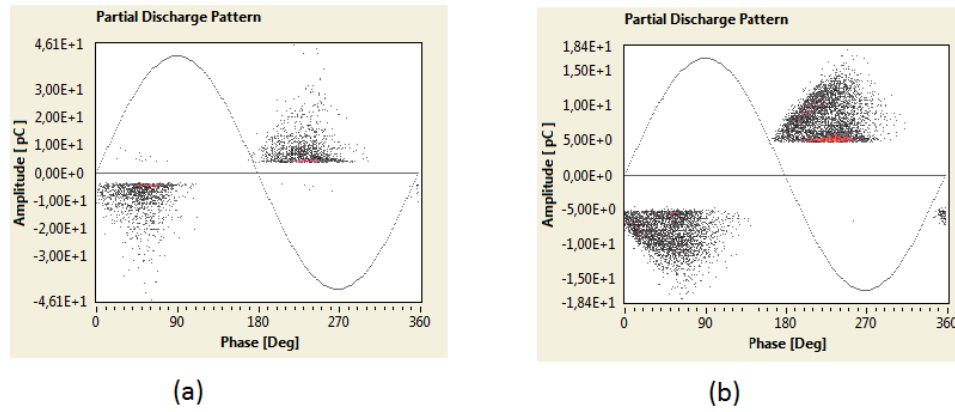


Figure 4.18: (a) PRPD pattern recorded at 15 kV (b) PRPD pattern recorded at 25 kV

3. **Conductive paint:** The silver conductive paint was applied to the surface of the rubber sample and was left for few hours to dry as seen in Figure 4.19. The dried sample was then placed in the oil. The electrode was placed at the proper distance from the conductive paint. The idea behind using the conductive paint is same as that of gold sputtered sample used previously. Different size and different electrodes such as cylindrical electrode, boot shaped electrode (electrodes used in last research [6]) was tried. However, the circular electrode design was finally used as it gave the better contact with the rubber sample compared to other electrodes and also adjustment of electrode around conductive paint was easy due to structure.



Figure 4.19: Experiment with conductive paint deposit on rubber sample

The distance between the electrode and conductive paint was approximately set. The voltage was increased gradually from 0. The PD signals were observed starting from 13 kV. The PD pattern observed with this setup at 15 kV and 25 kV is presented below in Figure 4.20 a and b respectively.

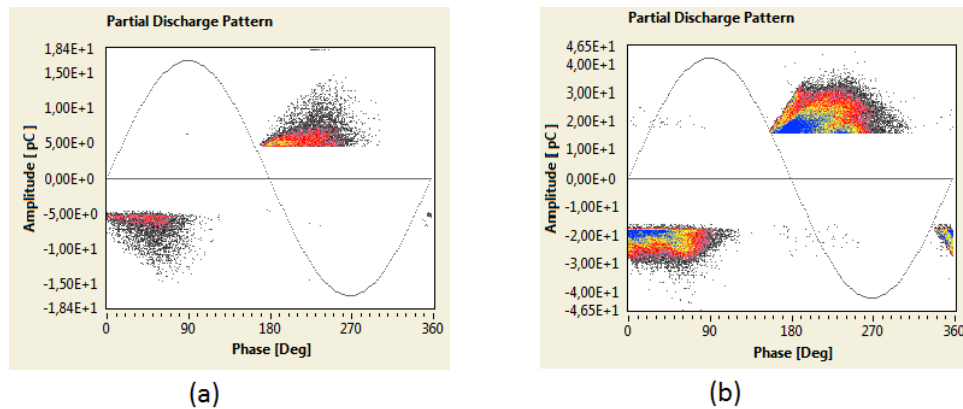


Figure 4.20: (a) PRPD pattern recorded at 15 kV (b) PRPD pattern recorded at 25 kV

Compared to the gold sputtered samples, these conductive paint samples gave surface discharge at much lower voltage as well as the magnitude and repetition rate was also higher.

4.2. Finalized setup/Conclusion

Seven steps were created each with some variants. The steps taken and the results are explained briefly in the previous section for each technique used. The methods successful in creating surface discharge on the rubber sample in the oil insulation are:

1. Needle electrode (3rd configuration)
2. Design 2: Two electrodes placed on the top of the rubber sample
3. Salted sample with circular base electrode
4. Conductive paint sample with circular base electrode

The first two techniques (suitable electrode configurations): needle and two electrodes on the top produce surface discharge at higher voltage of 35 kV. Furthermore, the time lag between the start of partial discharge and complete breakdown between the electrodes was few minutes. As a result, the reusability of these two setup will be time-consuming and challenging as the sample and the oil need to be changed after each breakdown. Also, the recording of data due to PD produced by these setup using the optical sensor in a short period of time will be difficult. The salted sample and conductive paint sample with circular base electrode are easily reproducible and there is very low chance of breakdown in the sample and oil. In fact, the breakdown in the sample can be completely avoided by using thicker sample. Finally, **conductive paint sample with circular base electrode** was finalized for producing surface discharge on the rubber sample due to less preparation time compared to the salted particles. Furthermore, the shape, pattern and size of conductive paint applied on the surface can be easily changed. The samples shown in Figure 4.21 were prepared for further testing of surface discharge in oil with optical sensors. The conductive paint size is similar to the object size mentioned in chapter 3 so that it can easily lie within the optical sensor range of detection.

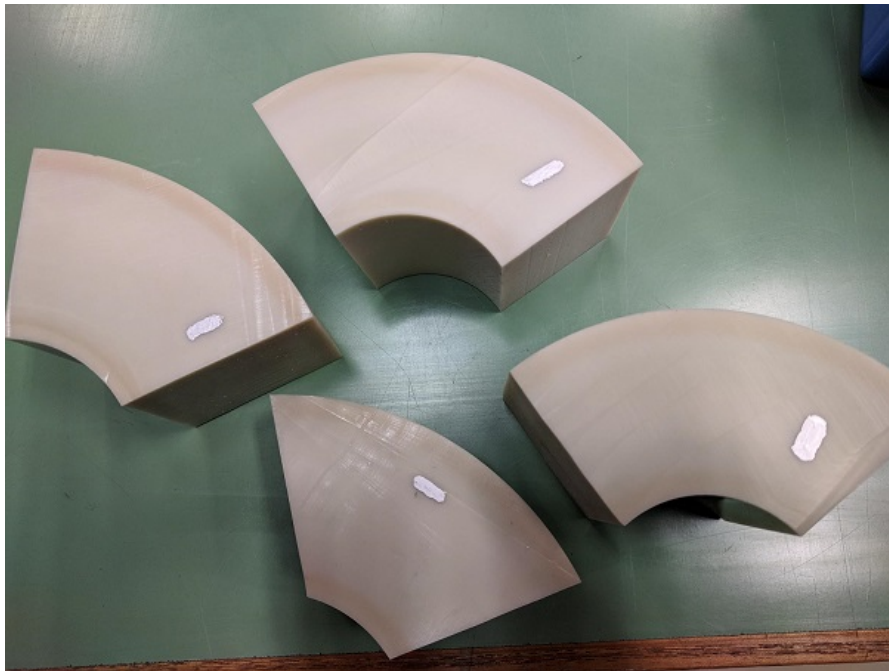


Figure 4.21: Finalized sample used for final measurements in this project

4.3. Oil sample preparation

The measurement of the partial discharge was not only done using the dry oil but also done using contaminated oil. The potential problem in actual oil-filled termination is mainly due to water ingress, therefore measurement of surface discharge at different level of moisture content in the oil had to be performed. This section explains the preparation of the oil sample with added moisture along with moisture measurement technique used in this thesis.

The climate chamber as shown in the Figure 4.22 of the HV lab, TU Delft, was used in order to prepare different oil samples. The device uses demineralised water for the humidifying process. The temperature and humidity level in the device is set and accordingly the addition of moisture inside the oil takes place. The dispersion of moisture also depends on the exposed area of oil inside the climate chamber and weight of the oil. The temperature inside the climate chamber while preparing the oil is always kept at higher degree (60°C) in order to reduce the viscosity of the oil so that the moisture can easily penetrate in the oil.



Figure 4.22: Climate chamber used for oil sample preparation of different moisture level (water activity)

Three samples were prepared with different level of moisture content. The container used for preparing all the oil sample was the same. The container is indicated in the Figure 4.22. The setting used for preparation of these three oil sample is mentioned in the Table 4.2.

Table 4.2: Settings used for preparation of different oil samples

Sample No	Temperature	Relative Humidity	Time	Weight of the sample	Area exposed
Sample 1	60° C	75%	52 hours	1.3 kg	14 cm circular diameter
Sample 2	60° C	50%	24 hours	1.44 kg	14 cm circular diameter
Sample 3	60° C	50%	12 hours	1.18 kg	14 cm circular diameter

4.3.1. Measurement of water content in the prepared oil sample

The amount of water content inside the sample should be known in order to perform any further analysis. Therefore, the water content in all these three samples prepared was measured using Vaisala HUMICAP device as shown in Figure 4.23. The Vaisala sensor is made of the capacitive thin-film polymer sensor having 4 layers namely: upper electrode, thin-film polymer, lower electrode and glass substrate. The probe MMP78 contains the sensor at the tip which comes in direct contact with the oil to be measured. Its operating temperature is -40°C to $+60^{\circ}\text{C}$. The sensor in the probe needs to be connected to the MI70 indicator for recording the measurements. MI70 operates at -10°C to $+40^{\circ}\text{C}$. This device gives the content of the moisture in the oil in terms of water activity. The indicator measures the temperature and water activity of the oil. The water activity indicates values from 0 to 1. 0 represents dry sample (no presence of water) and 1 represents saturated sample (oil is saturated with water). This measured by Vaisala for each sample indicate how close the oil is from getting saturated (1). The MI70 indicator has the capacity to store 1356 data points.

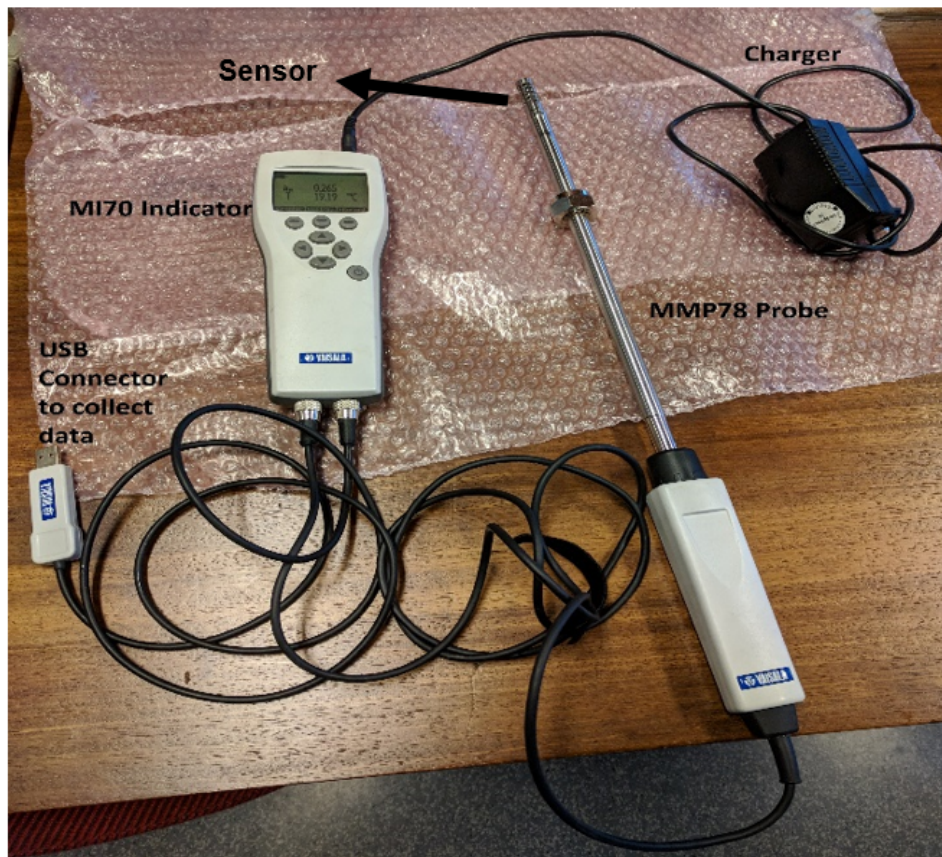


Figure 4.23: Vaisala MI70 indicator and MMP78 probe

A small quantity of the oil sample was taken out from the vessel and was placed in the tiny container for three samples prepared as shown in the Figure 4.24a. Each sample was then measured as shown in the Figure 4.24b. The holder was used in order to hold the probe at a constant position. The probe was dipped into the oil sample. It has to be made sure that the pores of the sensor should be completely dipped in the sample. The sensor is placed at the bottom of the probe. The sensor should be kept in the sample for 15-20 hours for measuring and recording of the water activity so that the thick oil can completely penetrate into the sensor making the reading more accurate and stable. Any exposure to the outside environment is prevented by wrapping the top of the flask with plastic wrap. It clings to the surface and remains tight throughout the cap of the flask without adhesive.

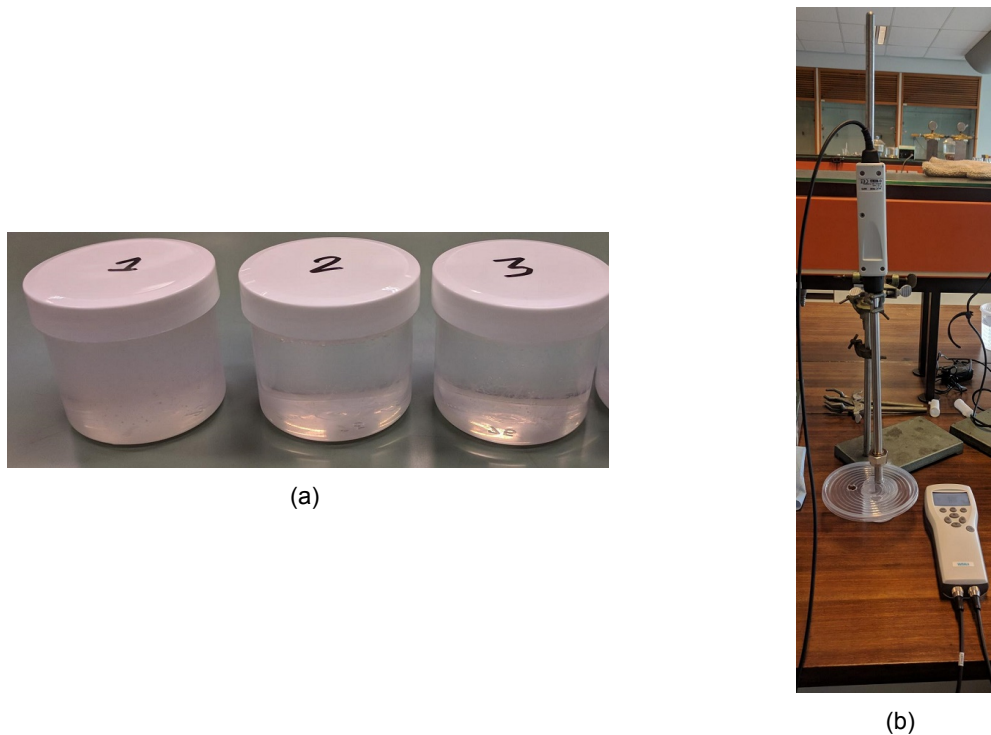


Figure 4.24: (a) Sample collected for water activity measurement (b) Oil sample measurement using Vaisala

The temperature and the water activity was recorded for each sample. Then, the recording was transferred and the average value was considered for each sample. Similarly, the measurements for sample 2 and 3 were also recorded. The stable average value of three sample is mentioned in Table 4.3.

Table 4.3: Water activity measured for different oil samples

Sample No	Water Activity
Sample 1	0.82
Sample 2	0.69
Sample 3	0.58

The reading is captured by MI70 indicator and is opened using *Vaisala MI70 link* software. The reading can be summarized in form of a graph also as shown in Figure 4.25. This graph is for sample 1 and the average value of the reading is taken. Similarly, graphs for sample 2 and 3 are shown in the appendix B Figure B.7 and B.8, respectively.

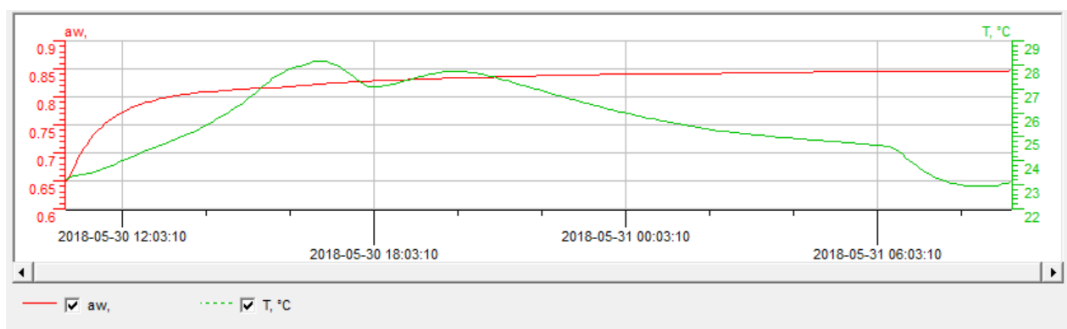


Figure 4.25: Vaisala measurements for sample 1

Measurement and results from electrical and optical PD detection

This chapter is dedicated to partial discharge measurements using both electrical and optical sensors. APD130A2 optical sensor is introduced for the first time in the field of partial discharge measurement, therefore, preliminary tests (such as corona and surface discharge in air) using the optical sensor simultaneously with the electrical detector were done. Finally, the surface discharge detection results using both electrical and optical detector in dry as well as in contaminated oil (oil with added moisture content) with the finalized setup obtained in the previous chapter are presented. The circuit diagram described in chapter 3 in Figure 3.17 is used throughout the measurement.

5.1. Preliminary testing with optical sensor

This section describes the measurements done for corona discharge and surface discharge on rubber sample in the air simultaneously using both electrical and optical detector. The measurements taken using both Techimp and high performance oscilloscope is presented.

5.1.1. Corona Source

The sharp needle as shown in the Figure 5.1 was used to produce corona discharge for detection.

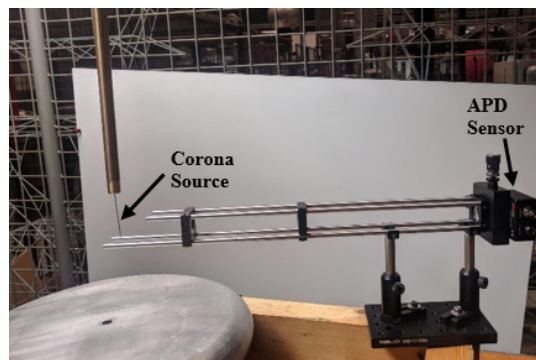


Figure 5.1: Corona source setup

The optical sensor was placed at approximately 600 mm from the needle to get the most efficient result as described in positioning calculation in the section 3.2.2 in chapter 3. The needle tip from where the discharge activity starts was aligned in the centre of the cage plate as seen from the Figure 5.1 to make sure that most of the light falls on the lens. The HFCT

was placed along with the coupling capacitor as described in the circuit diagram in the last section of chapter 3.

Measurements done using Techimp: Two Techimp instruments one for electrical sensor and one for the optical sensor was used. Partial discharge inception voltage (PDIV) of corona discharge with the setup shown above was 5.7 kV for both detectors. The waveform is shown in Figure 5.2 was captured at the same instant by two Techimp instruments at a voltage of 6.8 kV.

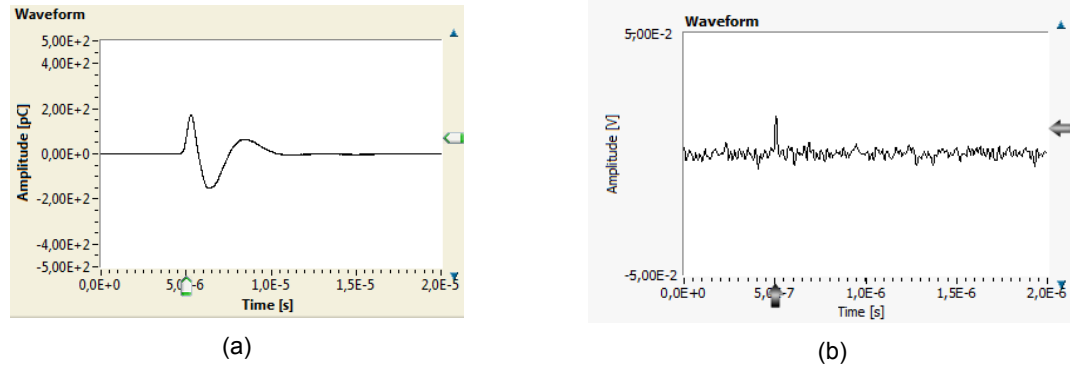
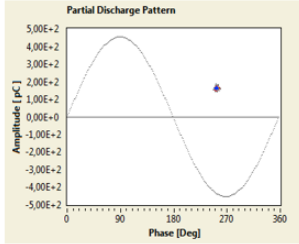
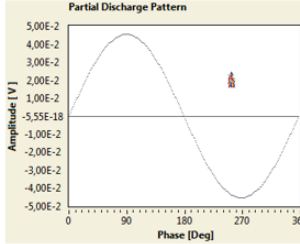
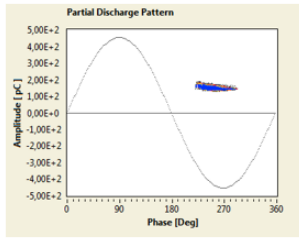
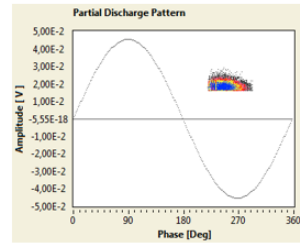


Figure 5.2: (a) Current pulse observed by electrical detector at 6.8 kV (b) Voltage pulse observed by optical detector at 6.8 kV

Table 5.1 exhibits a short comparison of the measurement taken by both the detector. As can be observed, the PDIV values and PRPD ¹ pattern recorded at different voltage are almost comparable. The repetition rate (average number of pulses per period) for both the measurement device is almost same which gives an indication that both sensor response at the same rate for the corona discharge.

Table 5.1: Comparison between electrical and optical measurements from corona source using Techimp device

Parameters	Electrical Measurement	Optical Measurement
Inception Voltage	5.7 kV	5.7 kV
Repetition Rate at 6.8 kV	8.82	8.93
PRPD pattern at 5.8 kV		
PRPD pattern at 8.12 kV		

¹PRPD pattern measured from electrical detector should be negative. However, polarity here is positive due to an internal property of Techimp PD detection technique explained in [30].

Measurements done using oscilloscope Tektronix DPO7354C: The measurements were also done using high end oscilloscope in order to see the pulse at same window at the same time instant. One oscilloscope with three channel: phase signal (sawtooth signal), electrical signal and optical signal were used. Figure 5.3 displays the signals of corona discharge taken at 9 kV.

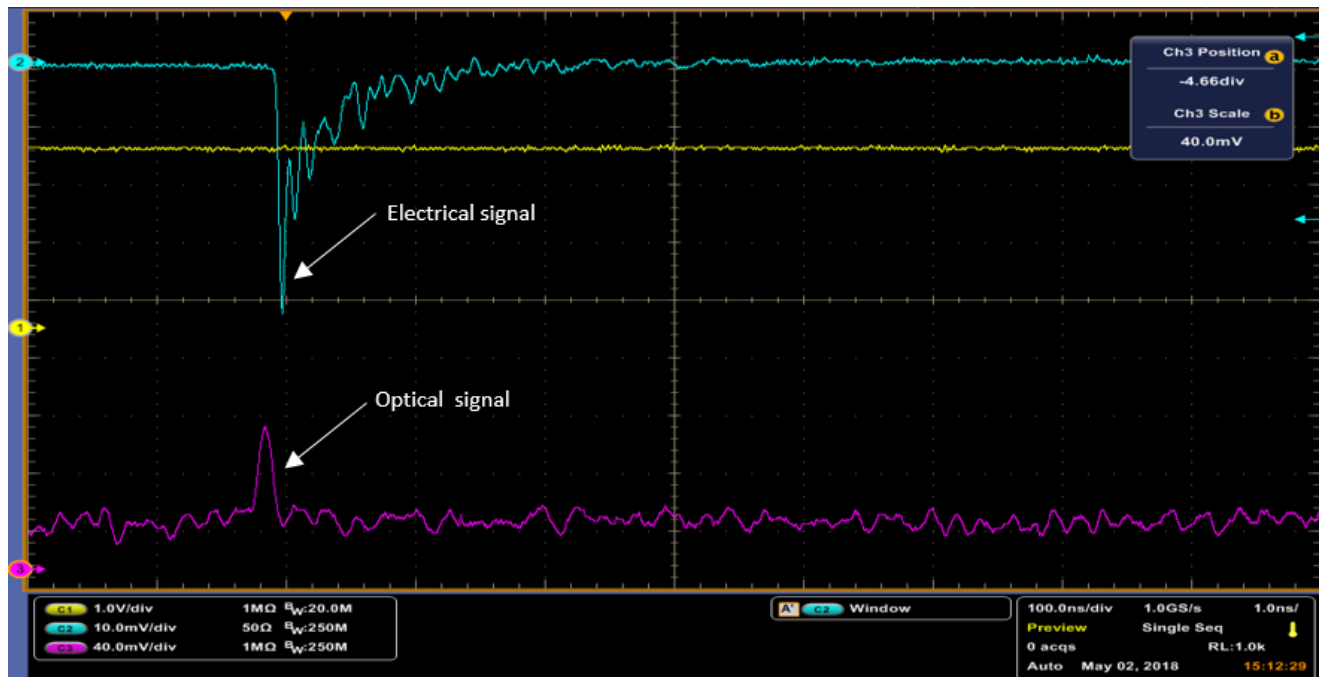


Figure 5.3: Signal obtained using oscilloscope from corona source

The distance of needle tip (corona source) from the ground plate was changed in order to observe the change in magnitude of the electrical and optical pulse. Table 5.2 summarizes the reading observed at a different distance of the needle from the ground. As expected, with the increase in the distance of needle from the ground, there was an increase in PDIV value (exactly same for both electrical and optical measurements). The charge magnitude detected by electrical sensor increases with the decrease in the distance. Furthermore, same increase was also observed in the voltage magnitude detected by the APD optical sensor. Therefore, it can be stated that the trend followed by both the sensors is the same.

Table 5.2: Comparison between electrical and optical measurements at different distance of corona needle from ground

Parameters	Corona at 18 cm	Corona at 15 cm	Corona at 11 cm
Electrical Parameters			
PDIV	9.9 kV	8.6 kV	7.6 kV
PD highest charge (at 10 kV)	-127.95 pC	-149 pC	-162 pC
PD charge average level (at 10 kV)	-95 pC	-125 pC	-133 pC
Optical Parameters			
PDIV	9.9 kV	8.6 kV	7.6 kV
PD highest voltage (at 10 kV)	81 mV	99.2 mV	110 mV
PD average voltage (at 10 kV)	50 mV	68 mV	78 mV

The PRPD pattern from both electrical and optical detector at 10 kV is displayed in Figure 5.4 a and b respectively. The pattern displayed here was recorded when the needle was at 11 cm far from the ground. The PRPD pattern for 15 cm and 18 cm distance is present in the appendix C Figure C.1 and C.2, respectively. The electrical PRPD pattern is in term of charge (picocoulomb: pC) whereas optical PRPD pattern is in term of voltage (mV) collected directly from APD sensor.

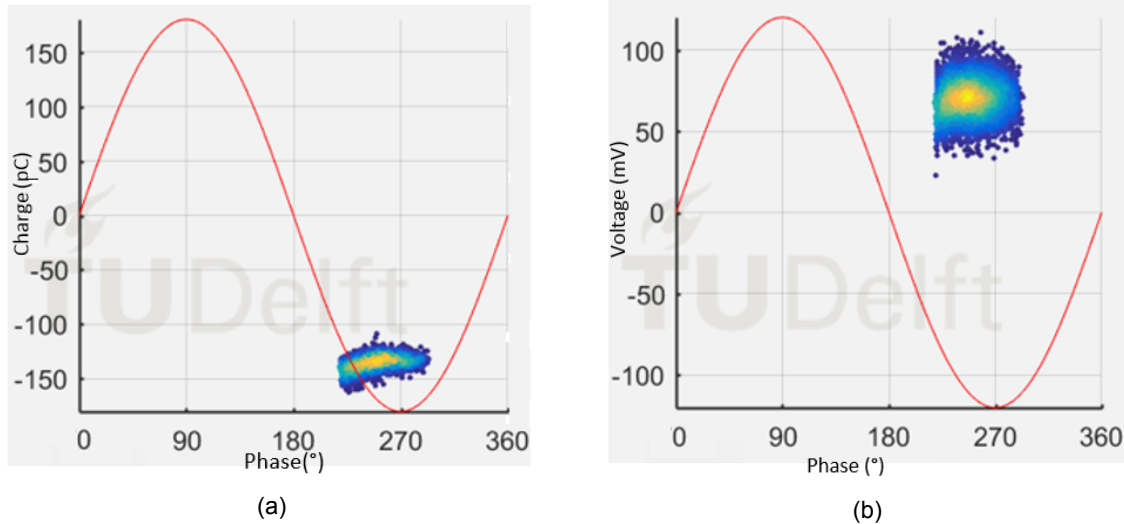


Figure 5.4: (a) PRPD pattern obtained from electrical detector at 10 kV (b) PRPD pattern obtained from optical detector at 10 kV

The PRPD patterns obtained from both the detector are comparable except for the polarity. The negative polarity is obvious for the electrical detector as the sharp point is at high voltage side. The optical measurements are based on light detection and it is known fact that light has no polarity, as a result, the signal or the PRPD pattern obtained from the optical sensor will always be positive.

5.1.2. Surface discharge on rubber sample in air

Another preliminary test was done using the rubber sample and cylindrical electrode to create surface discharges in the air as displayed in Figure 5.5. The optical sensor was placed as shown in the figure below in a such a way that the lens is focusing on the surface of the rubber close to the cylindrical electrode.

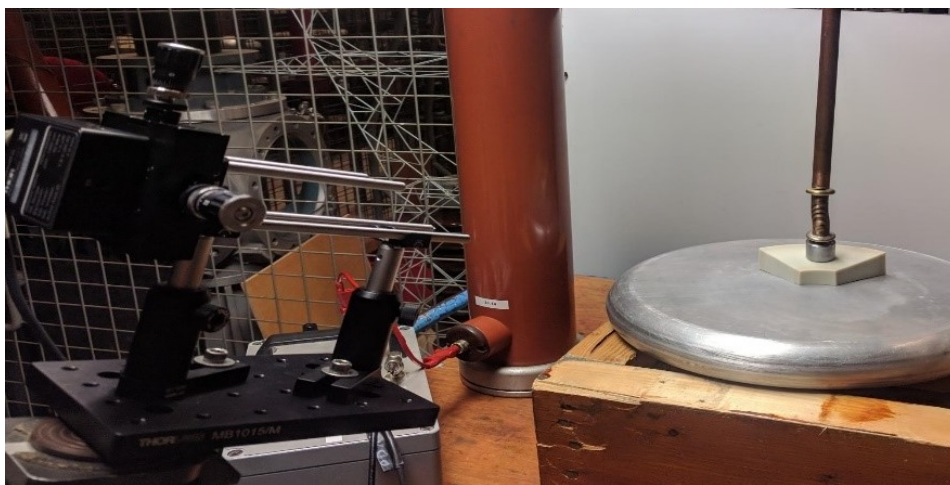
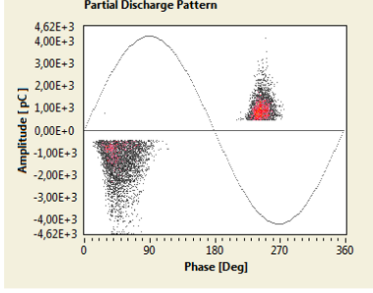
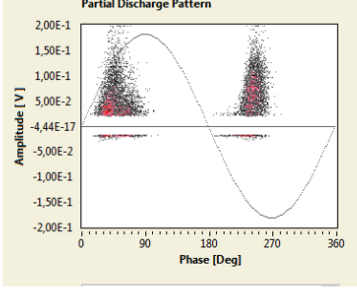
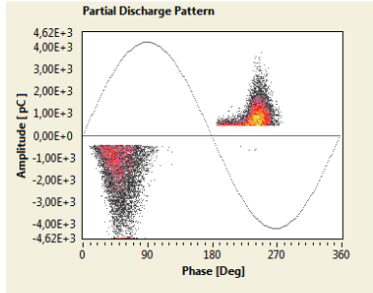
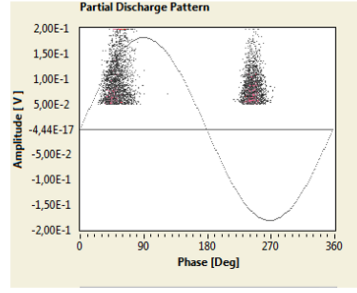


Figure 5.5: Setup for creation of surface discharge in air

Measurements done using Techimp: The results obtained by the Techimp instrument are summarized in Table 5.3.

Table 5.3: Comparison between electrical and optical measurements from surface discharge in air using Techimp device

Parameters	Electrical Measurement	Optical Measurement
Inception Voltage	11 kV	11.4 kV
Repetition Rate at 10 kV	0.83	0.35
At 12 kV		
At 13 kV		

PDIV value for optical measurement was slightly higher than electrical measurement. The repetition rate for the optical sensor was quite low compared to the electrical one. This is due to the fact that optical sensor was only able to focus on the limited area which falls under its coverage region whereas the discharges took place all around the rubber (which was captured by the electrical detector). Therefore, the setup has to be designed in such a way that the surface discharge only takes place in the area focused by the optical sensor. This will help us to directly compare electrical with optical signals.

Measurements done using oscilloscope Tektronix DPO7354C: The conductive paint was applied in a small area on the rubber sample as shown in the Figure 5.6.

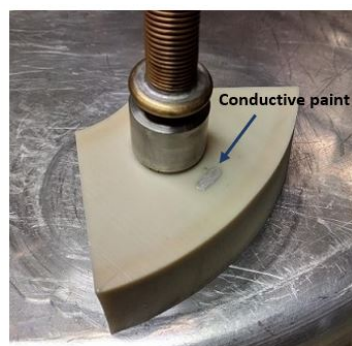


Figure 5.6: Setup for creation of surface discharge in air in particular area

The optical sensor was focused on that particular area of the rubber sample where the

conductive paint was present. Then, the voltage was applied and the results were recorded using the oscilloscope. The pulse obtained by both the detector is shown in the Figure 5.7 which was captured at around 11 kV. Table 5.4 summarize the result obtained from the improved setup shown in Figure 5.6.

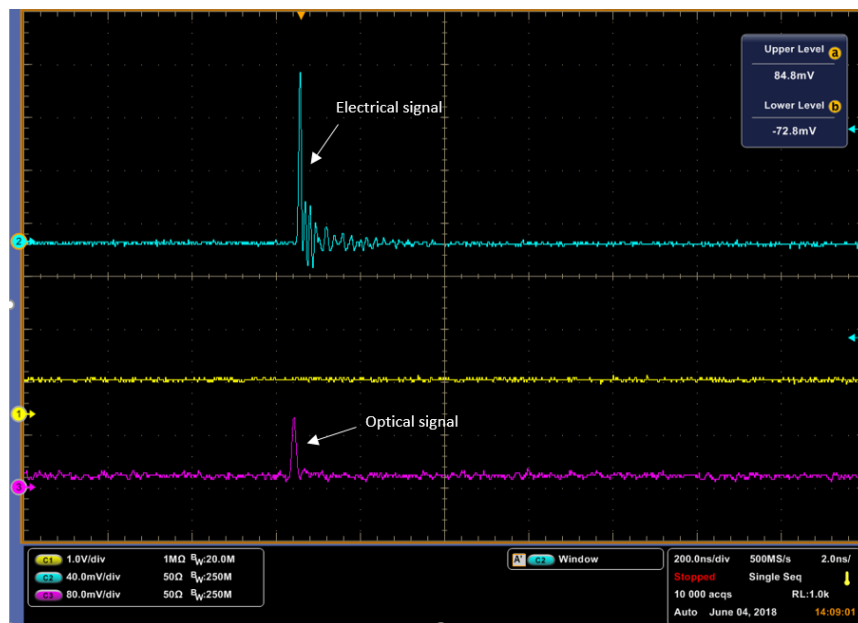


Figure 5.7: Signal obtained using oscilloscope from surface discharge

Table 5.4: Comparison between electrical and optical measurements obtained from oscilloscope from the setup shown in Figure 5.6

Parameters	Electrical Measurement	Optical Measurement
Inception Voltage	10.89 kV	10.89 kV
At 11.5 kV		
At 12.5 kV		

It is observed that the PDIV value is exactly the same. The number of pulses captured by both detectors for a specific time interval were also very close. It can also be observed that with the increase in voltage, there was an increase in magnitude for both the signal, as can be seen from the PRPD pattern captured at the different voltage for both the sensor in Table 5.4.

The preliminary tests based on both types of partial discharge showed good performance of the optical sensor in comparison with the electrical sensor. Therefore, it can be concluded from the above results that if the APD optical sensor is properly aligned then the sensitivity and characteristics of APD sensor is almost comparable to that of HFCT sensor.

5.2. Surface discharges on rubber sample in dry oil

The experimental tests conducted for detection of surface discharges on the rubber sample in dry oil insulation through both electrical and optical sensor is explained in this section. The actual experimental setup based on circuit diagram explained in Figure 3.17 in chapter 3 is displayed in Figure 5.8.



Figure 5.8: Experiment setup used for testing in HV lab, TU Delft

The optimum design to obtain surface discharges at the rubber-oil interface presented in section 4.2 in chapter 4 was used. The test object is seen in Figure 5.9. The distance between the electrode and conductive paint is approximately set to 2 mm. The oil is expected to be dry because it was kept in the vacuum oven at 50°C for 2 days. The oil was also measured using Vaisala device the next day and the average water activity value obtained was 0.19. The high voltage is applied to the circular electrode and the bottom of the vessel containing oil and sample is grounded. The voltage was increased gradually from 0 till the first PD pulse was observed. All the measurements were done using the oscilloscope and the analysis was done using *PDflex* software. The PD pulse detected by both detectors at 19.5 kV is seen in Figure 5.10.

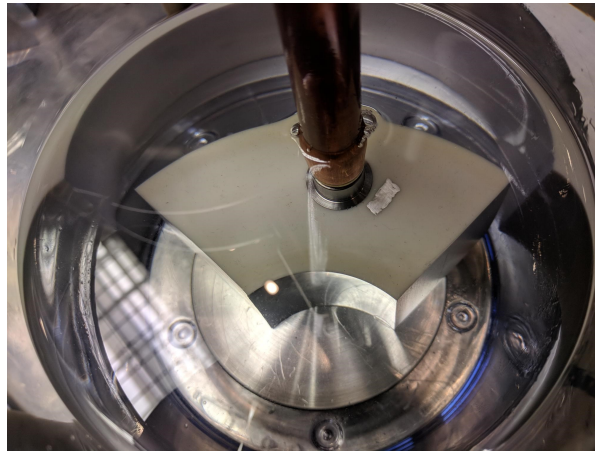


Figure 5.9: Test object in dry oil

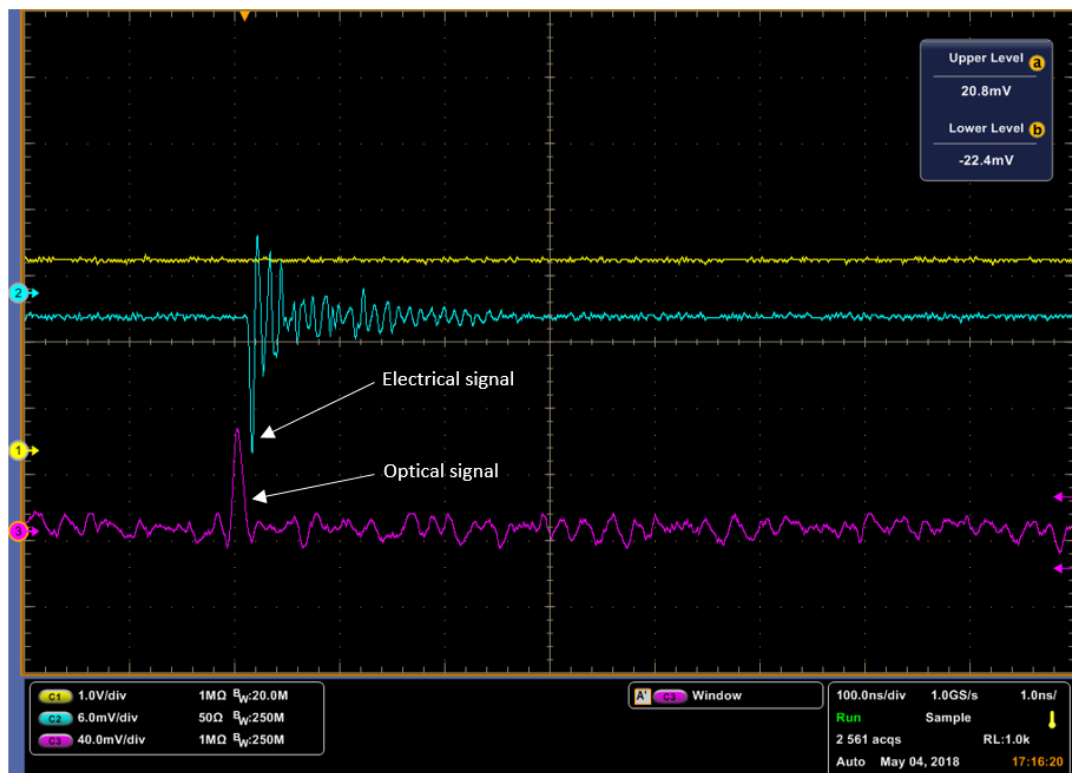
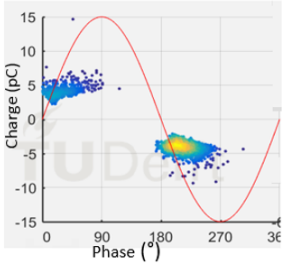
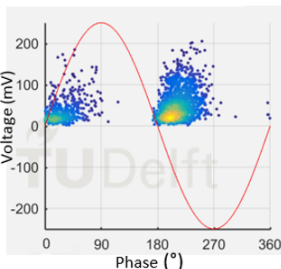
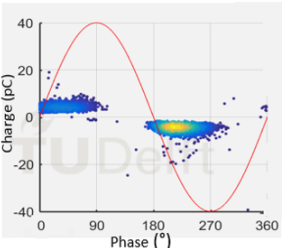
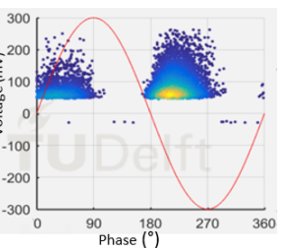


Figure 5.10: Signal obtained using oscilloscope from surface discharge in dry oil

Table 5.5 summarizes the readings obtained from both detectors. The PDIV values were very close to each other. The charge level as can be seen from the PRPD pattern obtained at 20 kV in Table 5.5 is very low. However, the optical sensor is able to detect such a low charge level as can be observed from PRPD pattern created from optical signals. There is a slight increase in the magnitude of both charge (from the electrical sensor) and voltage (from the optical signal) with the increase of applied voltage. However, a significant change in the values cannot be seen. It is worth mentioning here that the *PDflex* software uses a gain factor for obtaining current pulse according to HFCT sensor which is set in the software by default. This gain factor should be made to 1 in order to obtain exact voltage pulse from the APD sensor. This has been done for all the measurements obtained from the optical sensor when analysed by the *PDflex*.

Table 5.5: Comparison between electrical and optical measurements in the dry oil

Parameters	Electrical Measurements	Optical Measurement
PDIV	19 kV	19.1 kV
PRPD pattern at 20 kV		
PRPD pattern at 30 kV		

The values obtained in the oil from the optical sensor cannot be directly compared with the values obtained in the air or through corona discharge. The optical sensor detection is based on light emitted during the PD, this light emission varies with its medium, therefore the voltage pulse obtained cannot be matched. One more factor to keep in mind while doing the measurement in oil is that the container of the oil can also affect the optical detection. This was not the case in corona or surface discharge in the air since the optical sensor was focused directly on the PD source. However, here due to the limitation of the setup, the optical sensor is focused through this container towards the PD source which is present in the oil. Therefore, the readings obtained are not exact but give us a good estimation of how the optical signal will look like when PD activities occur in oil. The optical sensor even with the container in middle is very sensitive as it is still able to measure very low charge value, therefore its sensitivity will definitely increase with no container present in the middle. The measurement through oscilloscope can be done by setting the trigger either using the electrical signal or the optical signal at one instant of time. This helps us to check whether all the electrical pulse is been identified by the optical detector or not. This step is very important to decide the sensitivity of the optical sensor. The PRPD pattern obtained through both the detector at different trigger source for the same voltage applied in dry oil is presented in the appendix C Figure C.3 (electrical triggered) and C.4 (optical triggered).

5.3. Surface discharges on rubber sample in oil with added moisture content

This section deals with the measurement of PD done in the oil containing different level of water content. The three oil samples prepared as described in section 4.3 of chapter 4 are used here with same conductive paint rubber sample and electrode as used earlier in order to obtain surface discharges. The test results for PD measurements done using the optical sensor in comparison with the electrical sensor in each oil sample is discussed in the subsection below. All the measurements as described below have been conducted using an oscilloscope and the analysis has been done using *PDflex* software. HFCT sensor was used for the electrical detection.

5.3.1. Sample 1: Saturated oil with water activity of 0.82

The oil sample displaying the water activity of 0.82 as measured in section 4.3.1 of chapter 4 is used here. This sample had the highest water activity value, as a result, this was the most saturated sample prepared for this thesis testing. Therefore, the transmission index of this oil sample was also measured by the lambda 450 spectrophotometer using a similar procedure as described in section 3.1.1 of chapter 3. The result can be seen in the Figure 5.11. The transmission index of saturated oil is plotted in comparison with dry oil to get the idea of change in the behaviour of transmission characteristics of the saturated oil. There is significant 20-40 % decrease in the transmission capability of the saturated oil when compared to dry oil. This is due to the fact the sample prepared with climate chamber has opaque emulsion as seen from Figure 5.12. As a result, the light passing through the oil sample during the measurement experience scattering or is absorbed by the presence of water molecules or droplets to some extent. The transmission index of the saturated oil also gives some indication of the amount of light absorbed by the presence of water droplets in the oil. From [33], it is said that optical properties are principally determined by the characteristics of emulsion droplets (size, concentration, and refractive index). In case of micro-emulsion, the water gets completely dissolved with oil (refractive indexes of both oil and water matches) giving transparent view which would not effect the sensitivity of the optical sensor. However, in real life situation the termination doesn't face micro-emulsion as a result it is not investigated in this research work and all measurements are carried out with opaque emulsions. The experimental setup for measuring the surface discharge in the oil sample 1 is presented in the Figure 5.12.

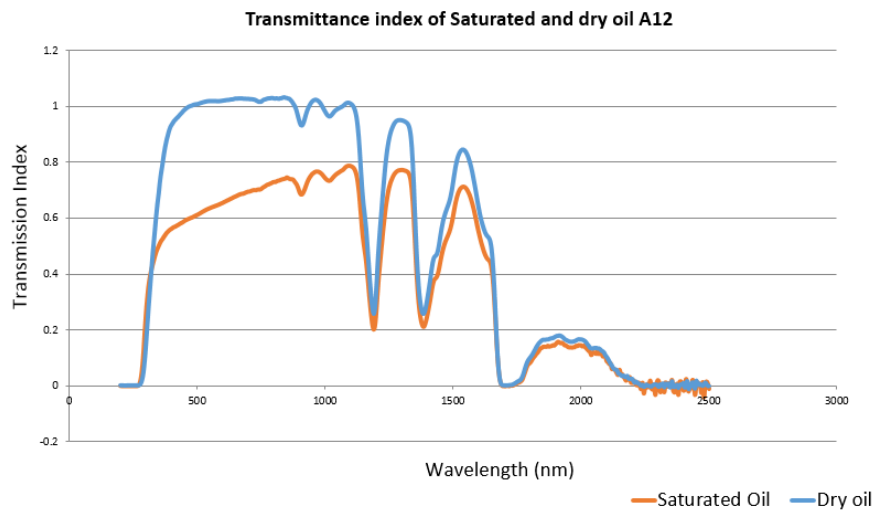


Figure 5.11: Transmission index of saturated oil compared to dry oil.

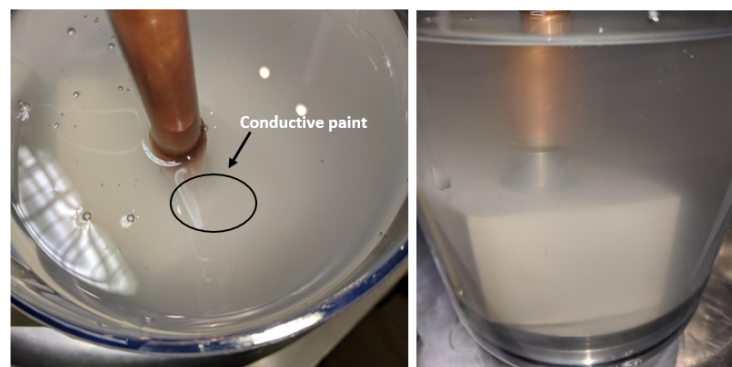


Figure 5.12: Experimental setup with oil sample 1

The same conductive paint rubber sample as described in section 4.2 of chapter 4 (also used for dry oil sample experiments) is placed in oil sample 1. As observed in the pictures above, the oil had the milky appearance. The conductive paint is present on the rubber sample as marked in the Figure 5.12. Therefore, as can be noticed setting the exact distance between the conductive paint and electrode was a challenge. At the start when the voltage was applied, the PDIV values of the electrical detector and the optical detector were 25 kV and 26.2 kV respectively. However, due to water contaminated oil, the PDIV values should be lower than compared to PDIV values obtained in the dry oil. This contrast situation was due to change in distance between the electrodes and conductive paint deposit as compared to that in dry oil. Therefore, the distance between electrode and conductive paint deposit was again adjusted in such a manner that it is approximately similar to the distance in the dry oil sample so that proper comparison of values can be done between different oil samples. The signals captured by the setup at 20 kV is presented in the Figure 5.13. Table 5.6 presents the results obtained with the finalized setup in the saturated oil sample 1.

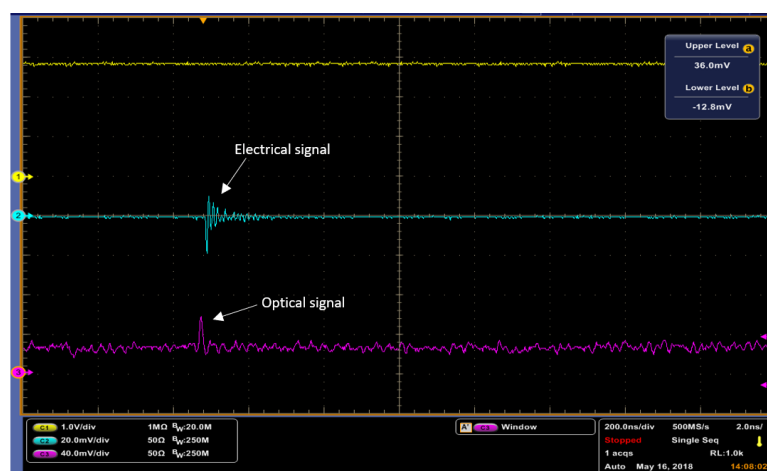


Figure 5.13: Signals obtained at 20 kV in oil sample 1

Table 5.6: Comparison between electrical and optical measurements in the oil sample 1

Parameters	Electrical Measurement	Optical Measurement
Inception Voltage	15.9 kV	17.8 kV
At 26 kV		
At 28 kV		

Now, as expected the PDIV value is lower than that in dry oil. However, the values for optical and electrical differ by almost 2 kV which can be explained by the reduction in transmission capability of the oil (due to the presence of water which may lead to scattering of light before it is detected by the optical sensor) under test which is shown in Figure 5.11. The PRPD pattern for both electrical and optical detector at 26 kV and 28 kV is presented in Table 5.6. The PRPD pattern of electrical measurement at 28 kV includes some noise due to interference from other instruments as shown which was ignored for further analysis.

5.3.2. Sample 2: Water activity of 0.69

The oil sample with water activity 0.69 was chosen next for testing the surface discharge. The oil sample 2 with similar conductive paint deposited rubber sample is displayed in the Figure 5.14.

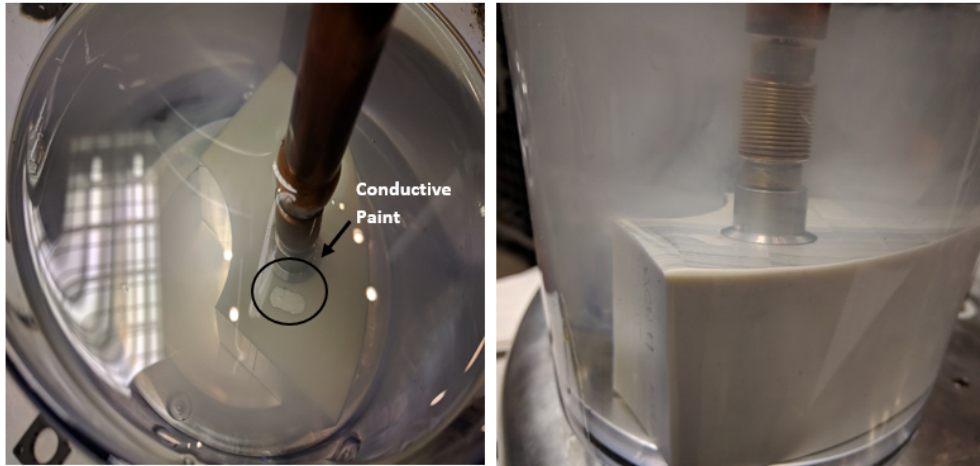


Figure 5.14: Experimental setup of oil sample 2

The distance between the HV electrode and conductive paint sample was kept approximately same as kept with other oil samples. The voltage was increased gradually from 0 till PDIV. The signal captured at 20 kV by both detection techniques is displayed in Figure 5.15.

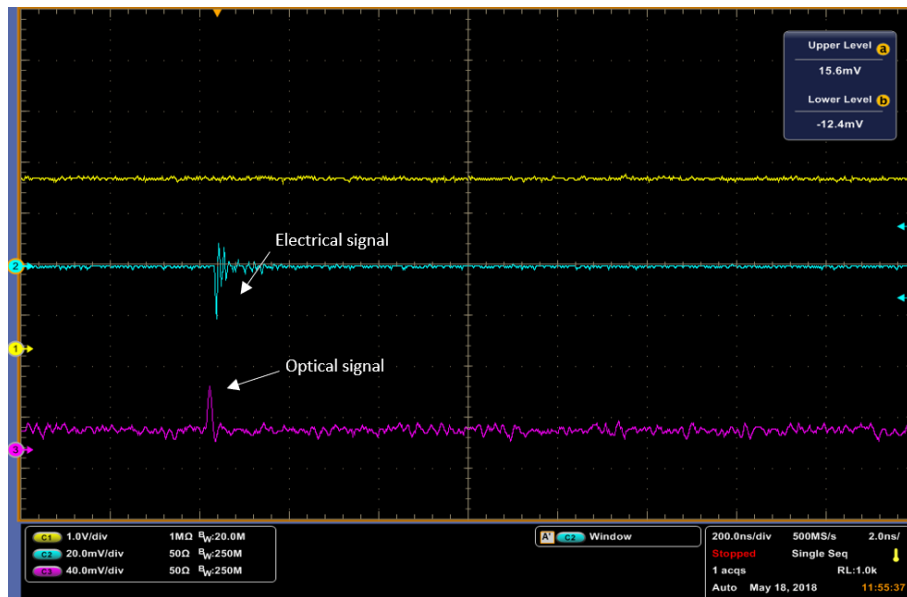
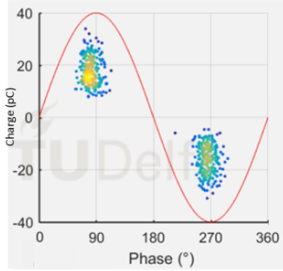
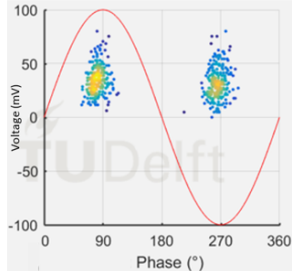
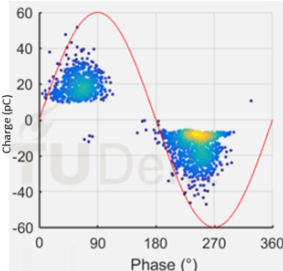
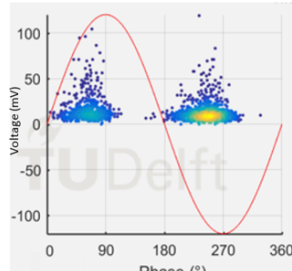


Figure 5.15: Signals obtained at 20 kV in oil sample 2

Table 5.7 presents the data collected while doing the measurement with oil sample having the moisture content of around 0.69 (water activity). As can be noticed, the PDIV value increased compared to the most saturated sample. Also, the difference in the PDIV value between electrical and optical measurement in oil sample 2 is around 1 kV which is less compared to the difference found in PDIV values in oil sample 1. The PRPD pattern captured at 25 kV and 36 kV is also presented in the table.

Table 5.7: Comparison between electrical and optical measurements in the oil sample 2

Parameters	Electrical Measurement	Optical Measurement
Inception Voltage	16.5 kV	17.6 kV
At 25 kV		
At 36 kV		

5.3.3. Sample 3: Water activity of 0.58

The final oil sample prepared with added moisture content (water activity of 0.58) was tested with the setup presented in Figure 5.16. The signal captured by both sensors at 20 kV is displayed in the Figure 5.17.

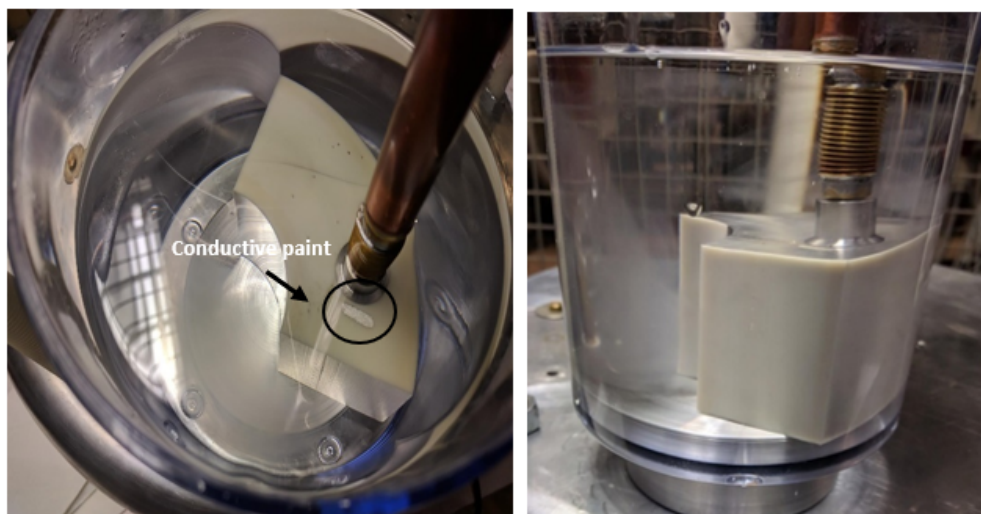


Figure 5.16: Experimental setup of oil sample 3

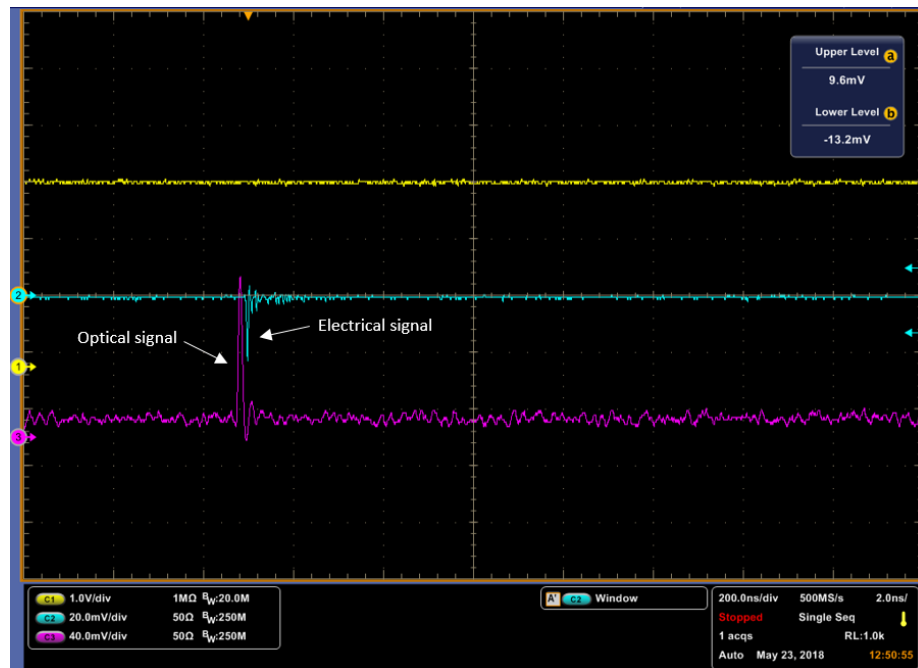


Figure 5.17: Signals obtained at 20 kV in oil sample 3

Table 5.8 summarizes the reading taken in oil sample 3. The PDIV value is quite close to each other. The oil sample as seen from the Figure 5.16 is almost clear in appearance with slight milky texture, as a result, the optical sensor detection is not much affected. The PRPD pattern captured at voltage 28 kV and 35 kV is presented in Table 5.8 as well.

Table 5.8: Comparison between electrical and optical measurements in the oil sample 3

Parameters	Electrical Measurement	Optical Measurement
Inception Voltage	18.1 kV	18.5 kV
At 28 kV		
At 35 kV		

In each oil sample tested for surface discharge, it was observed that with the increase in the voltage there is no significant difference in neither charge magnitude obtained from the electrical detection system nor in the voltage magnitude obtained from the optical detection system. However, the difference in PDIV values from both the detection system for each oil sample can be clearly noticed. It should be also kept in mind that not only water content will affect the PDIV values but also the distance between HV electrode and conductive paint deposit. Although, efforts were taken to adjust the distance in similar manner but there is good possibility of human error. This factors should be also considered when evaluating the sensitivity factor. Thus in conclusion, it can be said that with water activity in oil lower than 0.58, the sensitivity loss is less than 3% whereas maximum sensitivity loss of approximately 12% was observed with water activity of 0.82. Any delay in signal as obtained in Figure 5.3, 5.10 is due to different length of coaxial cable used for measurement from the sensors to oscilloscope. If same length is used, both the signal will get triggered at same instant. The PRPD pattern shown for all the discharges in the oil indicate that the type of PD is surface discharge. It is now evident from the measurements done in the thesis that the optical sensor is capable of detecting the surface discharge not only in the dry oil but even in saturated oil with some loss in sensitivity which can be defined according to water activity measurement of the oil.

After few days (approximately 7 to 11 days) of the sample preparations (with moisture content), it was observed that the milky texture of the oil got disappeared and water droplets got settled in the bottom. However, this is not the case in oil-filled termination under operation as effect of electric field also plays a role which would eventually lead to well-dispersed oil. These characteristics (water getting settled down and effect of electric field in long run) were not investigated in this research. However, use of this technology in real time application can be considered as possibility since the technique behind the detection is clear through the measurement performed and also it is easily comparable with the already existing electrical detection system.

5.4. Measurements of treeing phenomena

The optical sensor PD detection have already been tested for corona, surface discharge in air and surface discharge at the rubber-oil interface in different oil samples in this thesis. However, the research stated in [9] reveals that the optical PD detection can also be used for detecting internal discharges at interface of transparent or translucent stress cone with XLPE insulation of cable inside the termination. In order to cover this phenomena in our thesis using the selected optical sensor, plexiglass insulation was used due to unavailability of transparent or translucent rubber material. The setup constructed to replicate the phenomena of internal discharges is presented in Figure 5.18.

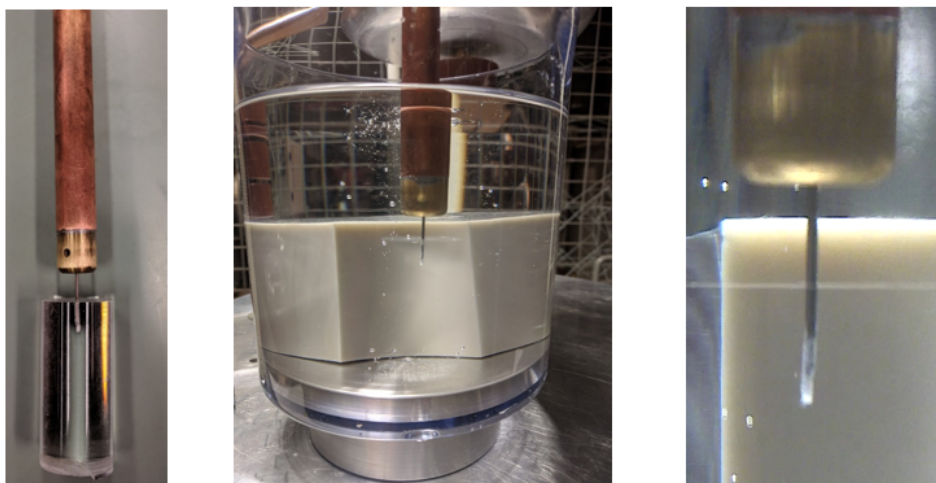


Figure 5.18: Setup used for creating internal discharge

The needle is inserted in the plexiglass and a void is created between the HV electrode and insulation material as seen in the Figure 5.18. The whole arrangement is placed inside the oil to avoid any concentration of electric field at edges and end of pipe of needle electrode. The electrical and optical sensor are placed at optimum position as shown in the Figure 5.19. The camera is also placed for capturing pictures and videos of the treeing process while measuring the PD. The results obtained from both the detectors are presented in Table 5.9.

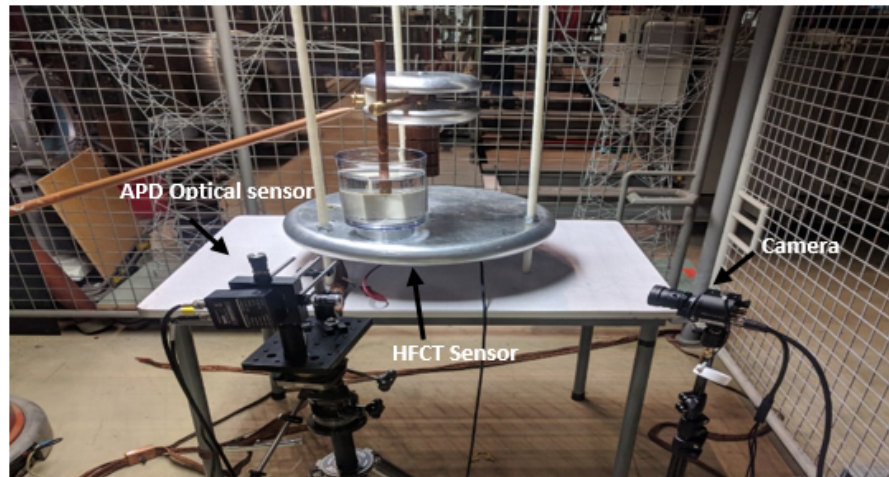


Figure 5.19: Sensors in position to capture the PD activity

Table 5.9: Comparison between electrical and optical measurements from treeing phenomena

Parameters	Electrical Measurements	Optical Measurement
PDIV (1 st attempt)	5.1 kV	6.5 kV
PDIV (2 nd attempt)	5.25 kV	5.25 kV
PRPD Pattern at 16 kV		
PRPD Pattern at 25 kV		

The PRPD pattern obtained during the experiments does not show internal discharge like pattern even by data collected using HFCT sensor. During start of treeing process, floating PD like pattern was observed. As the treeing increased, surface discharge like PRPD pattern was observed as shown in Table 5.9. The growth of tree can be easily observed from the Figure 5.20.

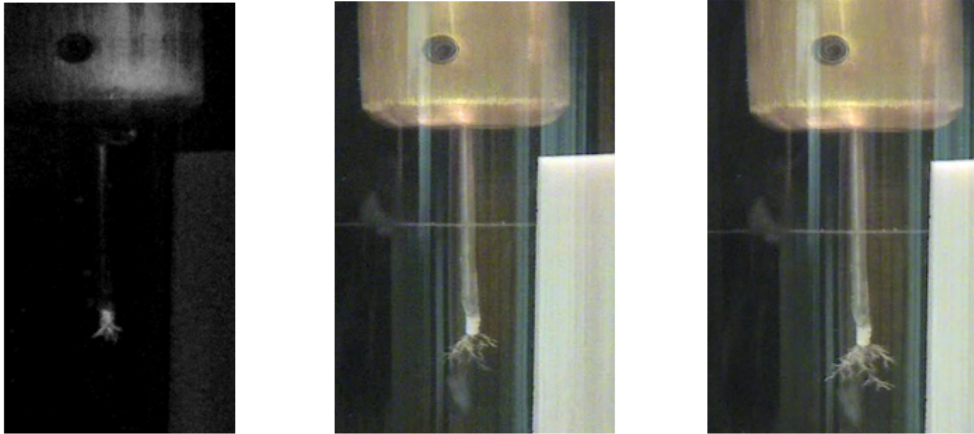


Figure 5.20: Growth of tree during testing

Analysis of results from electrical and optical PD detection

This chapter deals with the comparison, interpretation and explanation of the results obtained from the measurements presented in chapter 5. To investigate the actual performance of the APD optical based PD detection, comparative studies were performed for data collected from both optical and HFCT electrical sensor in terms of evaluating fundamental performance (such as output pulse for different type of discharges and electromagnetic interference immunity check for APD sensor in comparison with HFCT sensor), sensitivity analysis, stochastic features of PD pulse (including Weibull plot describing time interval between PDs and PRPD pattern comparison) detected by both the sensor for different types of PD sources. Furthermore, any possible correlation between the electrical and optical output of the PD signal is explored and discussed.

6.1. Basic Performance of optical based PD detection

The section discusses the fundamental behaviour of the APD sensor in comparison with the HFCT sensor. This includes discussion of PD output pulse for different types of discharges. Electromagnetic immunity which is the main advantage of the optical PD detection is also discussed in this section.

6.1.1. Typical output PD pulse

While detecting the partial discharges, the foremost attribute that is obtained is PD pulse. This is the first thing that we encounter while measuring PD before doing any further analysis. Most of the online PD measuring devices do the categorization of PD based on the PD pulse signal recorded. Therefore, the pulse/signal captured for different types of PD at a particular voltage for the same instant of time is compared in order to notice any features. Figure 6.1 display the signal captured by APD and HFCT sensor for corona source at 10 kV at the same instant of time.

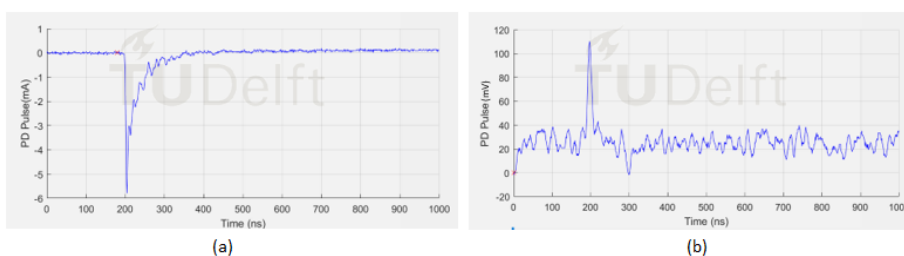


Figure 6.1: (a) PD pulse captured by HFCT sensor for corona source at 10 kV (b) PD pulse captured for corona source by APD sensor at 10 kV

Figure 6.2 displays the signal captured by APD and HFCT sensor for surface discharge in air at 12 kV at the same instant of time. Table 6.1 present signals captured from the PD in different oil samples at 30 kV. The PD pulse obtained from treeing phenomena is presented in appendix D Figure D.1.

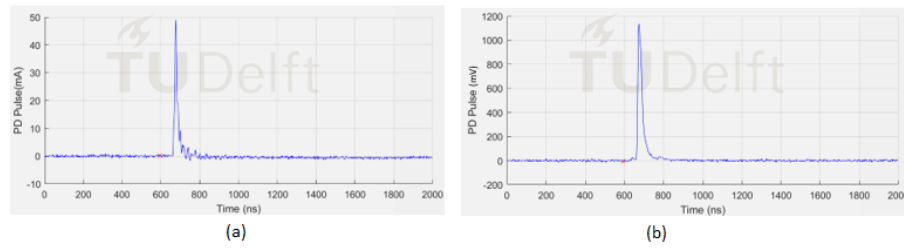


Figure 6.2: (a) PD pulse captured by HFCT sensor for surface discharge in air at 12 kV (b) PD pulse captured by APD sensor for surface discharge in air at 12 kV

Table 6.1: PD pulse captured by both the sensor in different oil samples

Parameters	Electrical Pulse	Optical Pulse
Surface Discharge in Dry oil at 30 kV		
Surface Discharge in Sample 1 oil at 30 kV		
Surface Discharge in Sample 2 oil at 30 kV		
Surface Discharge in Sample 3 oil at 30 kV		

The electrical pulses as seen above are different for corona and surface discharge. However, no significant difference in the optical pulse is observed apart from the magnitude change. The measurements taken in oil samples with different water content do not show

any differentiation for pulses captured from both sensors. Therefore, it can be concluded that the PD pulse obtained by the APD optical sensor only indicates the presence of light due to partial discharge but does not help to categorise the type of PD as there can be no distinction observed in the signal captured for the different kind of PD.

6.1.2. Electromagnetic immunity

The main reason for considering the use of optical PD detection for online measurements of HV equipment is because of the good interference immunity of the optical sensor. Unlike the electrical and vacuum PMT optical sensors, the solid state silicon based APD units in the APD sensor used in this research are insensitive to the magnetic fields in all the directions, which imparts a low level of device noise in the actual PD detection, particularly in the strong EM environments. Figure 6.3 shows an example of comparison between the signals obtained from HFCT and APD sensor in identical strong noise conditions. This noise condition was created by the breakdown tests which was on-going in one of the other test area in the lab. In spite, being far away from the breakdown testing setup the electrical sensor in PD detection circuit was influenced whereas no such effect was seen in the signals obtained from APD sensor.

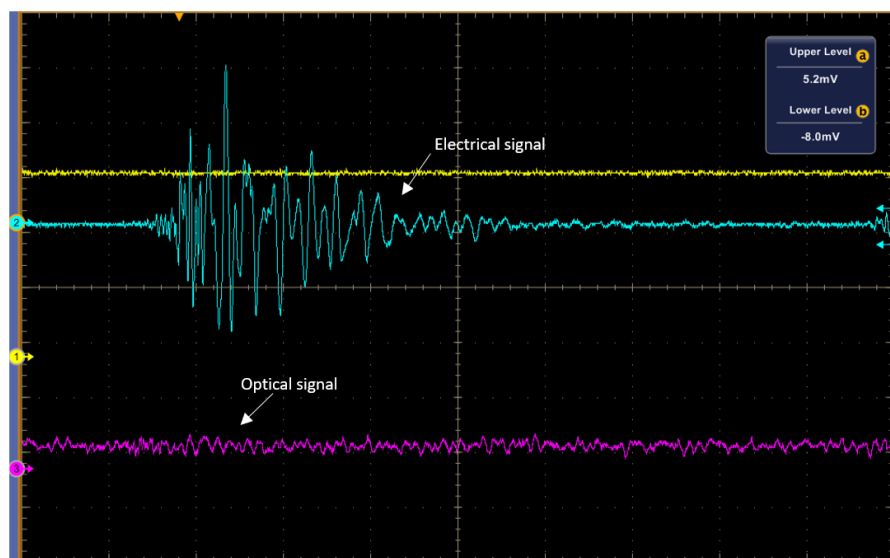


Figure 6.3: Signals captured by HFCT and APD sensor during noise condition

Apart from the ideal non-electromagnetic interference scenario, the components used for the electrical detection set up should be suitably installed. The resistor and inductor of right magnitude should be present in the loop where PD current circulates. If this is not taken care of, then the electrical channel will not show proper PD signal. Figure 6.4 is an example of such situation where no resistor nor inductor was included in the loop of coupling capacitors. As a result, it can be noticed that the electrical signal does not have smooth PD pulse unlike the signal received from the APD sensor. With the introduction of relevant resistor and inductor, based on setup prepared, the PD signal from HFCT sensor can be smoothened with better quality of the pulse. However, PD signals obtained from the APD sensor require no such additional configuration.

Therefore, by using the illustration of signals captured at various scenarios, it can be said that APD optical sensor is electromagnetic immune and insensitive to any noise conditions. Also, special attention to the use of additional elements in the test setup to get an ideal PD pulse is also not required. These qualities can be a significant advantage while doing online PD measurements.

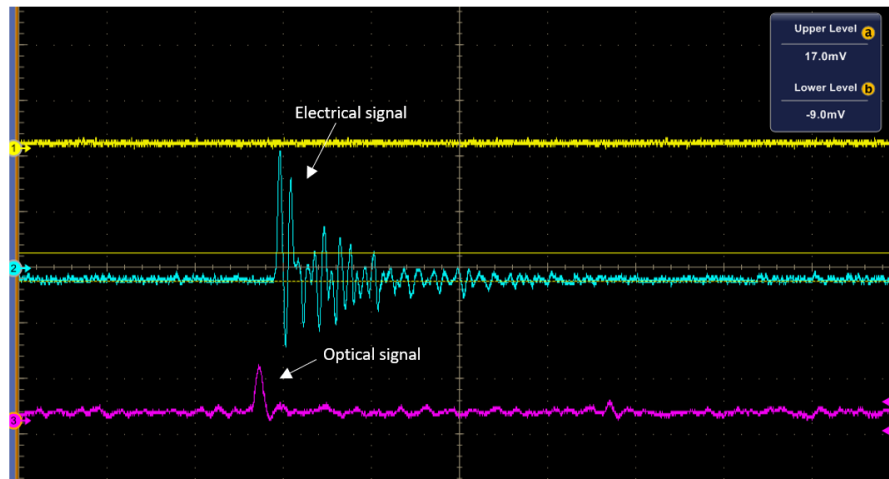


Figure 6.4: Signals captured by HFCT and APD sensor during PD activity

6.2. Sensitivity analysis

PD measurements are generally used for the diagnostic purposes. Therefore, PDs are expected to be detected at initial phases and mainly to prevent a total breakdown of the insulation system. Thus, the lower limit of a PD detection is crucial for the insulation examination. In order to verify the sensitivity of the APD optical sensor in comparison with the HFCT sensor, two parameters namely PDIV and minimum charge detection are considered suitable for this analysis [10].

6.2.1. Partial discharge inception voltage

In this study, the partial discharge inception voltage (PDIV) of the different PD models, described in chapter 5 (corona, surface discharge in air and surface discharge in oil) are discussed and analysed. Figure 6.5 shows a comparison of PDIV values for both electrical and optical sensor for different kind of discharges measured. The PDIV values of HFCT and APD sensor coincide. However, the standard deviation of PDIV for surface discharge in oil is higher comparatively due to the PD occurrence inside the highly viscous oil which is highly uncertain at times even with proper setup.

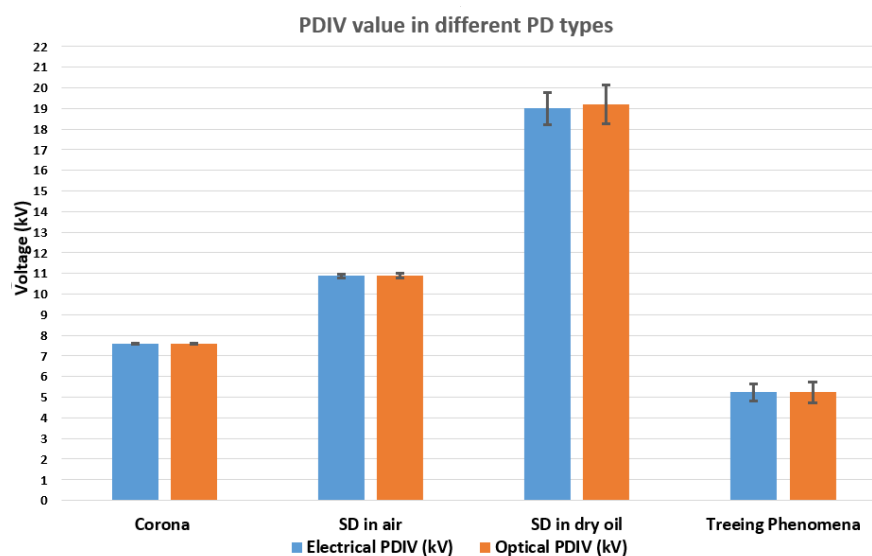


Figure 6.5: PDIV values comparison for different PD models in the experimental setups used

The comparison of PDIV values for oil samples prepared with different moisture content was done separately. The sensitivity factor based on PDIV values was calculated according to the formula given in the equation 6.1. This formula was devised based on the fact that PDIV obtained from HFCT sensor is always lower or equal to the PDIV obtained from the APD sensor. Therefore, this equation can give the percentage of error of PDIV values when compared with both sensors.

$$\text{Sensitivity} = \frac{\text{PDIV Value obtained from HFCT sensor}}{\text{PDIV value obtained from APD sensor}} \quad (6.1)$$

Figure 6.6 shows the plot for the sensitivity factor based on the equation above. This shows decrease in the sensitivity as the water content in the oil increases because the light gets scattered more (due to presence of minute water particles in the oil) before being detected by the APD sensor. However, even with the lower sensitivity for saturated oil, the decrease is not higher than approximately 12%. This decrease in the APD sensor's sensitivity can be acceptable if we consider other advantages of optical PD detection over HFCT sensors. Also, wet oil is not acceptable in the terminations. Thus, for monitoring the reliability of dry oil, the sensitivity of optical sensor is similar to the HFCT sensor.

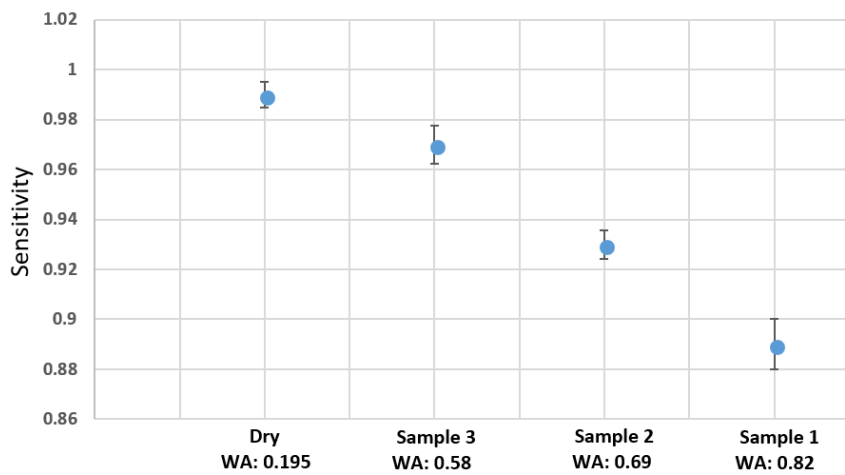


Figure 6.6: Sensitivity plot based on PDIV in different oil samples

6.2.2. Lower limit of detection

From the analysis based on PDIV values, it is noticed that the performance of the optical sensor is affected by the presence of moisture in the oil. This effect in the detection of the optical sensor should be known in terms of minimum charge level which can be detected by APD sensor compared to HFCT sensor. For this analysis, the following steps are followed.

- The trigger level of the oscilloscope is set to the electrical channel.
- The voltage is slightly increased from 0 to the PDIV value.
- The PD pulse during PDIV value is observed either by only electrical channel or by both channels based on the PD model under testing.
- If both channels do not observe the PD pulse, the voltage is increased until the PD signal is observed by optical channel also.
- Once the PD pulse is observed by both the channels, the data is recorded and processed by PDFlex software.
- The software will give detail magnitude of each pulse with the time instant. The maximum noise level of the APD sensor is known. The lowest charge detected by the electrical pulse is deduced for the particular recorded data, and its corresponding optical pulse

value is known due to the identical time stamp. If the corresponding pulse value is greater than the maximum noise level of APD, it can be said that APD sensor captures the PD pulse. This can be cross-checked by finding the optical PD pulse plot in PDFlex GUI.

These steps are repeated for all the kind of PD measured in this research. The analysis of minimum charge level is done for positive and negative half separately. Table 6.2 and 6.3 present the value deduced after the analysis indicating the minimum charge detected at positive and negative cycle, respectively.

Table 6.2: Comparison of the charge detected by both the sensor (Positive Cycle)

Type of discharge	Lowest charge detected by electrical detector (pC)	Lowest charge corresponding to electrical sensor detected by optical sensor (pC)
Surface Discharge in air	81.6	81.6
Surface Discharge in dry oil	1.57	1.57
Surface Discharge in most saturated oil: Sample 1	1.25	5.4
Surface Discharge in relative saturated oil: Sample 2	2.29	3.9
Surface Discharge in relative saturated oil: Sample 3	1.67	3.36
During treeing phenomena	197	197

Table 6.3: Comparison of the charge detected by both the sensor (Negative Cycle)

Type of discharge	Lowest charge detected by electrical detector (-pC)	Lowest charge corresponding to electrical sensor detected by optical sensor (-pC)
Corona	84	84
Surface Discharge in air	98.87	99.2
Surface Discharge in dry oil	1.75	1.75
Surface Discharge in most saturated oil: Sample 1	1.35	6.05
Surface Discharge in relative saturated oil: Sample 2	2.35	4.8
Surface Discharge in relative saturated oil: Sample 3	1.57	3.27
During treeing phenomena	100.5	100.5

The values by optical and electrical channels are both represented by the charge corresponding to the electrical sensor. This represents that for this charge value there was optical pulse detected and below this charge level only noise from the APD sensor was observed. The corresponding value obtained from the optical sensor (in terms of mV) is not represented here to avoid any confusion in the analysis. The relation between this charge value and its

corresponding optical pulse (voltage pulse) is done later in this chapter. It can be seen from the table (6.2 and 6.3) that lowest charge detected at corona, surface discharge in air, dry oil and during formation of tree is identical. However, as expected this trend changes with the different moisture content oil samples. This can be explained as follows: as the moisture level increases, the scattering and dispersion of light produced by the PD increases as a result certain minimum light level required for the detection of APD sensor varies with each pulse produced (this can be supported by transmission index calculation shown in Figure 5.11 in chapter 5 where the transmission capability of the oil decreases due the presence of water). The values considered in the table is taken into account after reviewing all the data obtained from several measurements recorded. For each reading, the minimum charge detected by both sensors varies. However, the values accounted for were the lowest quantity of charge recorded at minimum voltage possible (mostly PDIV of optical sensor). Figure 6.7 gives the graphical representation of lowest charge detected in the oil samples used in this research. The lowest charge detected by optical sensor increases with increase in the moisture whereas for electrical HFCT sensor this value almost remains constant. It is true that a lot of assumptions are taken into account as the physics of the entire process starting from ionisation to extinction which results in light radiation obtained during PD is not studied in this thesis. The lowest charge detected here for different oil sample cannot be used as the margin of detection when used in real time optical PD detection as the scenario and positioning of the optical sensor can be changed and altered. This analysis is done to establish a initial understandings of the sensitivity of the APD sensor in comparison with HFCT sensor under the conditions tested in this thesis.

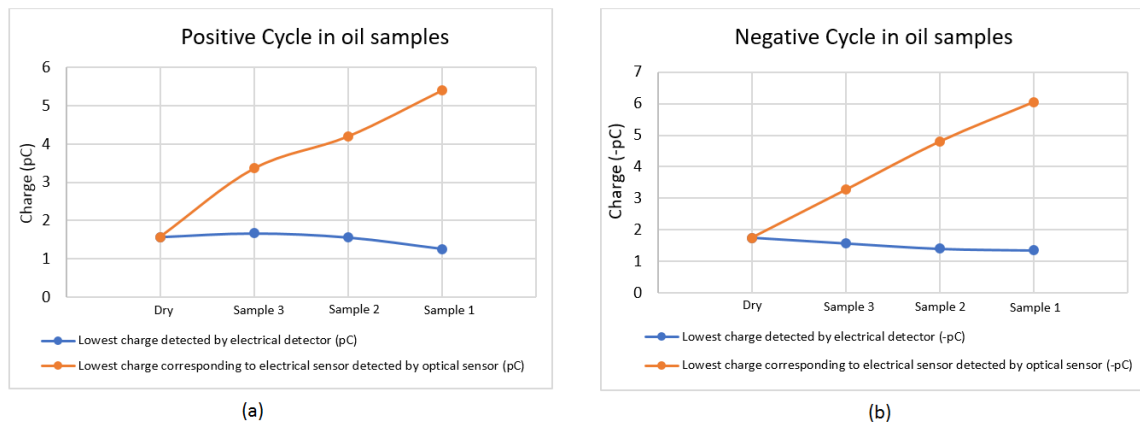


Figure 6.7: (a) Plot for minimum charge detected by both sensor (Positive Cycle) (b) Plot for minimum charge detected by both sensor (Negative Cycle)

6.3. Pulse resolution time :Weibull plots

A good pulse resolution of a PD detection system ensures that the PD events are precisely recorded specially for PRPD pattern analysis [10]. The pulse time resolution of the APD PD detection depends mostly on the response time of the cell to work at Geiger avalanche mode [9] and external matching circuit. To compare the APD sensor PD detection with HFCT current pulse response in terms of time resolution, the time interval between successive PD events, which are recorded by the oscilloscope is analysed by the Weibull probability distribution which is calculated by equation 6.2:

$$\ln(-\ln(1 - F(\Delta t))) = \beta \ln \Delta t - \beta \ln \Delta t_0 \quad (6.2)$$

Here, β is shape parameter and F is the probability as a function of the scale parameters (i.e Weibull time interval), Δt and β .

Reliasoft software named Weibull++¹ is used in order to plot the Weibull graphs. Weibull++ provides the most comprehensive tool-set available for reliability life data analysis, calculated

¹<http://www.reliasoft.com/Weibull/>

results, plots and reporting. Figure 6.8 shows the Weibull distribution of time stamp recorded during PD measurements by both electrical and optical channel for 5000 pulses each. The graph shows that the time interval of the signal recorded overlaps. This indicates that the pulse intervals recorded by the APD sensor have strong consistent Weibull parameters with those of HFCT. Thus, APD sensor can also be applied to stochastic PD detection with high accuracy in PD event recognition [10]. Almost all the data recorded show a similar behaviour. However, delay in detection by optical sensor can take place as shown in the Figure 6.9. This can be due to the occurrence of PD outside the coverage area of the optical sensor. However, this can be solved by correct positioning and use of multiple sensors in order to cover all possible area for PD occurrence.

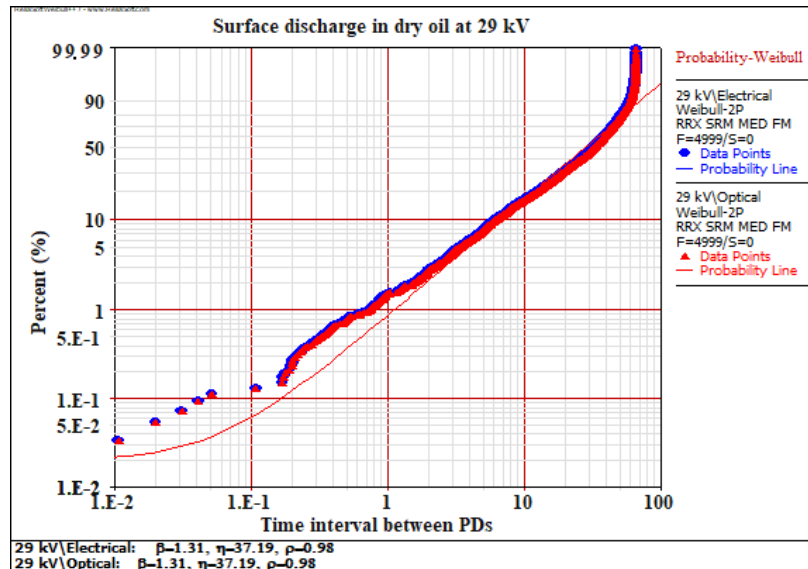


Figure 6.8: Weibull distribution of the time intervals between successive PD events recorded by HFCT sensor (blue) and APD sensor (red)

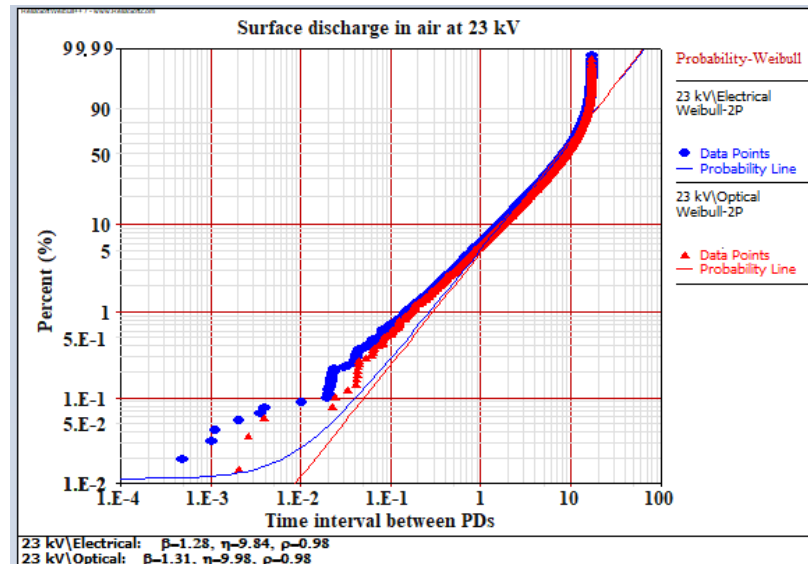


Figure 6.9: Weibull distribution of the time intervals between successive PD events recorded by HFCT sensor (blue) and APD sensor (red)

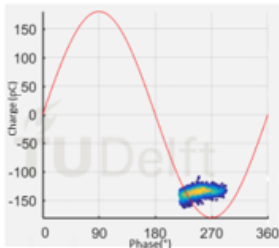
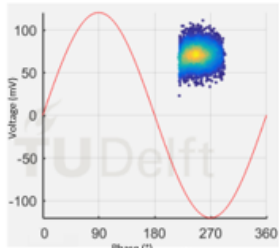
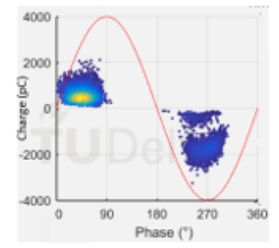
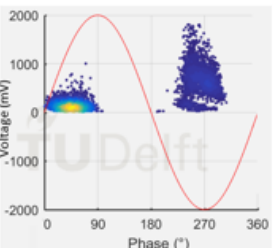
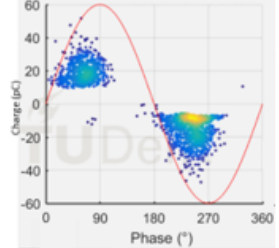
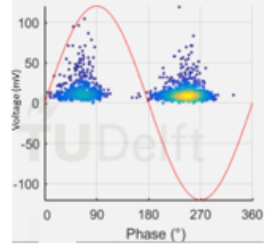
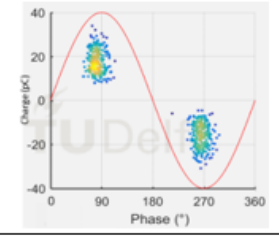
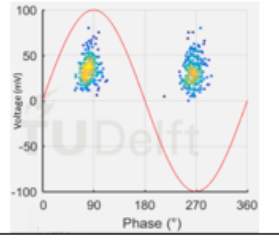
This analysis indicates that any comparison of data done between the detectors is based on the fact that HFCT and APD sensor record the pulse at the same time. It is also done to

ensure that signals to both the channels are captured from same discharge. It implies that one to one correlation of the PD signal received from HFCT and APD sensor is possible as both are recorded at the same time which is proved by the overlap of the time interval plot displayed in Figure 6.8.

6.4. Phase resolved partial discharge pattern

When an alternating current (AC) electric field is applied, the discharge activities periodically varies in terms of time lag and magnitude, based on which the phase resolved partial discharge (PRPD) pattern is proposed for PD diagnosis and defect recognition in insulation system under AC. The PD data in a certain number of applied voltage cycles are plotted on the phase axis in one voltage cycle. All the PRPD pattern has been displayed with the measurements results in chapter 5. However, this section is dedicated to summarising the insights acquired from PRPD pattern obtained from HFCT and APD sensor. Table 6.4 displays some of the PRPD pattern captured by electrical and optical detector simultaneously using the oscilloscope.

Table 6.4: Comparison of the PRPD pattern for different discharges captured

Parameters	Electrical Measurement	Optical Measurement
Corona		
Surface discharge in air		
Surface discharge in oil		
Surface discharge in oil		

PRPD pattern provides additional information including the physical properties and stochastic behaviours of the discharge. Similarly, the PRPD pattern can be used to analyse stochastic light pulses [10]. By comparison of the PRPD pattern displayed in Table 6.4, it can be said that the results from HFCT and APD measurements are considerably consistent with each other in term of both profile and distribution intensity. With each pattern displayed, the change in the phase, orientation and occurrence of the PD is similar for both the electrical and optical measurements. Therefore, it can be said that PRPD pattern obtained from optical signal can give a clear indication of the type of discharge happening in the setup. Consequently, with proper analysis software, it can be stated that the conventional PD diagnosis and defect recognition approaches can also be applied to APD optical based PD monitoring.

6.5. Correlation between electrical and optical output

A monotonic relationship between the signal response and the strength of a physical object is the premise for building a measurement system. The comparative study of APD sensor with HFCT sensor is incomplete if the relation between the output signal obtained from both the sensors is not investigated. The intensity of the light emitted from the discharge is positively associated with the quantity of PD charge and depends on the ratios among the probabilistic cross-section of the excitation, ionisation, recombination and attachment during a complete discharge process [10]. The most commonly used electrical PD detection gives the results in terms of charge or current pulse. The interpretation of PD in terms of electrical output is known. Generally, the intensity of the charge is used to determine the severity of the partial discharge. With the increase in the PD activities, the charge obtained from the electrical detector (in this case HFCT sensor) increases. The APD sensor is used first time for the PD detection application. Therefore, the relation of the intensity of the voltage (received from APD sensor) with the PD severity is unknown. As a result, this section will focus on any possible relationship that can be achieved between the output of HFCT and APD sensor.

In order to compare the direct voltage and current/charge obtained from APD and HFCT sensor respectively, the extraction and processing of the data should be performed first. The graph presented for each subsection (different PD source) is obtained using the following steps:

1. Set the appropriate trigger level. Collect the data from the oscilloscope through fast frame acquisition setup (any number of pulses up-till certain higher limit can be set). Save the waveforms (Channel 1: Phase detector pulse; Channel 2: electrical pulse from HFCT sensor; Channel 3: optical pulse from APD sensor) in terms of “.wfm” and time stamp in the form of “.txt”.
2. Open the channel 2 and channel 3 files separately in the PDflex software. Now, build a cluster such that only one cycle of the data displayed in the PRPD pattern is captured as shown in Figure 6.10. Save this cluster in the designated path. The file will get saved in terms of Matlab file “mat”. Do not forget to include the time stamp tick bar while saving the data. Repeat this for another cycle. This step should be done for electrical and optical channel separately.

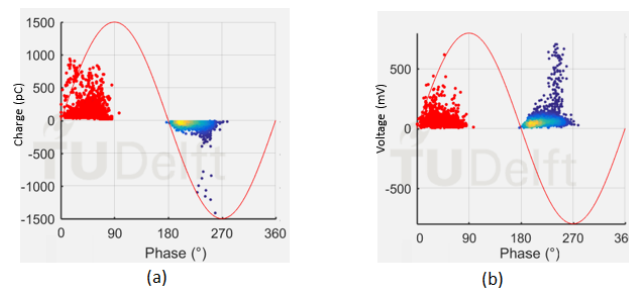


Figure 6.10: (a) Positive cluster of PRPD pattern obtained from HFCT sensor (b) Positive cluster of PRPD pattern obtained from APD sensor to save data for positive cycle part analysis

3. Open the data in Matlab obtained for both electrical and optical measurements derived from PDFlex for positive cycle first. Extract the values of charge, peak current and time stamp from electrical files whereas peak voltage and time stamp from optical files. Repeat this step for the negative cycle as well.
4. In Matlab or in excel align the data in such a way that the electrical signal and optical signal in each row of one column data is having a same time stamp. This step is important to ensure that data is aligned properly. For example, at 1 sec the electrical charge obtained is 5 pC and at 1 sec the optical charge obtained is 60 mV. As evident from Weibull plots displayed in section 6.3, mostly these data is already aligned.
5. Open “SFTOOL” window in Matlab. Insert X-axis as charge or peak current pulse obtained from electrical measurements and Y-axis as peak voltage pulse obtained from optical measurements.
6. In this case, through experiments, it was already noted that with an increase in average charge there was a linear increase in the magnitude of voltage pulse received from the optical sensor. Therefore, linear fitting with equation and correlation factor was best fitted for all the measurements taken.

All the plots mentioned below will contain electrical data in X-axis and optical data in Y-axis. The charge and pulse current from HFCT sensor for corona and negative cycle in all the other discharge type is negative. However, for analysis purpose, negative sign has been neglected and only absolute value has been considered.

6.5.1. Corona PD

This section presents the graphs obtained after correlating the charge or peak current pulse with peak voltage pulse. Figure 6.11 shows the graph in which charge obtained from electrical measurement is plotted against peak voltage derived from optical measurements. Similarly, Figure 6.12 shows graph between peak current pulse and peak voltage pulse.

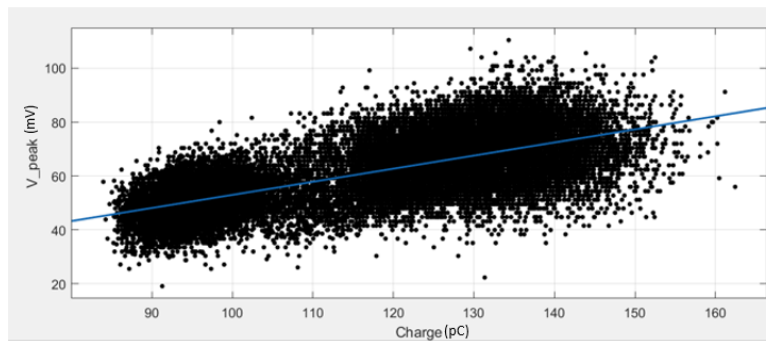


Figure 6.11: Plot of voltage pulse detected by APD sensor Vs apparent charge PD magnitude by HFCT sensor for corona data

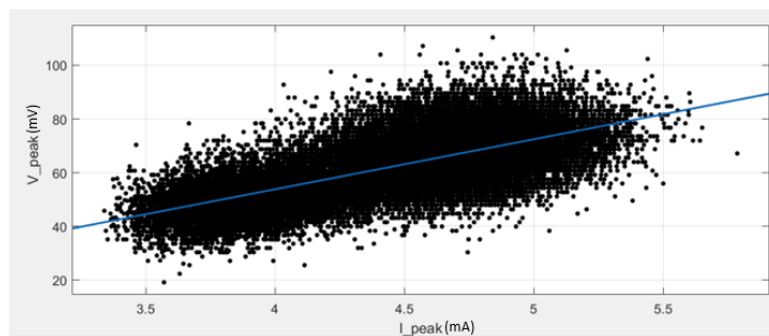


Figure 6.12: Plot of voltage pulse detected by APD sensor Vs peak current pulse (-ve) by HFCT sensor for corona data

The data obtained at the different distance of needle from the ground as discussed in section 5.1.1 of chapter 5 is combined and plotted in the graph above. This is done to obtain a more extensive range of both the charge and voltage pulse derived from the HFCT and APD sensor respectively. As can be said, there is a linear growth of voltage with an increase in the charge or current magnitude.

6.5.2. Surface discharge in air

This section will present the linear plot of data obtained from surface discharge in air experiments. Firstly, the main difference in the trend can be seen if the optical sensor is only covering a part of PD source whereas HFCT measures all the discharges possible from all the direction. Figure 6.13 illustrates such scenario in which optical sensor cannot capture all the pulses because of its limitation of the coverage area and directionality issues. Therefore, the graph obtained is disarranged and clustered at patches since the one to one relation between charge and voltage pulse cannot be deduced (as the signal captured by both the detector at one instant of time can be from different discharges and not from the same discharge). The graph is plotted by cumulating all the measurements data taken at different voltages. The intention was to obtain larger range of charge and voltage to have an aligned graph. The certain cluster in the graph is due to different trigger level set during the measurements at different voltages.

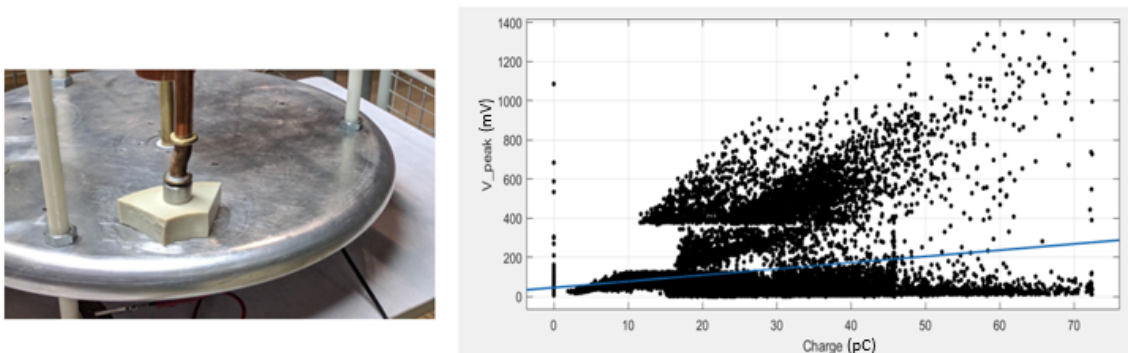


Figure 6.13: Plot of voltage pulse detected by APD sensor Vs apparent charge by HFCT sensor for surface discharge in air (setup 1)

Now, when the discharges produced at the PD source is limited to an area equivalent to the coverage area of the optical sensor, then the linear trend can be obtained as displayed in Figure 6.14 which was plotted by combining measurements taken at 11 kV and 12 kV. The high linearity is due to the fact that electrical and optical signal captured at certain time can be assumed to be coming from the same discharge.

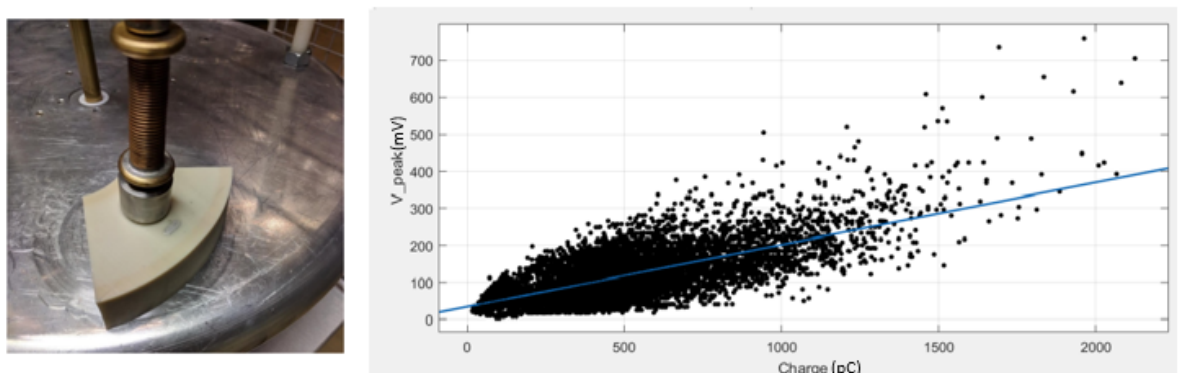


Figure 6.14: Plot of voltage pulse detected by APD sensor Vs apparent charge by HFCT sensor for surface discharge in air for positive cycle (finalized setup)

The change in plot and trend can be observed from both the figures. This concludes that focusing the optical sensor at right spot can lead to similar results as compared to HFCT sensor. The graph in Figure 6.14 which is obtained for positive cycle deduces that the voltage pulse magnitude of APD sensor linearly increases with the increase in apparent PD magnitude. The graph for negative half shown in the appendix which is also linear in nature. Similarly, the plot between voltage Vs current peak instead of charge and plot between energy of the pulse from both the sensors also presents linear drift. Some of these plots are present in the appendix D (Figure D.2 shows plot between voltage and current pulse for positive cycle, Figure D.3 shows plot between voltage and charge for negative cycle, Figure D.4 shows plot between energy of signals coming from both sensor for negative cycle).

6.5.3. Surface discharge in oil

Figure 6.15 and 6.16 give the plot for PD obtained in dry oil and in oil sample 3 (Water activity:0.58) respectively. As can be observed from the plot, the voltage pulse from APD sensor increases with the increase in charge but the scatter is too high to have a proper relationship between the quantities. This can be explained as follows: in the measurements done in air, the APD sensor was directly focused on the source of the PD at an appropriate distance whereas here the direct focus due to the limitation of the setup cannot be done. The oil as well the oil vessel is present in middle. The oil container is transparent but the width is around 5 mm as a result scattering of light is a big possibility. Moreover, the distance also increased as the PD source is somewhat placed in the middle of the container which cannot be directly focused. Therefore, these conditions should be weighed before making any further conclusions.

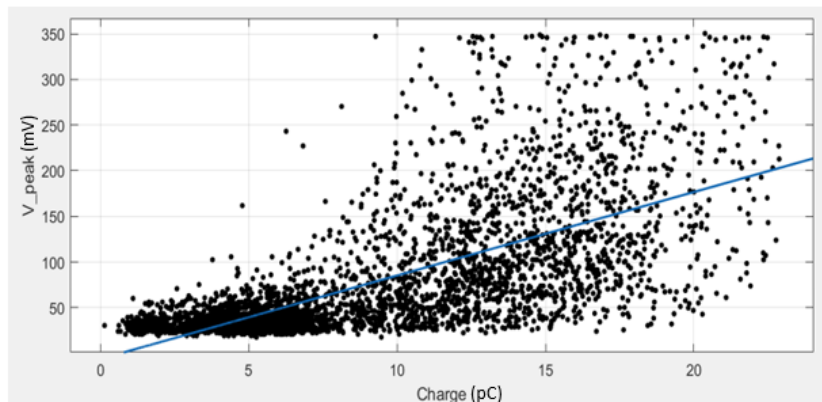


Figure 6.15: Plot of voltage pulse detected by APD sensor Vs apparent charge by HFCT sensor for surface discharge in dry oil for positive cycle

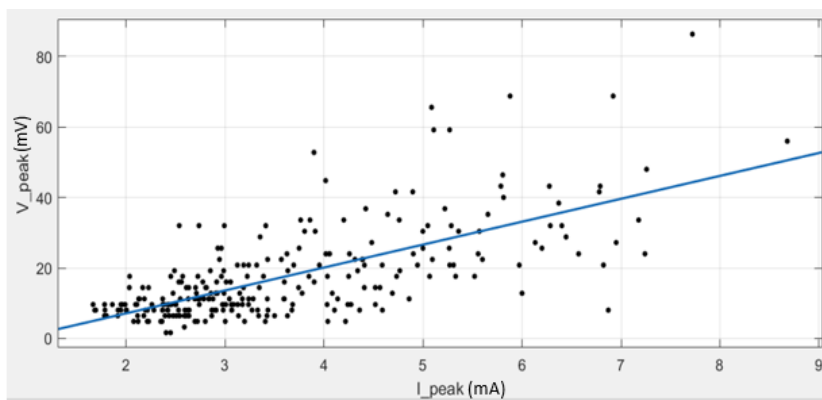


Figure 6.16: Plot of voltage pulse detected by APD sensor Vs apparent charge by HFCT sensor for surface discharge in oil sample 3 for positive cycle

The plot for the negative cycle and for the data obtained from other oil samples as well as from treeing phenomena is present in the appendix D (Figure D.5 for dry oil, Figure D.6 for sample 1, Figure D.7 for sample 2 and Figure D.8 for treeing sample). Similar, dispersion and scattering was observed in all the plots obtained from PD in the oil with different water content.

If the scattering or any outliers are neglected, then the relationship between the light intensity (given in terms of voltage pulse) and the apparent PD magnitude has approximately a single linear form as shown in the equation 6.3. The equation is valid for all the data obtained simultaneously from the optical and electrical sensor for different kind of PD measured.

$$\text{Light intensity (mV)} = A * \text{PD magnitude (pC or mA)} + B \quad (6.3)$$

where A and B are the slope and the constant value of the linear fitting line respectively.

To summarize the relationship of the data obtained from both the measurement, the correlation factor based on equation 6.4 is calculated for all the readings obtained.

$$CC = \frac{\sum x_i * y_i - \sum x_i * \sum y_i / n}{\sqrt{[\sum x_i^2 - (\sum x_i)^2 / n] * [\sum y_i^2 - (\sum y_i)^2 / n]}} \quad (6.4)$$

where x is the charge or the peak current obtained from the electrical HFCT sensor, y is taken as peak voltage obtained from optical APD sensor, n is the number of pulses or data. The correlation coefficient tells how closely the two values are related. If the $CC > 0.8$, strong correlation; $0.5 < CC < 0.8$, average correlation and $CC < 0.5$, weak correlation [9]. Table 6.5 present the correlation factor for all type of discharges measured in this thesis. The strong correlation was seen for some of the measurements. However, the correlation factor is average for most of the measurements obtained.

Table 6.5: Correlation coefficient obtained from all the PD data

Type of discharge	Correlation coefficient			
	Positive Cycle		Negative Cycle	
Electrical →	Charge Vs	I _{peak} Vs	Charge Vs	I _{peak} Vs
Optical →	V _{peak}	V _{peak}	V _{peak}	V _{peak}
Corona	NA	NA	0.70	0.69
SD in air	0.75	0.73	0.95	0.92
SD in dry oil	0.71	0.72	0.76	0.79
SD in sample 3	0.61	0.65	0.68	0.69
SD in sample 2	0.60	0.61	0.61	0.61
SD in sample 1	0.55	0.54	0.53	0.54
Treeing	0.77	0.92	0.77	0.89

The analysis presented in this chapter covers different aspects of the optical APD sensor in comparison with the electrical HFCT sensor. Since the APD is not used before for PD application, this initial examination of the data obtained had to be conducted. The PD pulse

obtained from optical sensor does not give any indication for the type of discharge but only indicate the magnitude of the light intensity. The PRPD pattern comparison showed that optical sensor is highly comparable with the electrical sensor in terms of phase and orientation of PD occurrence. The correlation plot obviously showed huge scattering but also indicated the linear behaviour of optical sensor output compared to the electrical sensor output. The similar study has been conducted in [9] also shows the discrepancy in correlation plots for different measurements conducted. The Weibull plot indicated high pulse resolution time of APD sensor compared to HFCT sensor. The strong immunity against interference was also checked under an adverse condition in which APD sensor surpasses HFCT sensor with its strong resistance ability against radiation and noise. These analyses laid a basic foundation for the usage of APD sensor for PD detection and explain the characteristics of the optical sensor.

Conclusion and recommendation

This chapter describes the findings of this thesis project through experiments and analysis performed throughout the research. The future outlook for the optical partial discharge detection technique and recommendations for further research work is also discussed at the end.

7.1. Conclusion

The main goal of this research was to check the feasibility of using the optical partial discharge detection technique in HV cable terminations. The following points summarize the conclusion for each research objective:

1. **Design for creating surface discharge**

Producing surface partial discharges at the rubber-oil interface was a challenge. Seven setups, each with some variations were designed and investigated. This was explained in chapter 4 of this thesis. Two suitable electrodes configurations with two suitable sample treatments were found for creating surface discharge at the oil-rubber interface. The circular base electrode with conductive paint deposit on rubber samples was used for all the final experiments due to its high reproducibility and ease of use.

2. **Parameters influencing the choice of optical sensor**

Partial discharge detection using optical sensors is quite new research field. As a result, no existing protocol or guideline is available to choose optical sensors for PD applications. This thesis identified several critical parameters to be considered before selecting the sensors. This was presented in section 3.1 of chapter 3. The main parameters are: light power level, light source spectral range, quantum efficiency and gain of the sensor, output bandwidth, cost and size.

3. **Selection of optical sensor**

Based on the specifications, there was three low light detection optical sensors available in the market which were evaluated in section 3.1.2 in chapter 3. The ThorLabs APD130A2 sensor was chosen for experiments in this research due to its optimum spectral and output bandwidth range, high immunity to EMI, no damage due to ambient light exposure, high quantum efficiency and its compatibility with fibre optics cable for future research.

4. **Testing of surface discharge in the oil by means of both electrical and optical sensor**

The final setup (circular electrode with conductive paint deposit on rubber sample) was used to perform experiments in dry oil as well as oil with different moisture content. The experimental setup and results with different oil samples were discussed in chapter 5. The PDIV values obtained from both electrical and optical detection system were

identical for corona, surface discharge in air and dry oil and for treeing phenomena in plexiglass. However, loss of sensitivity for optical sensor is observed with water contaminated oil samples. This difference in PDIV is not only due to the opaque emulsion of oil but can also be due to the variation in distance between the electrode and conductive paint deposit due to low visibility.

5. **Determination of optical sensor characteristics and possible relation with electrical detector**

The analysis and comparison of the electrical and optical detector based on the results obtained from experiments were done which is presented in chapter 6. Following points summarize the characteristics of the APD sensor in comparison with the HFCT sensor:

- The PD pulses received from the APD optical sensor only indicate light magnitude obtained from PD activity but it does not give a further indication for categorisation (for the different type of PD source).
- The immunity check conducted also indicate that the APD optical sensor is electromagnetic immune and insensitive to any noise condition, unlike HFCT sensor.
- The sensitivity analysis based on PDIV and lower limit detection concluded that optical sensor has the same sensitivity as that of HFCT sensor. However, with the water activity greater than 0.58, loss of sensitivity of the optical sensor was noticed due to the reduced transmission capability of oil with moisture content. The maximum loss of sensitivity was 12% which was obtained from the most saturated sample prepared in this research.
- The PRPD patterns obtained from both detector were comparable in terms of phases, orientation and occurrence except the magnitude, which was different in both cases (as two separate parameters are measured from PD activity) and polarity (since the optical sensor can only give output in positive).
- The correlation factor was calculated for electrical and optical output. It showed that they are moderately correlated and linear in trend. However, compared to the electrical measuring circuit, no direct calibration with respect to apparent charge was possible [9]. Furthermore, the optical signals (photons) propagating from the source must traverse different materials and penetrate interfaces (especially lens arrays) before being detected by the opto-electrical converter and converted into electrical signals inside the sensor itself in case of APD sensor used in this thesis.

If the comparison between the change in magnitudes, PRPD pattern and pulse resolution time is taken into account, then optical measurements are comparable with the electrical measurements.

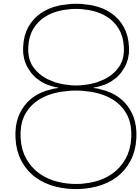
6. **Possibility of usage of the optical sensor in real on-field detection**

With the analysis done in this thesis, it can be concluded that the data obtained from the optical sensor can be analysed using the existing PD analysis tool which is currently used for electrical measurements. The working and detection results of the optical sensor with respect to electrical sensor were also discussed. Therefore, optical PD detection through suitable sensors can be used for monitoring PD activities inside the HV cable termination if further research as suggested in next section is carried out. In [25], the initial approach towards placement of optical sensor is presented (also presented in the appendix Figure E.1). However, a lot of research has to be done in order to finalise the installation of sensor inside termination.

7.2. Future scope and recommendations

The research conducted in this thesis can be seen as the first step towards usage of this technology in real application. However, a lot of research still needs to be performed to utilise this technology in real operations. The following points gives the recommendations based on this thesis:

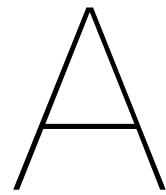
- The human error due to the difference in distance between HV electrode and conductive paint deposit in different oil samples can be reduced with an improved setup in the future.
- The correlation as observed between data collected from electrical and optical sensor for same PD source was not close to one. Therefore, the optimisation of the analysis procedure should be the next task. This will include a detailed study of the physics behind the light emission during PD activity. This will help to set upper and lower bound for the data collected thus minimizing the scattering in the plot. The question like whether each PD emit light?, how the light intensity changes with growth in PD activity? etc should be investigated.
- The APD sensor used in this research is fibre optic cable compatible. This allows more options for performing optical PD detection online. The laboratory experiments with standard and special fluorescent fibre cable along with optical sensor should be performed to study its characteristics. Various ways of using it in termination can be explored and tried.
- A feasibility study of using optical sensors for detecting internal discharge in translucent and transparent stress cone should be conducted. In this thesis, due to unavailability of transparent or translucent stress cone material, plexiglass was used to create the same effect. However, typical internal discharge type PRPD pattern was not observed by both electrical and optical sensor with the setup tried in this thesis. Therefore, an internal discharge at the interface of transparent or translucent rubber stress cone with XLPE insulation as described in [9] can be tested with proper design setup.
- The various other options of APD sensors with the wider active area and smaller overall size can be explored such that its integration inside the termination without the lens can be a possibility.
- The optical sensor is highly directional, as a result, its integration inside the cable termination will be a big challenge. Therefore, the number of sensors, its positioning and field of view of the optical sensors should be investigated. The optical and electrical simulation should be done in order to know whether the calculated positioning will work under the operating condition. The functionality of an oil-filled cable termination due to the presence of these optical sensors inside should not be compromised. Thus, the connection to outside communication system should be established at no or low electric field zone. Also, the change in the mechanical and other properties of terminations due to installation of optical sensor also need to be researched.



Bibliography

- [1] IEC 60050 International Electrotechnical Commission, *Electrical accessories*, IEC ref: 442-06-06.
- [2] K. B. Liland, A. K. Bjørke, S. Hvidsten, H. Faremo and E. Bjerkan, "Failure Modes and Condition assessment of High Voltage Oil Filled XLPE Terminations", *IEEE Electrical Insulation Conference*, Montreal, Canada, June 2009.
- [3] K. B. Liland, S. Hvidsten, G. Birkenes, F. Mauseth, G. A. Ward and E. Bjerka, "Development of a Simple Method for Condition assessment of oil Filled XLPE Terminations", *8th International Conference on Insulated power cables*, Versailles, France, June 2011.
- [4] [Online], Available: <http://www.inmr.com/looking-future-cable-accessory-design-ehv/3/>. Accessed on: 20-04-2018
- [5] J. Y. W. Wen, "Condition Assessment of water in High Viscosity Insulating Cable Termination Oil", Master thesis Report, Dept. Power Eng., Delft University of Technology, November 2016.
- [6] H. Di, "Investigation on termination oil-rubber interface parallel to electric field with water contamination", Master thesis Report, Dept. Power Eng., Delft University of Technology, August 2017.
- [7] A. Rodrigo Mor, "Monitoring and Diagnostics: High Voltage Cable System", Delft University of Technology, 2018.
- [8] H. Gerd and V. Klaus, "Optical PD detection in High Voltage Cable Accessories", *International Conference on Insulated Power Cables*, JiCable 2015.
- [9] S. Behrend, "Optische und elektrische Untersuchungen zu Teilentladungen in transparenten Silikonelastomeren", Ph.D. dissertation, Fakultät IV - Elektrotechnik und Informatik, Technischen Universität Berlin, 2015.
- [10] M. Ren, J. Zhou, B. Song, C. Zhang, M. Dong and R. Albarracin, "Towards Optical Partial Discharge with Micro Silicon Photomultiplier", *MDPI Sensors*, 2017.
- [11] C. L. Wadhwa, "Non-Destructive Insulation test techniques", *High Voltage Engineering*, Second edition, New age International Limited Publishers, pg 181-183, 2007.
- [12] F. H. Kreuger, "Partial Discharge", *Industrial High Voltage Volume 2*, Delft university Press, pg 117-157, 1992.
- [13] A. Rodrigo Mor, L.C. Heredia, and F.A. Muñoz, "Clustering Plots for the separation of partial discharge sources based on amplitude, charge and energy of PD pulses", *INSU-CON 2017 13th International Electrical Insulation Conference*, Birmingham, UK, 2017

- [14] IEC 60270, *High-voltage test techniques- partial discharge measurements*.
- [15] R. Cselko, Z. A. Tamus, A. Szabo and I. Berta, "Comparison of Acoustic and Electrical Partial Discharge Measurements on Cable Terminations", *IEEE Conference*, 2010.
- [16] L. E. Lundgaard, "Partial Discharge- Part XIII: acoustic Partial Discharge Detection-fundamental Considerations", *IEEE Electrical Insulation Magazine*, Vol.8, 1992.
- [17] M. M. Yaacob, M. A. Alsaedi, J. R. Rashed, A. M. Dakhil and S. F. Atyah, "Review on Partial discharge detection technique Related to High Voltage power Equipment using Different Sensors", *Photonics sensors*, Vol.4, 2014.
- [18] R. Schwarz, M. Muhr and S. Pack, "Evaluation of partial discharge impulses with optical and conventional detection systems", *XIVth International Symposium on High Voltage Engineering*, Beijing, China, August 2005.
- [19] R. Schwarz and M. Muhr, "Partial discharge measurement as a Diagnostic Tool for HV-Equipments", *IEEE Conference*, 2006.
- [20] A. K. Lazarevich, "Partial Discharge Detection and Localization in High Voltage Transformers Using an Optical Acoustic Sensor", Master thesis Report, Dept. Electrical Eng., Virginia Polytechnic Institute and State University, May 2013.
- [21] R. Schwarz, M. Muhr and S. Pack, "Partial discharge detection in oil with optical methods", August 2005.
- [22] R. Schwarz and M. Muhr, "Modern Technologies in Optical Partial Discharge Detection", *Annual Report Conference on Electrical Insulation and Dielectric Phenomena*, 2007.
- [23] T. Jiagui, Y. Jinggang, Y. Gaoxiang and T. Ju, "A System Using Fluorescent Fiber for Partial Discharge Detection in Transformer", *IEEE Conference*, 2016.
- [24] L. Shiyan, Z. Tao, L. Yunpeng, L. Yansong and L. Qiang, "Detections of ultrasonic sensor and PMT on partial discharge in oil under DC voltage", *IEEE International Conference on Liquid Dielectrics*, Bled, Slovenia, 2014.
- [25] C. Lothongkam, "Dielectric strength behaviour and mechanical properties of transparent insulation materials suitable to optical monitoring of partial discharges", Ph.D. dissertation, Fakultät für Elektrotechnik und Informatik, Gottfried Wilhelm Leibniz Universität, 2014.
- [26] Hamamatsu PMT guide, *Photomultiplier: Basics and Applications*, Third edition.
- [27] Hamamatsu SiPM guide, *Silicon Photomultiplier: Basics and Applications*, Third edition.
- [28] A. Gohler, "Detectors for microscopy-CCDs, sCMOS, APDs and PMTs", March 2015.
- [29] Thor Labs Avalanche Photodetectors, *APD130x Operation Manual*, Version 1.1.0, 2017.
- [30] A. Rodrigo Mor, L.C. Heredia, D.A. Harmsen, F.A. Muñoz, "A new design of a test platform for testing multiple partial discharge sources", *Electrical Power and Energy Systems*, 2018.
- [31] Techimp PDBaseII, *Operator's Manual*, software release 1.01.09.
- [32] [Online], Available: <http://pdflex.tudelft.nl/>, Accessed on: 27-02-2018
- [33] B.G. Park, I. Park, J. Han, S. Lee, C. Lee and C. Ha, "Characterization of Optical properties in Water-in-Oil Emulsion", *Journal of Dispersion Science and Technology*, Volume 34, 2013



Appendix: Chapter 3

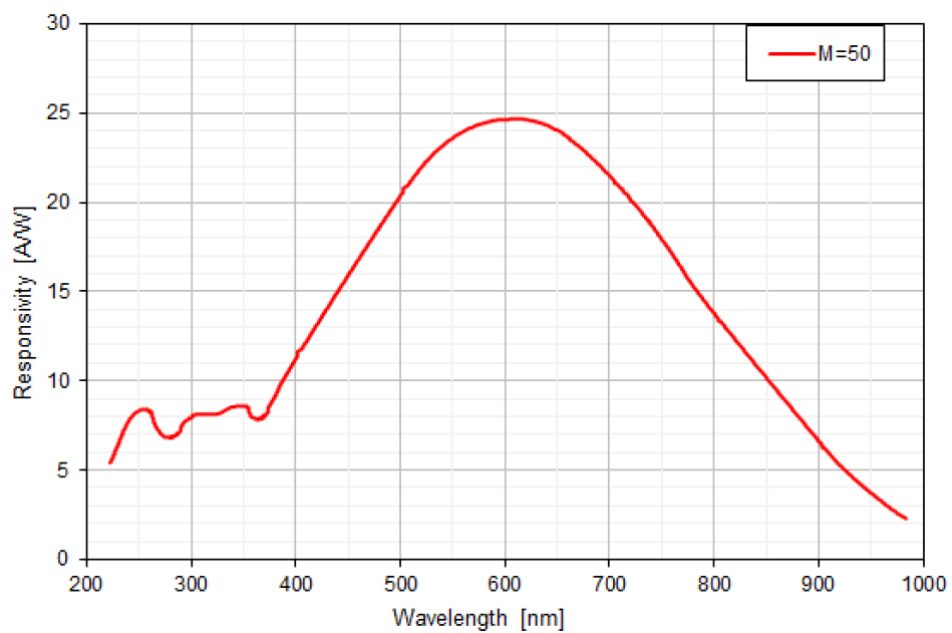


Figure A.1: Detector responsivity response of APD130A2

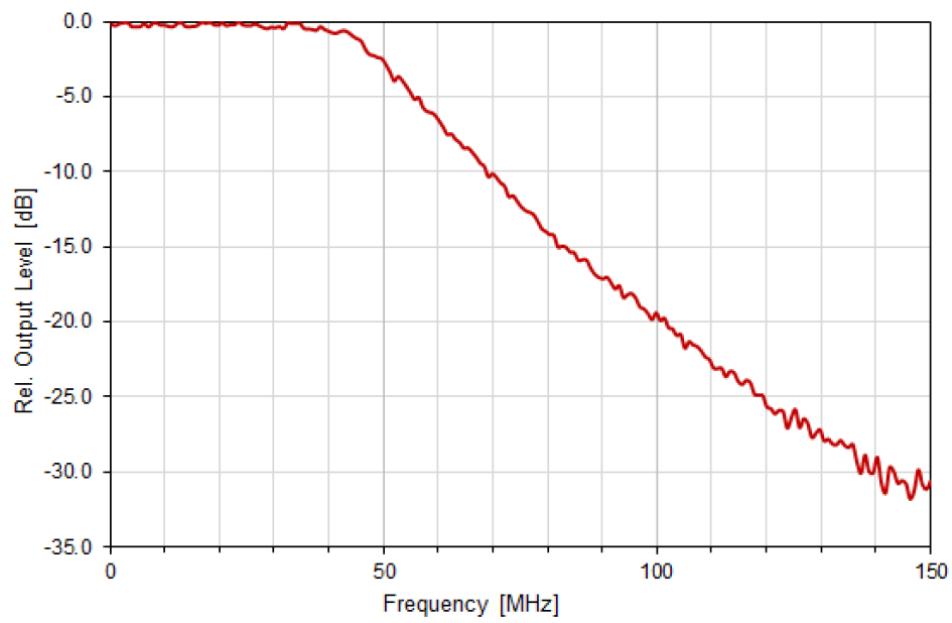


Figure A.2: Output frequency response of APD130A2

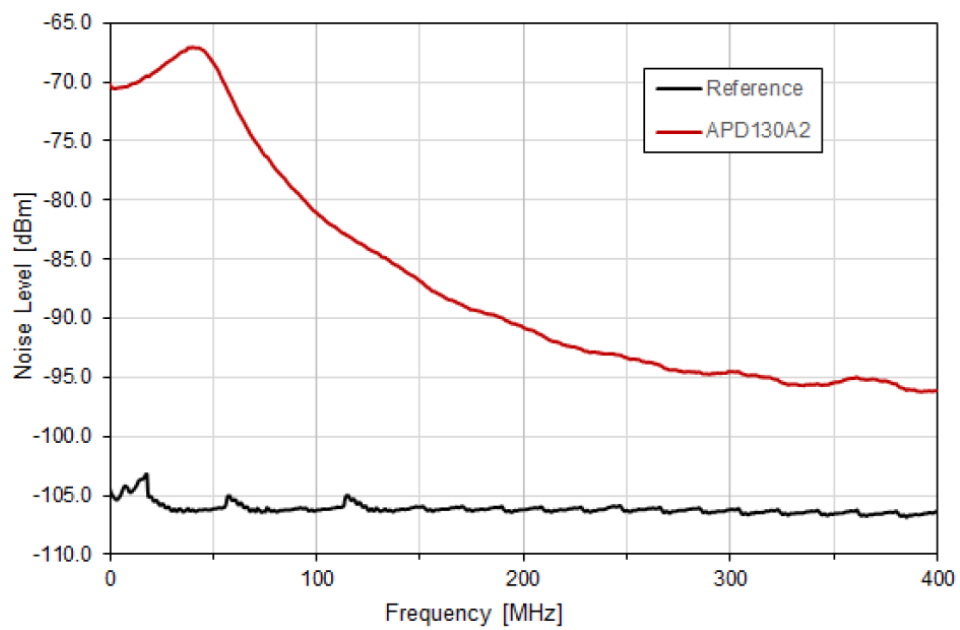


Figure A.3: Spectral noise response of APD130A2

B

Appendix: Chapter 4

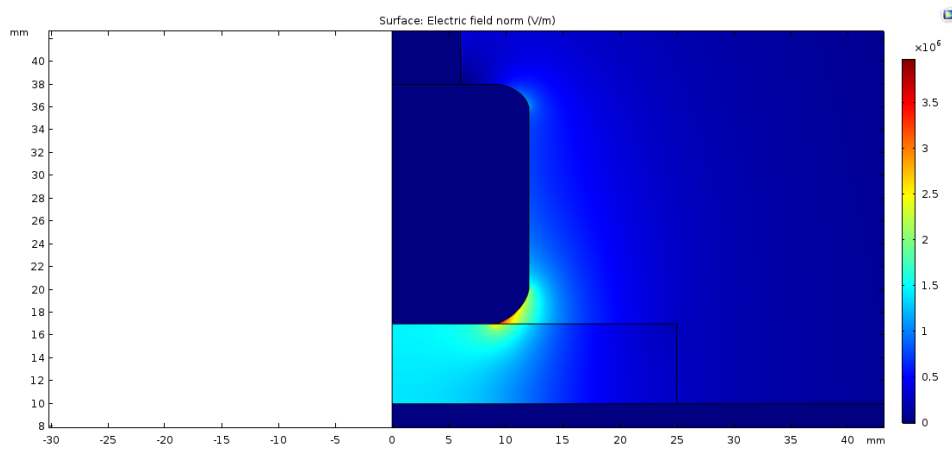


Figure B.1: COMSOL Simulation for cylindrical electrode (Setup 1)

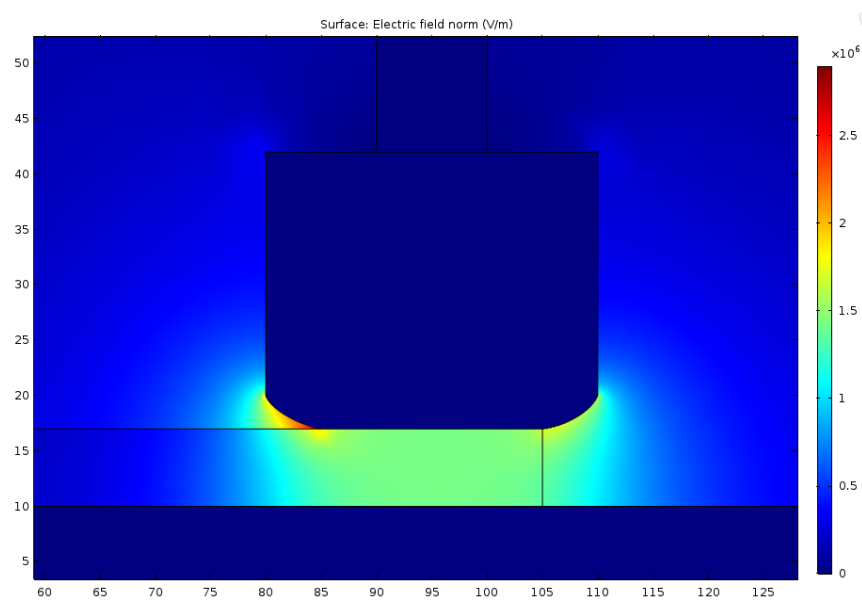


Figure B.2: COMSOL Simulation for cylindrical electrode (Setup 2)

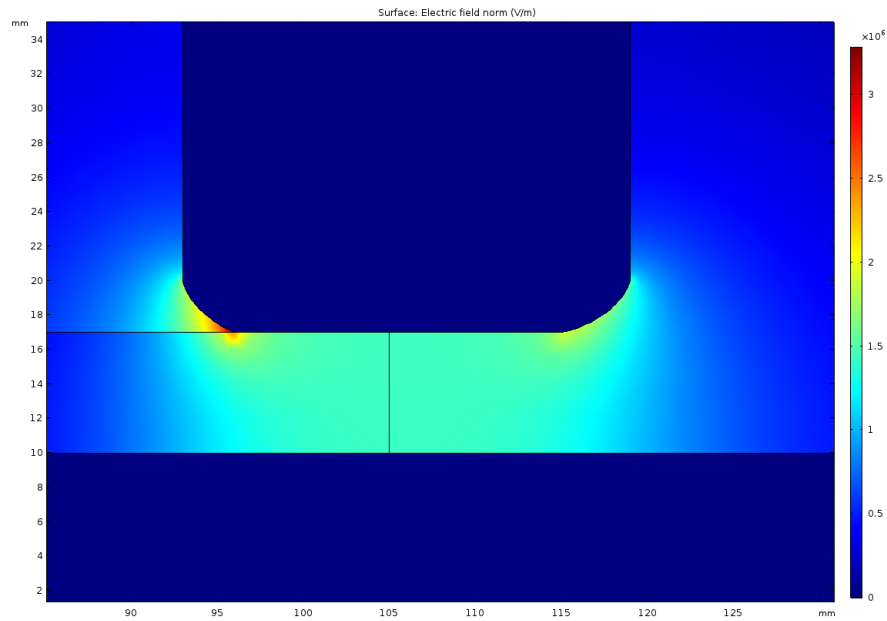


Figure B.3: COMSOL Simulation for cylindrical electrode (Setup 3)

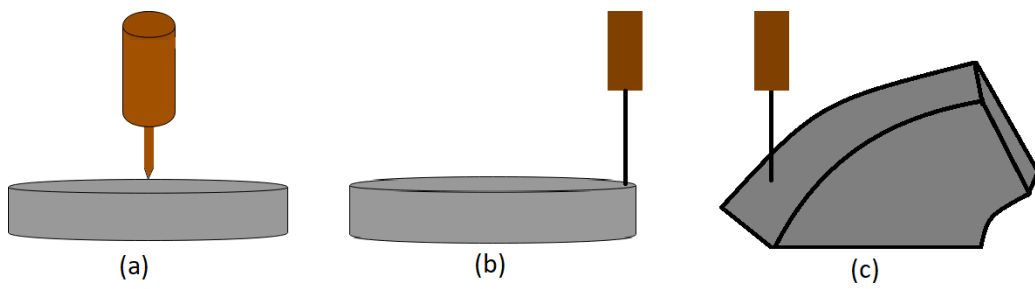


Figure B.4: Different needle electrode orientation

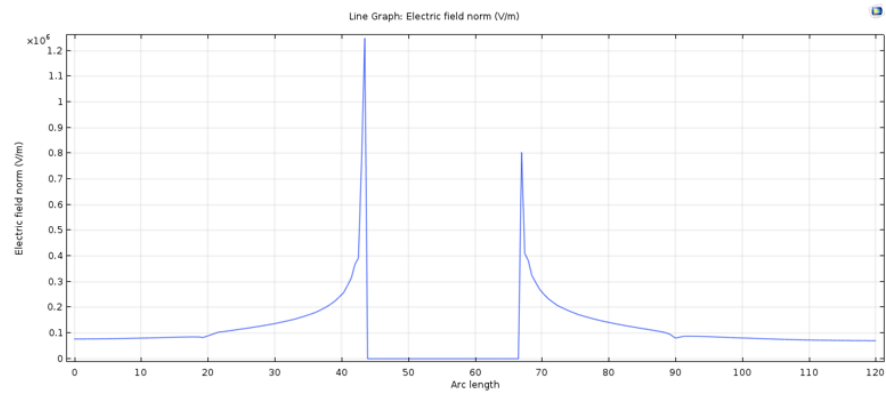
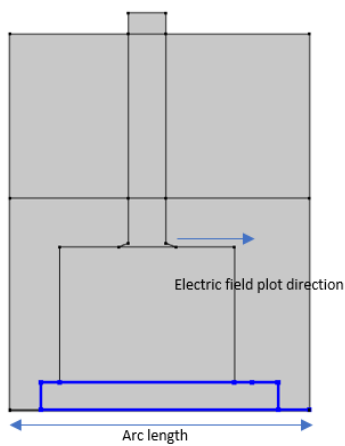


Figure B.5: Plot of electric field without side ground electrode for 10 kV voltage applied

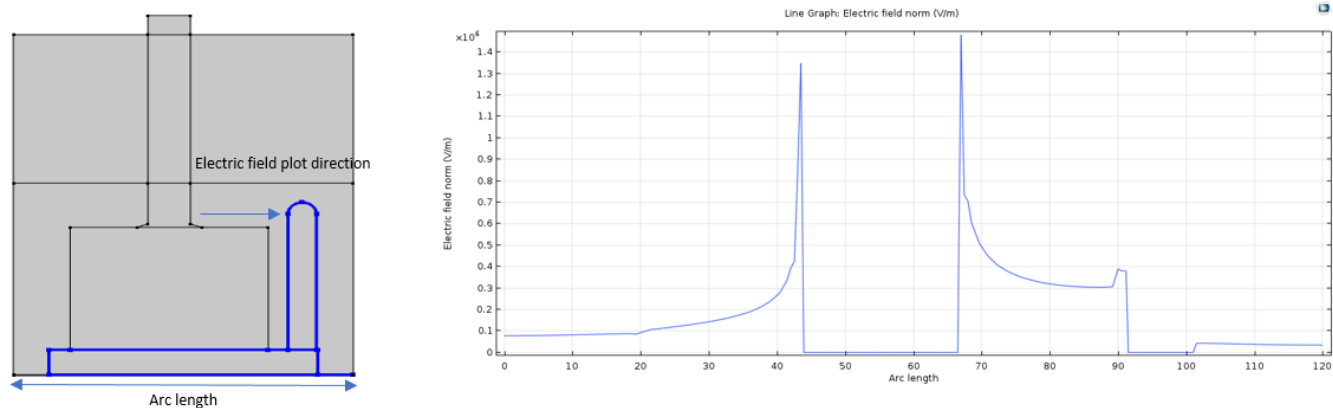


Figure B.6: Plot of electric field with side ground electrode for 10 kV voltage applied

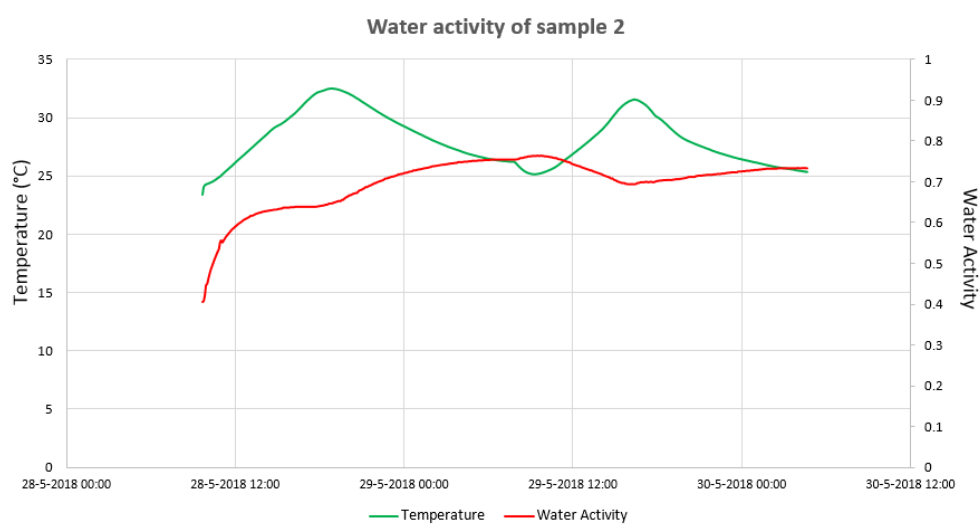


Figure B.7: Vaisala measurements for sample 2

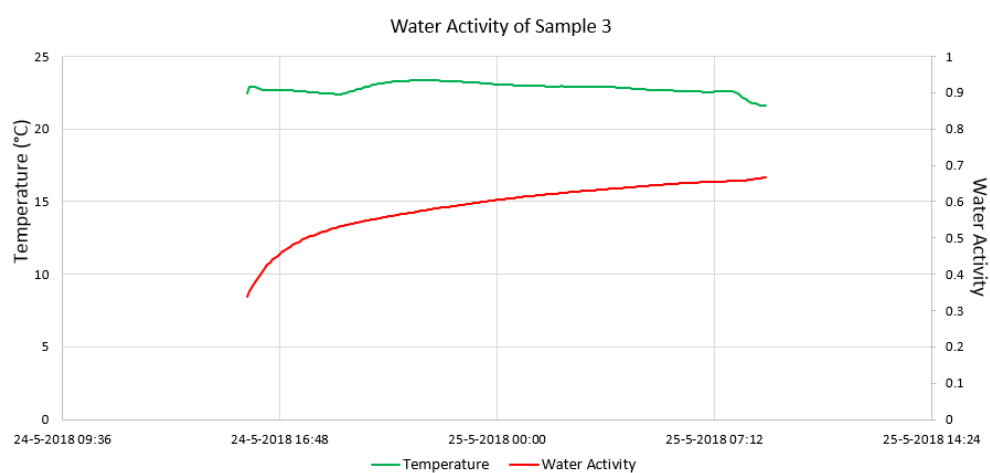


Figure B.8: Vaisala measurements for sample 3

C

Appendix: Chapter 5

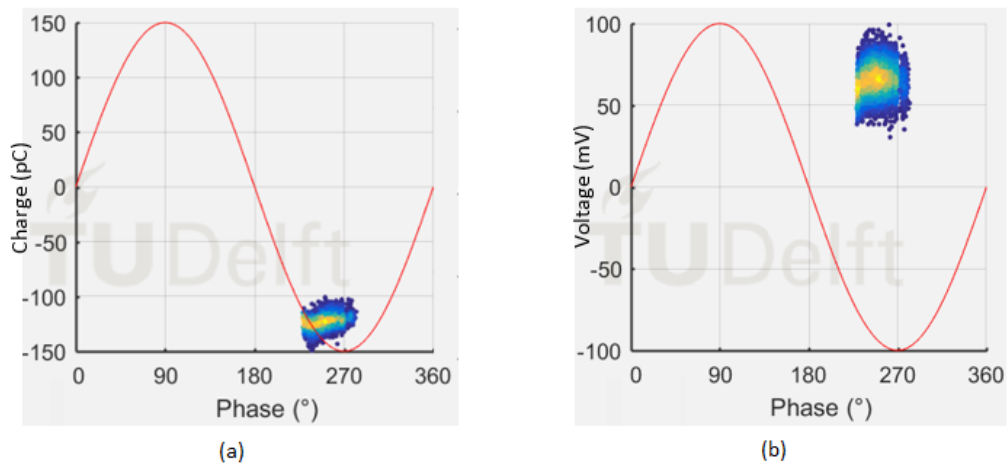


Figure C.1: PRPD pattern of corona source 15 cm from ground at 10 kV (a) From electrical detector (b) From optical detector

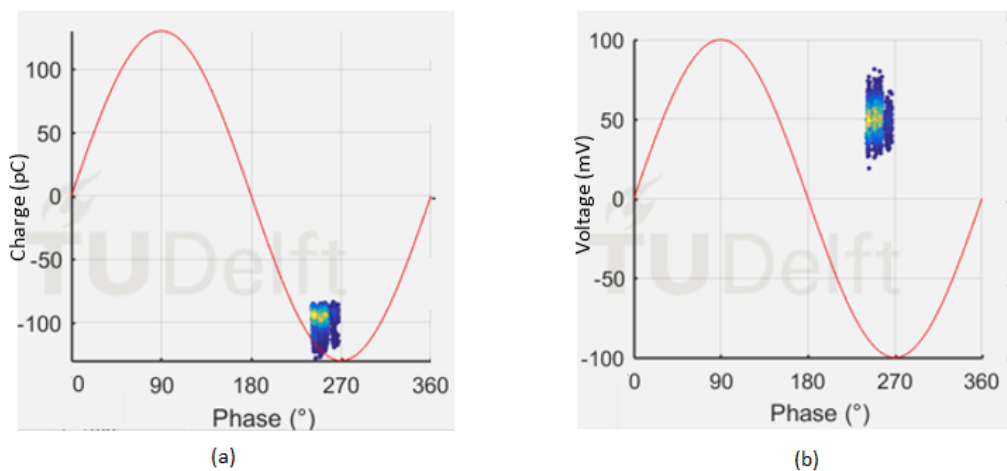


Figure C.2: PRPD pattern of corona source 18 cm from ground at 10 kV (a) From electrical detector (b) From optical detector

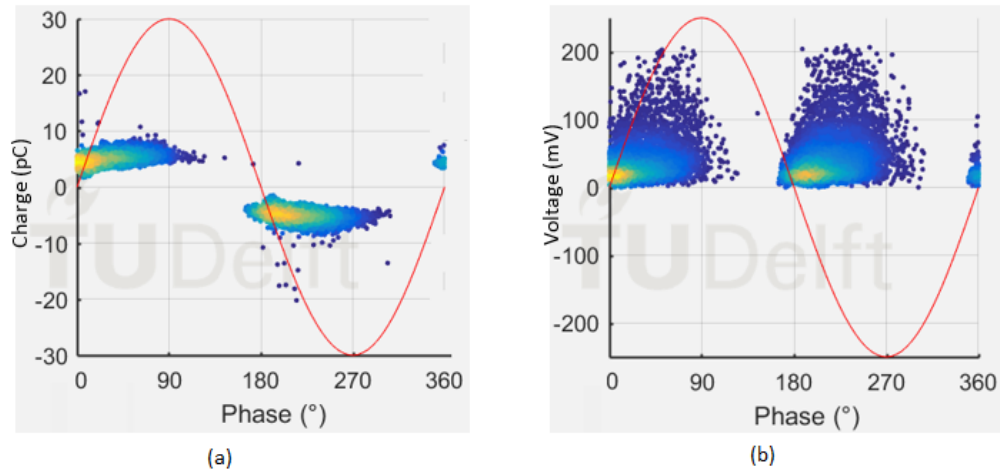


Figure C.3: PRPD pattern collected with electrical signal triggered for surface discharge in dry oil at 22 kV (a) From electrical detector (b) From optical detector

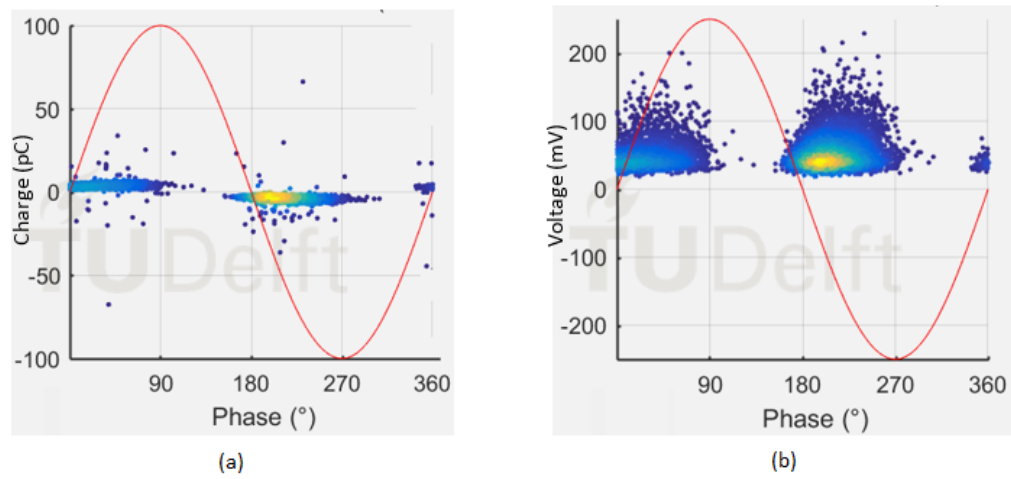


Figure C.4: PRPD pattern collected with optical signal triggered for surface discharge in dry oil at 22 kV (a) From electrical detector (b) From optical detector

D

Appendix: Chapter 6

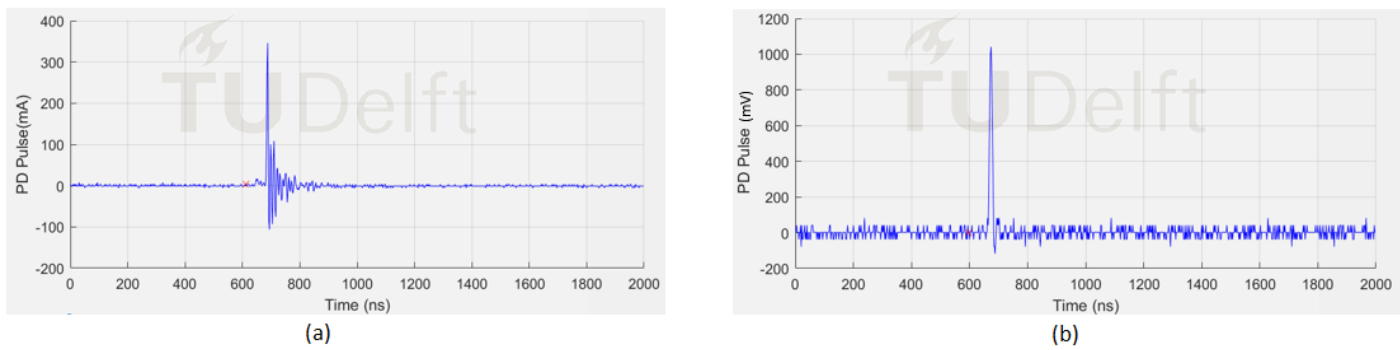


Figure D.1: (a) PD pulse captured by HFCT sensor for treeing phenomena at 25 kV (b) PD pulse captured by APD sensor for treeing phenomena at 25 kV

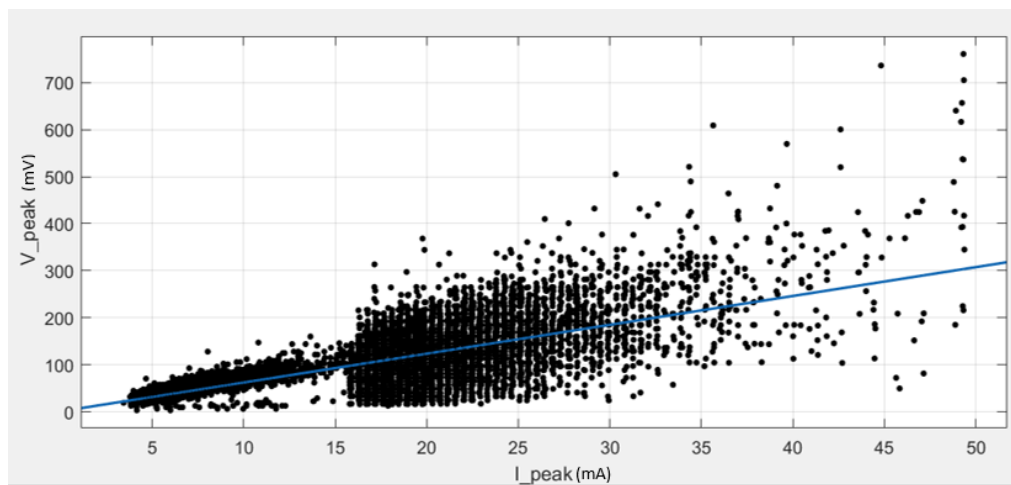


Figure D.2: Plot of peak voltage pulse detected by APD sensor Vs peak current pulse by HFCT sensor for surface discharge in air for positive cycle

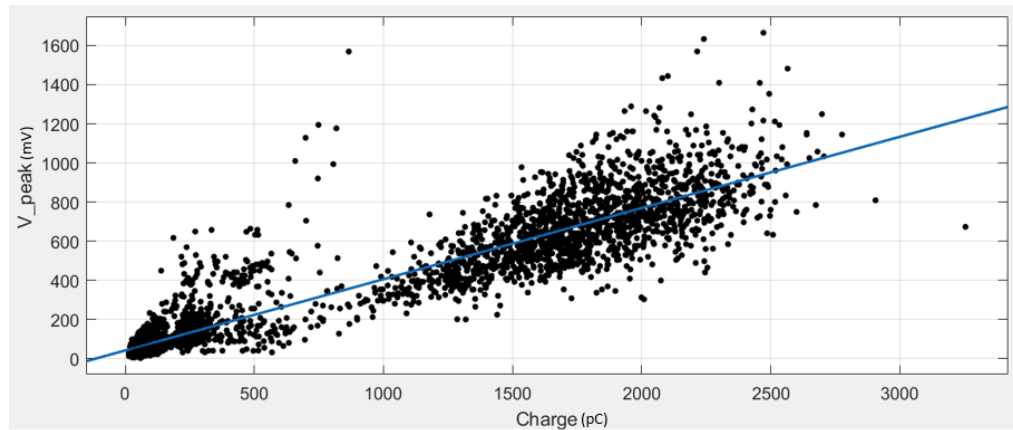


Figure D.3: Plot of peak voltage pulse detected by APD sensor Vs apparent charge by HFCT sensor for surface discharge in air for negative cycle

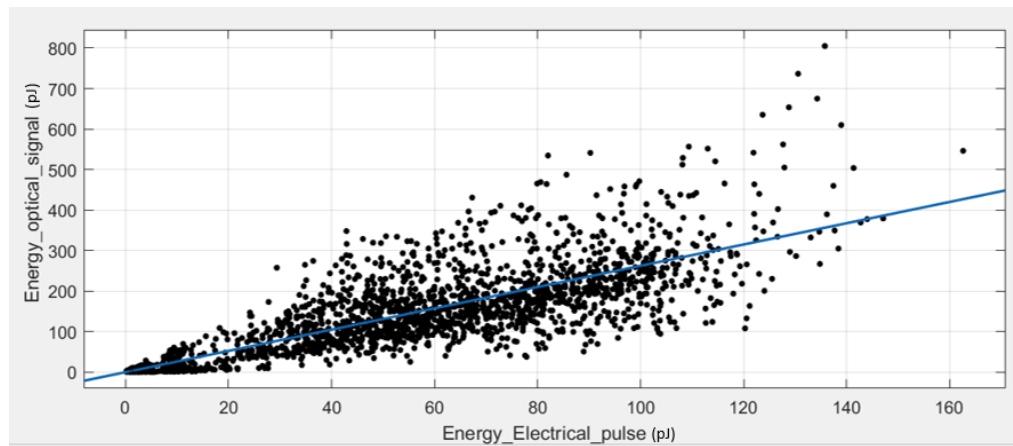


Figure D.4: Plot of energy of signal detected by APD sensor Vs energy of signal (-ve) by HFCT sensor for surface discharge in air for negative cycle

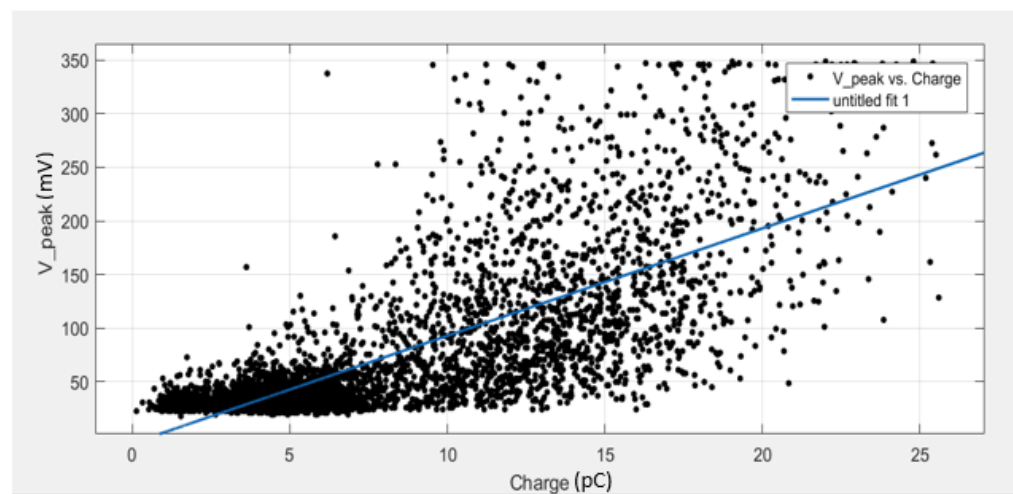


Figure D.5: Plot of peak voltage pulse detected by APD sensor Vs apparent charge by HFCT sensor for surface discharge in dry oil for negative cycle

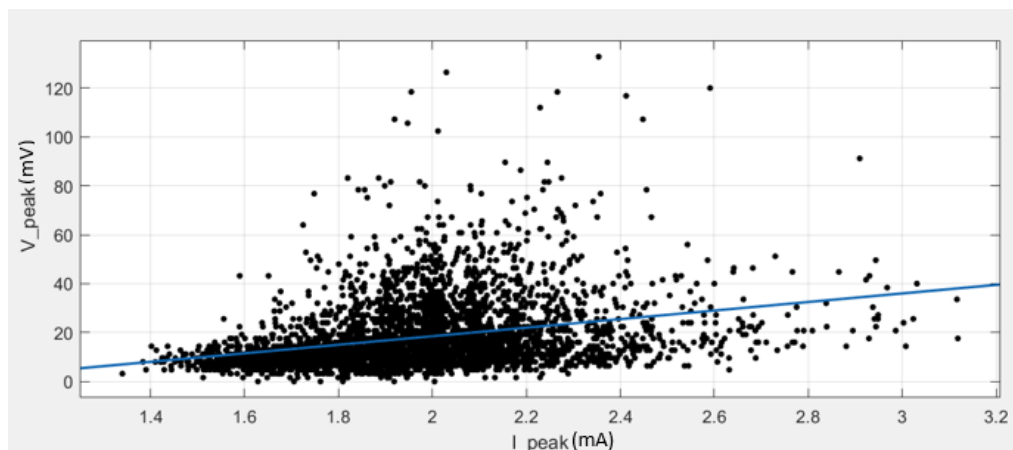


Figure D.6: Plot of peak voltage pulse detected by APD sensor Vs peak current pulse (-ve) detected by HFCT sensor for surface discharge in oil sample 1 for negative cycle

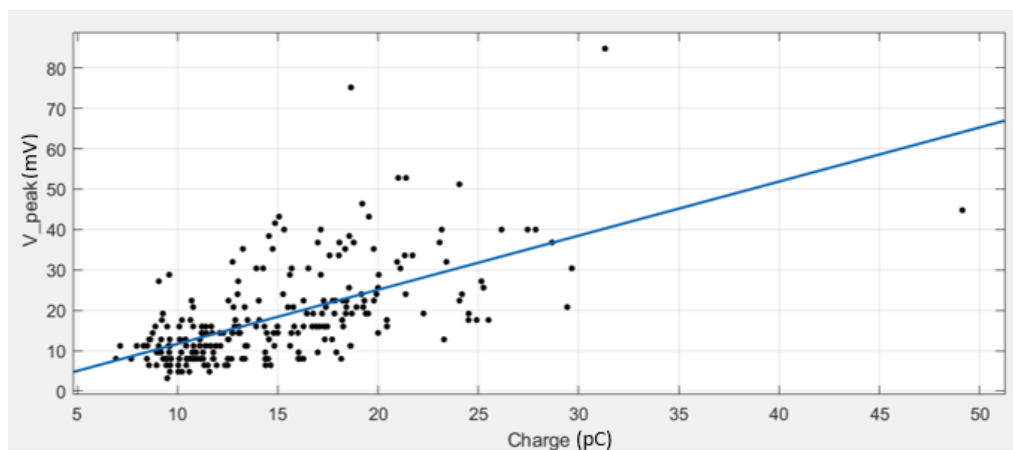


Figure D.7: Plot of peak voltage pulse detected by APD sensor Vs apparent charge by HFCT sensor for surface discharge in oil sample 2 for positive cycle

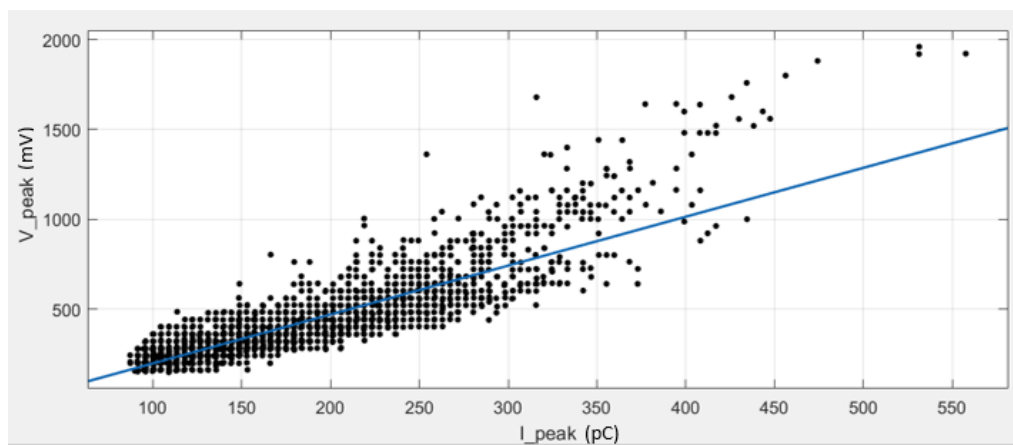
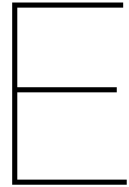


Figure D.8: Plot of peak voltage pulse detected by APD sensor Vs peak current pulse detected by HFCT sensor during treeing phenomena for positive cycle



Appendix: Chapter 7

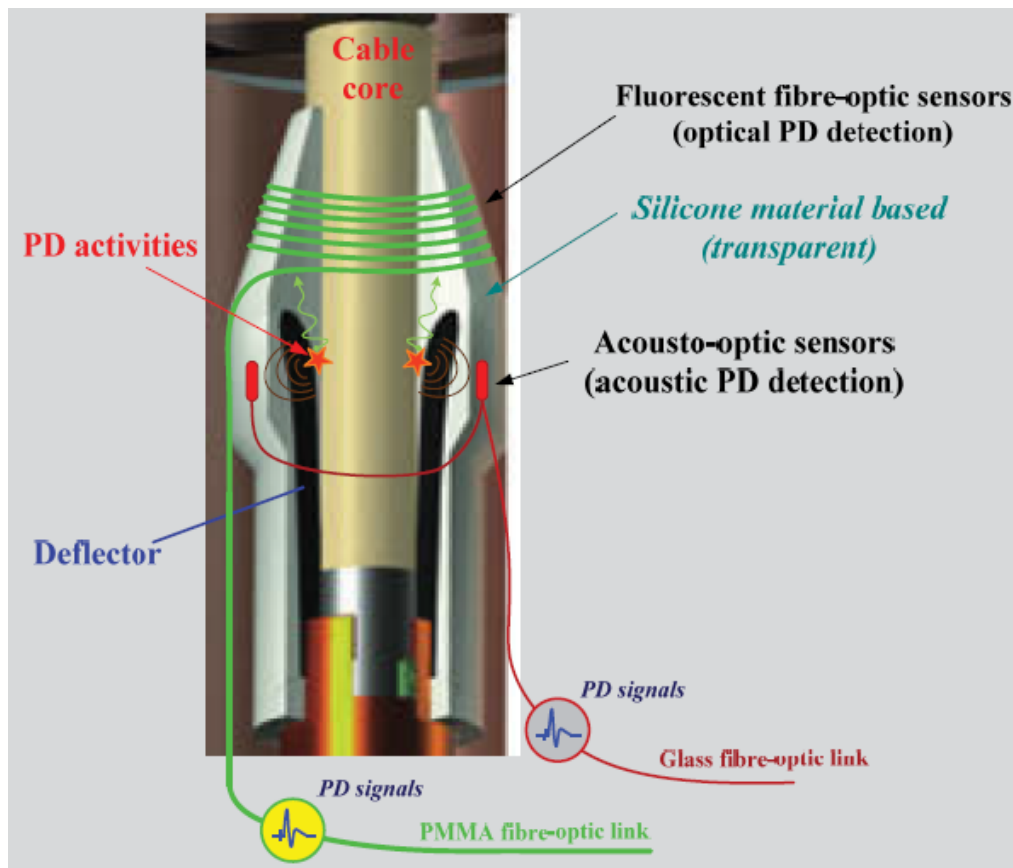


Figure E.1: Idea presented in [25] for positioning the different kind of optical sensors inside termination

